

INDRAPRASTHA INSTITUTE OF INFORMATION  
TECHNOLOGY, DELHI

DOCTORAL THESIS

---

**SPATIO-TEMPORAL LINEAR  
STABILITY OF VISCOELASTIC  
SAFFMAN-TAYLOR FLOWS**

---

*Author:*  
Dipa GHOSH

*Supervisor:*  
Dr. Sarthok SIRCAR

*A thesis submitted in fulfillment of the requirements  
for the degree of Doctor of Philosophy  
to the*

Department of Mathematics  
Indraprastha Institute of Information Technology Delhi



INDRAPRASTHA INSTITUTE of  
INFORMATION TECHNOLOGY DELHI

March 20, 2024



# CERTIFICATE

This is to certify that the thesis titled “SPATIO-TEMPORAL LINEAR STABILITY OF VISCOELASTIC SAFFMAN-TAYLOR FLOWS” being submitted by DIPA GHOSH to the Indraprastha Institute of Information Technology Delhi, for the award of the degree of Doctor of Philosophy, is an original research work carried out by her under my supervision. In my opinion, the thesis has reached the standards fulfilling the requirements of the regulations relating to the degree.

The results contained in this thesis have not been submitted in part or full to any other university or institute for the award of any degree/diploma.

January, 2024

Dr. Sarthok SIRCAR



**Indraprastha Institute of Information Technology Delhi**  
**New Delhi 110020**

# DECLARATION

This is to certify that the thesis titled “SPATIO-TEMPORAL LINEAR STABILITY OF VISCOELASTIC SAFFMAN-TAYLOR FLOWS” being submitted by Dipa GHOSH to the Indraprastha Institute of Information Technology Delhi, for the award of the degree of Doctor of Philosophy, is a bonafide work carried out by me. This research work has been carried out under the supervision of Dr. Sarthok SIRCAR.

The study pertaining to this dissertation has not been submitted, in part or in full, to any other university or institute for the award of any other degree or diploma.

**January, 2024**  
**Dipa GHOSH**

A handwritten signature in black ink that reads "Dipa Ghosh". The signature is written in a cursive style with a loop at the end of the last name.

**Indraprastha Institute of Information Technology Delhi**  
**New Delhi 110020**

INDRAPRASTHA INSTITUTE OF INFORMATION TECHNOLOGY, DELHI

# *Abstract*

Doctor of Philosophy

## **SPATIO-TEMPORAL LINEAR STABILITY OF VISCOELASTIC SAFFMAN-TAYLOR FLOWS**

by Dipa GHOSH

This thesis is about an analytical study of viscoelastic fingering that solves the problem of predicting the finger width when a Newtonian fluid (with negligible viscosity) drives a non-Newtonian (power-law) fluid. The finger thinning and widening phenomena in non-Newtonian fluids have been empirically explained in a large number of prior studies, but an analytical expression derived via a single, unified theory explaining both of these features has remained elusive until now. This work aims at deriving an expression and contrast the findings with the *in vitro* and *in silico* data that are already accessible. The dispersion relation is also derived in a rectilinear channel for the power-law fluids, which is utilized in the linearized model. The description of the five chapters is as follows:

- The classical Saffman-Taylor instability in a Hele-Shaw cell is introduced in the first chapter, along with a summary of earlier findings from direct numerical simulations as well as experimental and analytical findings for both Newtonian and non-Newtonian fluids. It gives an overview of both a qualitative and a quantitative investigation of viscous fingering in the linear and non-linear regimes. Additionally, its significant interest in a wide range of fields, including physics, biology, applied mathematics, and industrial research, is highlighted.
- In the second chapter, the basics of the various categories of instability modes are discussed briefly. The phrase "temporal modes" refers to situations where the real wave number determines the instability in the complex frequency. The convectively unstable modes result in wave packets that eventually leave the medium in its undisturbed state after traveling away from the source. In contrast, a point-source disturbance gradually contaminates all of the absolutely unstable modes. If both of the merging modes develop from waves traveling in the same direction, evanescent modes (or the direct resonance mode) will appear. To discern between these instabilities, elementary knowledge of the branch or pinch point and the Cusp-Map diagram is required. An example of the Briggs' contour integral method is used to discover the flow-material properties contributing to stability-instability regions.

- The third chapter highlights an analytical approach to the problem of predicting the finger width of a simple fluid driving a non-Newtonian (power-law) fluid. The analysis is based on the Wentzel-Kramers-Brillouin (WKB) approximation by representing the deviation from the Newtonian viscosity as a singular perturbation in a parameter, leading to a solvability condition at the fingertip, which selects a unique finger width from the family of solutions. This solvability theory provides a reasonable mechanism for the selection of the pattern, and it is done by constructing a function called the cusp function, whose zeros will determine the possible solutions for the pattern. It is found that the relation between the dimensionless finger width,  $\Lambda$  and the dimensionless group of parameters containing the viscosity and surface tension,  $v$ , has the form:  $\Lambda \sim \frac{1}{2} - \mathcal{O}(v^{-1/2})$  for shear thinning case, and  $\Lambda \sim \frac{1}{2} + \mathcal{O}(v^{2/(4-n)})$  for shear thickening case, in the limit of small  $v$ . This theoretical estimate is compared with the existing experimental finger width data as well as the one computed with the linearized model, and a good agreement is found near the power-law exponent,  $n = 1$ .
- The issues that have been encountered during this study, as well as some recent developments and potential future concerns requiring thorough spatiotemporal stability assessments on the dynamics of fingering patterns, are discussed in the final chapter. The potential future work includes but is not limited to the impact of changing the viscosity contrast parameter on the dynamics of fingered structures, the competition between the typical Saffman-Taylor single-finger stationary solution, and other attractor systems characterized by closed bubbles dominates the long-time asymptotics, the existence of topological singularities in the form of interface pinch-off, wetting effects, and applications to other issues like interface roughening in the fluid invasion of porous media, recent results on rotating Hele-Shaw flows, the impact of boundaries like elastic boundaries and occlusions, the evolution of the moving interface, etc.

## Statement of Originality

The analytical investigation of viscoelastic fingering, also known as Saffman-Taylor instability in a Hele-Shaw cell, is the focus of this thesis. It provides an answer to the challenge of forecasting the finger thinning and widening phenomena for various polymeric liquids. My original contributions to this thesis are listed below.

- Chapter 2: This chapter provides a clear understanding of the basics of temporal and spatiotemporal stability analysis using linear stability theory, the concepts of cusp map, branch, and pinch point (Bansal, Ghosh, and Sircar, 2021, Schmid and Henningson, 2001, Koch, 1986, Kupfer, Bers, and Ram, 1987).
- Chapter 3: The competition between the viscous and capillary forces on the advancing front leads to the emergence of a characteristic length scale that determines the relative finger width,  $\Lambda_{Temp}$ . The remarks on the determination of  $\Lambda_{Temp}$  using linear stability analysis and identifying this as the most unstable mode, followed by the analysis of Chuoke, van Meurs, and van der Pol (Chuoke, Van Meurs, and Poel, 1959), were done in this chapter (Bansal, Ghosh, and Sircar, 2023, Bansal, Chauhan, and Sircar, 2022, Bansal, Ghosh, and Sircar, 2021) by deriving a dispersion relation in a rectilinear channel for the power-law fluids.

In the mathematical model section: the derivation of McLean and Saffman's (McLean and Saffman, 1981) equations in order to consider the non-Newtonian effect in the surface tension parameter. The extension of the solvability theory of Hong and Langer (Hong and Langer, 1986) to include the shear-dependent viscosity effect in the modified Darcy's law ( (3.2), Bansal, Ghosh, and Sircar, 2023), which is the starting point of this analysis. Next is the estimation of the shear rate,  $\dot{\gamma} \approx \frac{q}{b}$ , in the power-law model (3.5) (Bansal, Ghosh, and Sircar, 2023).

In the main result section: the derivation of the relation between  $\Lambda$  and  $v_0$  using the WKB expansion and also using the concept of branch point for the cases  $\beta > 1, \beta < 1$ . The proof of solvability theory for the power law fluids, the derivation of the cusp function. All nonlinear terms at the level of the Wentzel-Kramers-Brillouin (WKB) approximation are included in the recomputed cusp function instead of just the leading order term (Bansal, Ghosh, and Sircar, 2023).

In the validation part: the comparison of the theory and the dynamical simulation with the experiments of Bonn and Meunier (Bonn and Meunier, 1997, Lindner et al., 2002). In the conclusion part: there is a need to extend the theory for strong shear thinning cases and include the elastic stresses as well.

- Chapter 4: In the first section, a discussion is made on the limitations of the work of Chapter 3 with Dr. Diksha Bansal and Dr. Sarthok Sircar (the co-author and corresponding author, respectively). In the second section, potential future research is addressed on the dynamics of fingering patterns and the impact of varying the viscosity contrast parameter, as well as the existence of topological singularities in the form of interface pinch-off, wetting effects, and applications to other problems from the previous study (Casademunt, 2004, McCloud and Maher, 1995) like interface roughening in the fluid invasion of porous media, rotating Hele-Shaw flows, etc.

Summary: 1) Contribution of Dipa Ghosh in Bansal, Ghosh, and Sircar, 2021 (Physics of Fluids): Part of the numerical derivations, part of the write-up and finding the cusp map using zero contours.

2) Contribution of Dipa Ghosh in Bansal, Ghosh, and Sircar, 2023 (SIAM Journal on Applied Mathematics): The estimation and the form of the shear rate and the complete mathematical derivations of the main results, compiling all the derivations in latex, part of the numerical validation of the theoretical results and concluding remarks.



## *Acknowledgements*

As I approach the completion of yet another thrilling chapter in my life, I want to express my gratitude to everyone who has supported me personally and academically in reaching this point. Firstly, I would like to extend my heartfelt gratitude to my mentor and guide, Dr. Sarthok Sircar, who had so graciously accepted me for the Ph.D. program and guided me all along, pushing me to be better every day.

I am also deeply indebted to Dr. Subhashree Mahapatra for her kind understanding and caring personality. She has been an inspiration all along. To Dr. Kaushik Kalyanaraman, I express my gratitude for his insightfulness and for helping me enhance my knowledge. To Professor K.C. Sivakumar, I will always be grateful for his unconditional support since my MSc. days at IIT Madras and for guiding me whenever I needed his help. I will always be appreciative of Professor Bhaba Kumar Sarma, IIT Guwahati, for his guidance during the MTTS program. My knowledge and comprehension of mathematics have increased as a result of his mentoring and instruction. Additionally, I owe a debt of gratitude to Dr. Sukalyan Mistry for inspiring me to seek a career in mathematics.

I also extend my sincerest gratitude to IIIT Delhi and the CSIR-UGC council for providing me with all the financial and academic means necessary and for supporting me in making this journey healthy and insightful. Also, to my beautiful colleagues at IIIT Delhi, I would really like to thank you. Tanisha, Shivani, Divya, Dr. Diksha, Dr. Neelam, and Dr. Manashi Debnath (from JNU), without you guys this journey wouldn't have been easy. Our late-night discussions and chats over a cup of tea have been one of the best moments of this journey.

Now, to the two wonderful personalities without whom this journey would only have been a dream; my brother, Dr. Kausik Ghosh, and my husband, Mr. Sohom Ghosh. I will always be indebted to them for their unmatched contributions to my career. Last but not least, I want to express my gratitude to my brother, Mr. Manojit Ghosh, my in-laws, and my parents for always having faith in me and for being the greatest support system anyone could ask for. Finally, I thank you, God, for giving me the strength and perseverance to follow my dream and for guiding me through all the ups and downs in life.

I sincerely ask all of my loved ones, friends, teachers, and well-wishers to continue showering me with love and blessings as I prepare to enter a new chapter of my life that will undoubtedly bring with it its own set of obstacles and hardships. This will inspire me to work even harder and will help me succeed in all of my new endeavors.

**Dipa Ghosh**

# Contents

<b>Acknowledgements</b>	<b>ix</b>
<b>1 Introduction</b>	<b>1</b>
1.1 Classical Saffman-Taylor instability in a Hele-Shaw Cell . . . . .	1
1.2 Newtonian Saffman-Taylor instability . . . . .	3
1.2.1 Computational results . . . . .	3
1.2.2 Experimental results . . . . .	6
1.2.3 Analytical results . . . . .	10
1.3 Non-Newtonian Saffman-Taylor instability . . . . .	13
1.3.1 Computational results . . . . .	13
1.3.2 Experimental results . . . . .	16
1.3.3 Analytical results . . . . .	21
1.4 Industrial applications of Saffman-Taylor flows . . . . .	23
<b>2 Basics of spatiotemporal instability</b>	<b>26</b>
2.1 Introductory remark . . . . .	26
2.2 Temporal instability . . . . .	28
2.3 Absolute and Convective instability . . . . .	29
2.4 Notion of Evanescent modes . . . . .	30
2.5 Pinch points and Branch points . . . . .	32
2.6 The Cusp map . . . . .	33
2.7 Briggs' method . . . . .	35
2.8 Concluding remark . . . . .	41
<b>3 An analytical approach to the WKB approximation method</b>	<b>43</b>
3.1 Introductory remark . . . . .	43
3.2 Mathematical model . . . . .	44
3.3 Main results . . . . .	48
3.4 Experimental and numerical validation . . . . .	64
3.5 Concluding remark . . . . .	69
<b>4 Conclusion</b>	<b>71</b>
4.1 Introductory remark . . . . .	71
4.2 Limitations of the current work . . . . .	71
4.2.1 In formulating the mathematical model . . . . .	71
4.2.2 In determining a unique value of $\Lambda$ . . . . .	72
4.3 Future problems . . . . .	73
4.3.1 The role of viscosity contrast . . . . .	73
4.3.1.1 Basin of attraction of Saffman-Taylor finger . . . . .	74
4.3.1.2 The competing attractors of Taylor-Saffman bubbles . . . . .	75

4.3.1.3 Rotating Hele-Shaw flows . . . . .	77
4.4 Concluding remark . . . . .	79
<b>Bibliography</b>	<b>80</b>
<b>List of publications</b>	<b>93</b>
<b>Curriculum Vitae</b>	<b>94</b>

# List of Figures

1.1	Schematic of (a) fingering patterns in Rectilinear Hele-Shaw cell, and (b) fingering patterns in Radial Hele-Shaw cell (Singh, Singh, and Pandey, 2020) . . . . .	2
1.2	(a) Interface between air (less viscous fluid) and glycerine (more viscous fluid) at an early stage of the instability, (b) Development of instability (fingering patterns), (c) Inhibiting effect of a finger which gets ahead of its neighbor (beginning of a single propagating finger) (Saffman and Taylor, 1958) . . . . .	7
1.3	Numerical simulation of miscible viscous fingering (defined in equations (1.1)-(1.3)), with a constant flux of solvent (on left of image) into oil, and $M$ (mobility ratio) = 5, $Pe$ (Péclet number) = 3000. (Booth, 2010) . . . . .	15
1.4	Shear-Thinning: Narrower fingers differs from the classical limit of $\Lambda = 0.5$ (Lindner and Wagner, 2009) . . . . .	17
1.5	(a) Oil spill cleanup (b) Oil, gas recovery (c) Dendrite formation (Open source) . . . . .	24
2.1	(a) Convective, (b) Absolute instability (Source (Schmid and Henningson, 2001)) . . . . .	30
2.2	Effect of direct resonance on amplitude evolution (Source (Koch, 1986))	31
2.3	Sketch illustrating the cusp map method (Source (Kupfer, Bers, and Ram, 1987)). . . . .	34
2.4	Outline of the numerical procedure for detecting branch points in the $w$ -plane used in the cusp map method (Source (Kupfer, Bers, and Ram, 1987)). . . . .	35
2.5	Illustration of the numerical procedure for detecting saddle points in the $\alpha$ -plane used in the Briggs' method (Source (Schmid and Henningson, 2001)). . . . .	36
2.6	Sketch of contour deformation procedure for Briggs' method. Left: complex $w$ -plane, right: complex $\alpha$ -plane (Source (Schmid and Henningson, 2001)). . . . .	38
2.7	An example in the schematic of an absolute instability created by the intersection of two $\alpha$ -roots with three crossing of the $\alpha_r$ -axis ( $\alpha_i = 0$ ). The vertical ray from $w_0$ cuts the $\alpha_i = 0$ contour in the three places in the double-sheeted $w$ -plane (Source (Yeo, Khoo, and Zhao, 1996)). . . . .	39
2.8	Map of the complex $w$ -plane into the complex $\alpha$ -plane under the dispersion relation (2.18)(Source (Schmid and Henningson, 2001)).	41
3.1	Schematic diagram of a Saffman-Taylor finger in the laboratory frame, assumed symmetric about the $\tilde{x}$ -axis. . . . .	46

3.2	Contours of integration for the evaluation of the cusp function, $\mathcal{C}$ (3.21):Cusp	57
3.3	Finger width as a function of $1/B$ for solutions of (a) Xanthane for concentrations of 50 ppm ( $\bigcirc$ ), 100 ppm ( $\square$ ), 500 ppm ( $\triangle$ ), 1000 ppm ( $+$ ), and at fixed cell geometry, $w = 2.0\text{cm}$ and $b = 0.25\text{mm}$ (Source: (Lindner, Bonn, and Meunier, 2000)), (b) Xanthane at different cell geometries, $w = 2.0\text{cm}$ and $b = 0.66\text{mm}$ ( $\bigcirc$ ), $w = 2.0\text{cm}$ and $b = 0.25\text{mm}$ ( $+$ ), $w = 4.0\text{cm}$ and $b = 0.5\text{mm}$ ( $\triangle$ ), $w = 4.0\text{cm}$ and $b = 0.25\text{mm}$ ( $\square$ ), and at fixed concentration of 1000 ppm (Source: (Lindner et al., 2002)), (c) PEO for concentrations of 5 ppm ( $\bigcirc$ ), 50 ppm ( $\square$ ), 500 ppm ( $\triangle$ ), and at fixed cell geometry, $w = 2.0\text{cm}$ and $b = 0.5\text{mm}$ (Source: (Lindner et al., 2002)). (---) predictions from the linear stability analysis (equation (3.105)). (—) predictions from the theoretical estimate (equations (3.72), (3.77)).	68
4.1	Two types of finger dynamics observed for $c = 0$ (Upper plot) and $c \neq 0$ (Lower plot) (Casademunt, 2004)	74
4.2	Bubble shaped region for a given surface tension and viscosity contrast (Casademunt, 2004)	76
4.3	Typical experimental pattern of low viscosity contrast fingering under rotation (Casademunt, 2004)	77
4.4	Typical experimental pattern for $c = 1$ , with air as the outer fluid, if the cell is initially dry (Casademunt, 2004)	78

*Dedicated to my brother Kausik and my loving husband  
Sohom*

# Chapter 1

## Introduction

The following chapter provides an overview of the theoretical, experimental, and numerical study of Saffman-Taylor instability in its linear/non-linear regime with the motivation of understanding the instabilities of the interfaces between two fluids in a narrow channel, which is known as the Hele-Shaw cell.

In accordance with the experiments, the less viscous fluid pushes the more viscous fluid into the Hele-Shaw cell, forming finger-like patterns at the interface referred to as the viscous fingering phenomenon. This phenomenon of viscous fingering leads to pattern formations, which have been a topic of acute interest in Physics, applied mathematics as well as industrial research communities for many years as it is responsible for a ubiquitous range of physical phenomena like: the breakup of falling fluid into droplets, vortex patterns of fluid jets, crystal formation, dendritic shape of snowflakes etc.

In order to get a clear understanding of the study, a concise summary of certain important topics like classical Saffman-Taylor flows in a Hele-Shaw cell, delineation of previous observations of direct numerical simulations, experimental and analytical results for both Newtonian fluids and non-Newtonian fluids will be discussed below. Finally, some industrial applications of Saffman-Taylor flows will also be discussed in further course.

### 1.1 Classical Saffman-Taylor instability in a Hele-Shaw Cell

The first theoretical treatment of the stability of an immiscible fluid-fluid interface in a Hele-Shaw cell (see Figure-1.1) was published in a seminal paper in 1958 by Saffman-Taylor (Saffman and Taylor, 1958) preceding which the viscous fingering instability is commonly known as the Saffman-Taylor instability.

The classical Saffman-Taylor instability occurs when a less viscous fluid pushes a more viscous fluid into a narrow channel. As an instance, if air (with a negligible viscosity) pushes a more viscous fluid (with viscosity  $\eta$ ), in a Hele-Shaw cell of height  $b$  and width  $W$ , and if the surface tension between the two fluids is  $\sigma$ , then the flow in the confined geometry governed by Darcy's law gives the mean velocity (averaged across the channel thickness) of the fluid as a function of an applied pressure gradient  $V = \frac{-b}{12\eta} \nabla p$ . Due to the incompressibility of the fluid,  $\nabla \cdot V = 0$ , and hence the pressure field is Laplacian, i.e.,  $\Delta p = 0$ . The pressure jump at the interface is given by  $\delta p = \sigma(\frac{2}{b} + k)$ , where  $k$  is the curvature in the direction of the channel width. In

this two-dimensional approximation, the set of equations together with the boundary conditions completely determine the problem (Lindner and Wagner, 2009).

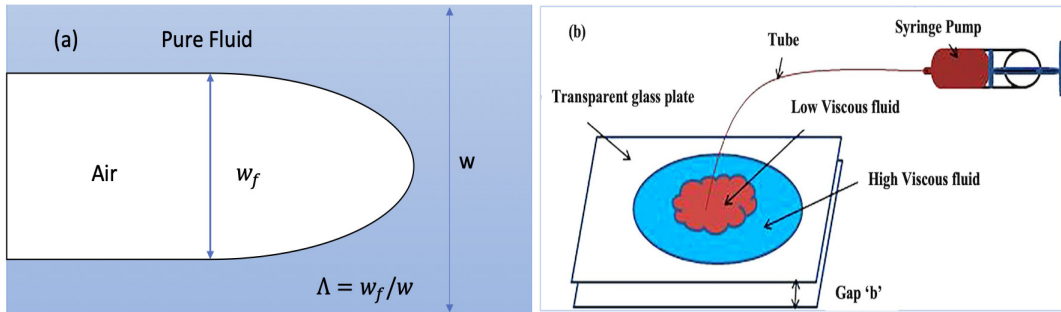


FIGURE 1.1: Schematic of (a) fingering patterns in Rectilinear Hele-Shaw cell, and (b) fingering patterns in Radial Hele-Shaw cell (Singh, Singh, and Pandey, 2020)

An initially straight interface becomes unstable when the less viscous fluid pushes the more viscous fluid, and minor perturbations increase the pressure gradient and velocity in front of the perturbation. Surface tension, on the other hand, tends to stabilize the initially straight interface. The rivalry between viscous and capillary forces produces a characteristic length scale, which can be estimated using linear stability analysis. The little fingers eventually expand and begin to compete with the more advanced fingers. As a result of the non-linear development process, a single finger may be observed propagating through the cell. The control parameter  $1/B = 12Ca(\frac{w}{b})^2$  gives the relative width of a single finger as  $\Lambda$ , defined as the ratio between the finger width  $w_f$  and the cell width  $w$ ; that is, the ratio between the two length scales of the system  $w$  and the maximum growth rate for a wavelength  $l_c = \frac{\pi b}{Ca^{1/2}}$  (where  $Ca$  is capillary number). The outcomes achieved in various cell geometries as a function of the control parameter  $1/B$  follow a universal curve. As fingertip velocity  $U$  increases, viscous forces become more dominant than capillary forces, and relative finger width falls. At high velocity,  $\Lambda$  does not go to zero but rather settles near a plateau value of  $\Lambda = 0.5$ . Saffman and Taylor described this instability in 1958 (Saffman and Taylor, 1958); however, they were unable to explain the finger selection mechanism, and by ignoring surface tension, they discovered a family of analytical solutions for the shape of the interface (Lindner and Wagner, 2009) that agrees well with experimental observations but fails to clarify the selection of a given finger width.

Taking surface tension into consideration, McLean and Saffman in 1981 (McLean and Saffman, 1981) numerically explained the selection mechanism of a given finger width. Analytical results of the selection process describe the fact that surface tension represents a singular perturbation leading to a solvability condition at the fingertip, which was solved much later (Hong and Langer, 1986; Shraiman, 1986; Combescot et al., 1986).

An ideal two-dimensional problem was the targeted point of discussion so far. However, when the problem is viewed in three dimensions, a thin wetting layer can be seen between the advancing finger and the glass plate. This causes the pressure fluctuation at the interface to be continuously altered, effectively causing minor



modifications in finger width observed between different experimental geometries (Lindner and Wagner, 2009; Tabeling and Libchaber, 1986).

## 1.2 Newtonian Saffman-Taylor instability

This section will be primarily focused on highlighting the various methods used for studying Newtonian flow instability like direct numerical simulations (DNS) and computational bifurcations, experimental observations, and analytical results, respectively.

### 1.2.1 Computational results

In current times, much attention has been devoted to controlling the fingering patterns (Karmakar et al., 2022), tip splittings, and reduction of the growth of the interfacial fingers (Karmakar and Shukla, 2023) using direct numerical simulations on Newtonian fluids that have been reported here chronologically.

One of the significant aspects of the enduring interest in Newtonian fluid flow in Hele-Shaw cells is its close similarity to quasi-static solidification (Kondic, Palffy-Muhoray, and Shelley, 1996). In particular, it has also been reported that the fluid-fluid interface plays the same role as the Mullins-Sekerka instability of the solidification front (Kondic, Palffy-Muhoray, and Shelley, 1996). The features such as the growth of stable dendritic fingers and side branching are associated with solidification, which has also been observed in fluids with an imposed anisotropy.

Over the last decade, large-scale numerical simulations have emerged as a useful new tool, which often can access information that is difficult to extract experimentally by using a simple conventional method like finite difference approaches (Christie, Jones, and Muggeridge, 1990; Christie, Muggeridge, and Barley, 1993; Sorbie, Zhang, and Tsibuklis, 1995). Also, several experimental and computational investigations on the role of permeability heterogeneities in viscously unstable displacements (Araktingi and Orr, 1993; Tchelepi et al., 1993; Sorbie et al., 1994) have been analyzed. However, the detailed numerical work by Tchelepi (Tchelepi et al., 1993) was able to break new ground in this regard. The author employs a mixed computational approach in both two- and three-dimensional homogeneous as well as heterogeneous media that combines a traditional Eulerian finite difference discretization for the pressure equation with Lagrangian particle tracking for the concentration equation in order to analyze the transition from viscosity- to density-dominated displacements. It is worth noting that if gravitational forces strongly dominate viscous forces, two- and three-dimensional simulations display similar behavior. In all of the above computational investigations, the governing equations are formulated in terms of velocity and pressure variables. Due to the familiarization of primitive variables like velocity and pressure, this approach may have the advantage that most researchers are familiar with, but there are also some drawbacks, such as, in this formulation, the equations do not allow a clear separation of the various physical effects. So, as an alternative, rectilinear homogeneous miscible displacements with gravity override are analyzed by Ruith et al. (Ruith and Meiburg, 2000) by means of direct numerical simulations on the basis of the vorticity-streamfunction formulation of the governing equations. This vorticity-based point of view often provides a clear overview of

these flow characteristics to the effects of viscosity differences, density differences, or impermeable boundaries. In particular, from this literature, one can understand the formation of the gravity tongue in terms of a focusing mechanism. The author also provides the numerical simulations for different values of the governing parameters that lead to scaling results, which demonstrate that the thickness of the gravity tongue grows with  $(G/Pe)^{1/2}$ , where  $G$  is the gravity parameter and  $Pe$  is the Péclet number.

Density-driven instabilities between miscible fluids in a vertical Hele-Shaw cell are investigated by Fernandez et al (Fernandez et al., 2002) by means of both experimental and two-three dimensional numerical simulations. In their article, their work focuses on the initial stage of the growth instability, and they provide detailed information about the growth rates as well as the most amplified wave numbers as a function of the governing Rayleigh number,  $Ra$ . Gravitationally unstable interfaces, i.e., interfaces that separate a lighter fluid from the heavier fluid located above it in a gravitational field, are less understood in a vertical Hele-Shaw cell. Here, the flow is dominated by viscous forces, while inertial forces, i.e., when the Reynolds number ( $Re$ ) is small, are negligible. So, the velocity profile is no longer parabolic across the gap; hence, the Hele-Shaw equation is unable to provide an accurate description of the flow. Despite all the above facts, some successful nonlinear simulations based on gap-averaged equations have been used to investigate nonlinear interaction mechanisms among the evolving fingers.

Moreover, in the vertical Hele-Shaw setup, Goyal et al. (Goyal and Meiburg, 2006) had also done a computational study based on the Stokes equations to investigate the effects of gravitational forces on miscible displacements. Using nonlinear simulations (provide the quasi-steady displacement fronts in the gap of the cell), they examined the stability of spanwise perturbations by means of linear stability analysis. Due to gravity, the two-dimensional simulations indicate a marked thickening or thinning and slowing down or speeding up of the displacement front for flows stabilized or destabilized. In order to investigate the transition between viscously driven and purely gravitational instabilities, a comparison between displacement flows and gravity-driven flows without net displacements is presented by them (Goyal and Meiburg, 2006).

Miscible porous media displacements have also been investigated by E. Upchurch and E. Meiburg in 2008 (Upchurch and Meiburg, 2008) unlike Fernandez et al. and Goyal et al. (Fernandez et al., 2002; Goyal and Meiburg, 2006), by non-vertical injection wells. In their investigation, they provide insight into the mechanisms that dominate variable viscosity and density. The numerical results reveal a significant difference compared to vertical injection wells, which strongly influence breakthrough times and recovery times. Due to the presence of a density difference, interesting interactions and competitions between the dominant fingers and the emerging gravity tongue are observed, and for sufficiently large mobility ratios, dendritic fingering instabilities appear prominently on the flanks of the dominant finger along the exposed side of the gravity tongue.

3D Navier-Stokes simulations of viscously unstable, miscible Hele-Shaw displacements have been discussed by Oliveira et al. in 2011 (Oliveira and Meiburg, 2011). Quasi-steady fingers whose tip velocity increases with the Peclet number and unfavorable viscosity ratio that shows the widest finger near the tip but progressively narrower one towards the root have been observed. Their simulations also reveal a

new mechanism which is inner tip-splitting, fundamentally different from the familiar tip-splitting mechanism. It is furthermore observed that the Péclet number plays an important role in miscible flow displacements that differs from the capillary number for the case of immiscible flows (since inner splitting is delayed for large Pe numbers, whereas higher capillary number promotes tip-splitting).

M.O. John et al. (John et al., 2013) performed direct numerical simulations of the variable density and viscosity Navier-Stokes equations in order to explore 3D effects within miscible displacements in horizontal Hele-Shaw cells. These simulations identify a number of mechanisms concerning the interaction of viscous fingering with a span-wise Rayleigh-Taylor instability.

Gravitationally and viscously unstable miscible displacements in vertical Hele-Shaw cells have been investigated via 3D Navier-Stokes simulations (Heussler et al., 2014). These unstable vertical displacements show a strong vorticity quadruple along the length of the fingers, which does match with the recent observations for neutrally buoyant flows. It can also be noted that the velocity of the 2D base flow at the front usually increases due to viscosity contrast and destabilizing density difference. While displacement fronts moving faster than the maximum velocity of the Poiseuille flow exhibit a single stagnation point in a moving frame of reference, gravitationally stable fronts, on the other hand, move more slowly than the Poiseuille flow which causes complex streamline patterns and form spike-like structures at the tip. These findings are in line with the earlier observations for corresponding capillary tube flows (Oliveira et al., 2014).

In the same year, Luis et al. (Cueto-Felgueroso and Juanes, 2014) proposed a continuum model of two-phase (or multiphase) flow in a Hele-Shaw cell, which describes a 3D flow in the cell gap using gap-averaged quantities such as fluid saturation and Darcy flux. In the gap, viscous and capillary coupling between the fluids leads to a non-linear fractional flow function. Within a phase-field framework, capillarity and wetting phenomena are modeled to design a free energy function that induces a phase segregation at equilibrium. Though the model has been tested through the bubbles and viscously unstable displacement simulations, the behavior of the model has been analyzed as a function of capillary number, viscosity contrast, and cell geometry. This model has a great impact on wetting and flow rate on the performance of microfluidic devices and geological flows through fractures (Cueto-Felgueroso and Juanes, 2014).

It is worth noting from the previous observations that multiphase flow in porous media has an enormous impact on industrial as well as environmental applications at several spatiotemporal scales. Zaleski et al. (Lagrée, Zaleski, and Bondino, 2016) focused on the sharp-interface method in porous media with a simplified Darcy-scale approach and simulations of Saffman-Taylor fingering by modeling multiphase flows. Thus, they measured the scaling properties of the fractal viscous fingering patterns that can be seen in the numerical simulations. The scaling properties are fractal or of Hausdorff dimension (DF), and variations of the area ( $A$ ) of the viscous fingering cluster are defined by the simple power law relation  $A \sim L^\alpha$ , where  $L$  is the length of its perimeter. This helps to indicate an increase in recovery of the high-viscosity fluid behind the fingering front, which is caused due to the reduction of the viscosity contrast.

In recent studies, it has been noticed that the addition of a low dose of nanoparticles to the base fluids can well influence the dynamics of fingering patterns due to a substantial increase of viscosity, and because of this potentiality, nanoparticles are used to control the viscosity driven instabilities (Madhavan et al., 2023). This phenomenon and its applications in recent times have been registered in the paper of Sabet et al. (Sabet, Hassanzadeh, and Abedi, 2017). The impact of nonreactive nanoparticle's presence on the stability and subsequent mixing of an originally unstable binary system is investigated through linear stability analysis (LSA) and pseudo spectral-based through direct numerical simulations (DNS). The investigated result shows that nanoparticles have the capability to lessen the instability of an originally unstable system.

Numerical investigation of controlling instabilities at the interface in non-standard Hele-Shaw cells like angled or tapered was reported by Morrow et al. in 2019 (Morrow, Moroney, and McCue, 2019) and also in the same year by D. Lu et al. (Lu, Municchi, and Christov, 2020). Their numerical simulations show how these non-standard Hele-Shaw configurations influence the morphological characteristics of the inviscid-viscous fluid interface.

Besides, D. Lu et al. (Lu, Municchi, and Christov, 2020) computationally analyzed interfacial dynamics in order to formulate a three-regime theory based on the critical capillary number ( $Ca_c$ ). To present a theoretical and numerical study on the stability or instability of the interface between two immiscible liquids, they have considered two types of cells; one is diverging cells with a positive depth gradient, and the other one is converging cells with a negative depth gradient. A modified linear stability analysis is employed to construct an expression for the growth rate of perturbations on the interface. Their 3-regime theory describes different growth rate situations of the interface stability or instability. In regime I, the growth rate is always negative, and thus, it shows a stable interface. In regime II, the growth rate remains zero (parallel cells) but changes from negative to positive (converging cells) or from positive to negative (diverging cells); the interface stability or instability possibly changes its type at some location in the cell. In regime III, the growth rate is always positive and hence causes an unstable interface. This study shows that the dynamic properties possibly change during the interface's propagation (Lu, Municchi, and Christov, 2020). In this paper, they used 3D simulations to verify the mathematical model (i.e., the theory part) for the growth rate of the interface.

## 1.2.2 Experimental results

The results of experiments involving the Saffman-Taylor instability (Hele-Shaw, 1898; Saffman and Taylor, 1958), known as viscous fingering, is a classical interfacial instability that arises in a Hele-Shaw cell (Sandnes et al., 2007) when a low viscosity fluid displaces a higher viscosity fluid (refer Figure-1.2(a)). A fingering phenomenon occurs due to the instability at the moving interface, and the little fingers gradually grow and compete with the more advanced fingers, repressing the less advanced fingers (refer Figure-1.2(b)). As a result, one can finally see a single finger propagating (refer Figure-1.2(c)) across the cell (Lindner and Wagner, 2009).

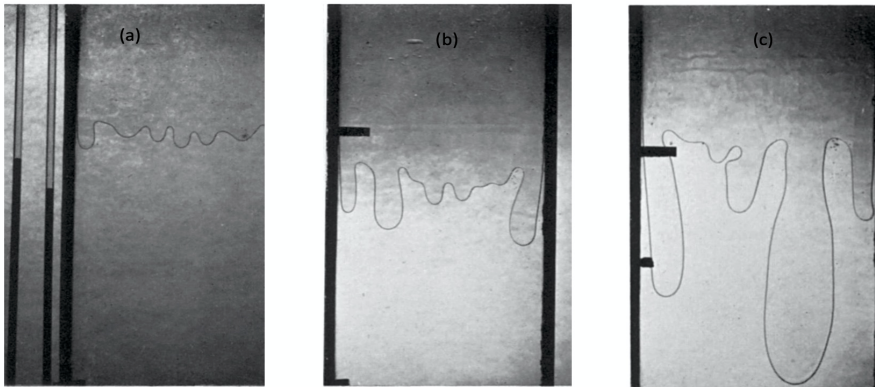


FIGURE 1.2: (a) Interface between air (less viscous fluid) and glycerine (more viscous fluid) at an early stage of the instability, (b) Development of instability (fingering patterns), (c) Inhibiting effect of a finger which gets ahead of its neighbor (beginning of a single propagating finger) (Saffman and Taylor, 1958)

A fundamental topic in fluid mechanics, the two-phase displacement flow in a constrained geometry has applications in biomechanics (biological fluid dynamics (Nelson et al., 2021), microfluidics (Mannan and Leiderman, 2020; Eastham et al., 2020), biofilms (Nooranidoost et al., 2023) and infectious diseases (Nooranidoost et al., 2023)), geophysics, and industrial. The primary dynamic parameter is the capillary number  $Ca = \mu U_{f_*}/T$ , which quantifies the ratio of viscous to surface tension forces when a viscous fluid (oil) is displaced by an inviscid one (air) and the geometry is small enough to ignore gravitational and inertial effects. Here,  $\mu$  is the oil viscosity,  $T$  is the interface's surface tension, and  $U_{f_*}$  is the advancing interface's velocity. The remaining characteristics that affect the behavior are all geometric in nature. The Hele-Shaw channel, based on the classic work of Saffman and Taylor (Saffman and Taylor, 1958), is the tube geometry that has gotten the most attention: an axially uniform tube with a rectangular cross-section of large aspect ratio  $\alpha = W_*/H_* \gg 1$ , where  $W_*$  is the width and  $H_*$  the height of the cross-section. In the absence of surface tension, Saffman and Taylor (1958) proposed a depth-averaged model of the system with symmetric and asymmetric (Saffman, 1959; Chuoke, Van Meurs, and Poel, 1959) families of solutions. A single modified capillary number  $1/B = 12\alpha^2 Ca$  is used in the depth-averaged system, which combines geometric and dynamic effects. Only a single symmetric family of solutions is ever found in experiments, and the fractional finger width  $\lambda = \frac{\lambda_*}{W_*}$ , where  $\lambda_*$  is the dimensional finger width, does indeed collapse onto a master curve when plotted as a function of  $1/B$ , provided  $1/B < 7000$  (Tabeling, Zocchi, and Libchaber, 1987).

For  $1/B > 7000$ , Tabeling et al. (Tabeling, Zocchi, and Libchaber, 1987) discovered aberrations from the symmetric finger shape with tip splitting. When the roughness was adjusted from 0.3% to 3% of the channel height, the instability occurred at lower  $1/B$ , implying that minor, uncontrollable geometric non-uniformities were the cause of the instability. Chevalier (Chevalier, Lindner, and Clément,

2007) demonstrated early destabilization owing to controlled interface perturbations, Lindner and Clément (Chevalier, Lindner, and Clément, 2007) studied fingering in a granular suspension in a viscous liquid, where the perturbation amplitude was proportional to the grain size.

An experimental study of dissolution-driven convection from first contact between  $KMnO_4$  (potassium permanganate) solute and water solvent through to 65% saturation in a Hele–Shaw cell for Rayleigh numbers  $Ra$  in the range  $100 < Ra < 1700$  has been presented by Slim et al. in 2013 (Slim et al., 2013). They described dynamical details and quantified global measures throughout the evolution. Their work is consistent with earlier experimental and numerical studies but also goes beyond them in providing details of the dynamics at both a local and global level in a single unifying, universal framework through the advection–diffusion scalings (based on the distance over which advection and diffusion balance) and they also showed that using a simple coarse-grained Howard-style phenomenological model, aspects of the behavior (such as flux decay) can be captured (Slim et al., 2013).

The bulk fingering instabilities in viscous liquids confined in Hele-Shaw cells, also known as the Saffman-Taylor instability, have been the subject of much experimental and theoretical (Hirata, 1998) effort. This instability translates into a fingering to fracture transition in the context of the liquid to solid transition (in gels (Park and Durian, 1994), foams (Lemaire et al., 1991), yield stress fluids (Coussot, 1999; Lindner, Coussot, and Bonn, 2000; Mora and Manna, 2010), and Maxwell liquids (Ghatak et al., 2000)) (Saintyves, Dauchot, and Bouchaud, 2013).

Instabilities revealed through spatiotemporal analysis are thought to be antecedents to topological transitions of fluid surfaces in Hele-Shaw flows, according to Goldstein (Goldstein, Pesci, and Shelley, 1993). The transition between the two classes of flows, namely absolutely unstable and convectively unstable flows, has been empirically demonstrated in a variety of Newtonian flow scenarios. In liquid jets, absolute instability was recently experimentally confirmed by Shoji (Shoji et al., 2020). There is also a large body of literature on Newtonian wakes and mixing layers, including the blunt body tests mentioned by Oertel (Oertel, 1990). Overall, these investigations discovered that limited boundaries and their existence have a destabilizing effect, as well as a transition to absolute instability in the near wake region.

In a horizontal Hele-Shaw cell, Haudin et al. (Haudin et al., 2014) investigated a buoyancy-driven instability that occurs when a viscous fluid is injected into a miscible, less viscous fluid. Even if the displacement is stable from a viscous standpoint, if the density difference between the two solutions and the gap of the cell is significant enough, a pattern consisting of very thin stripes aligned perpendicularly to the miscible interface arises. In a vertical cell, though, it vanishes. As a result, buoyancy plays a role in this phenomenon. They used a parametric experimental analysis of viscously stable miscible displacements in a horizontal Hele-Shaw cell with radial injection to investigate this buoyancy-driven instability and the striped pattern that goes along with it. They also define the impact of the flow rate and the thickness of the material. In a horizontal cell with radial injection, the pattern, which appears after a given onset time, consists of radial stripes. Further away from the injection point, splitting of the stripes is observed (Haudin et al., 2014).

Though the dynamics of a droplet confined between solid walls and pushed by a surrounding liquid is an old problem, Huerre et al. (Huerre et al., 2015) in their

letter, has developed recently an unexplored theory which is related to the study of the motion of droplets in a confined, micrometric geometry, by focusing on the lubrication film between a droplet and a wall. They noticed when capillary forces dominate, and the lubrication film thickness evolves nonlinearly with the capillary number due to the viscous dissipation between the meniscus and the wall. However, due to the thinness of this film (tens of nanometers), intermolecular forces come into play and affect classical scalings. They have resolved topographies of the shape of the interface experimentally, which yields new insights into droplet dynamics in microfluidics. They have also reported two dynamical regimes; one is for low capillary numbers, where the film thickness is constant and set by the disjoining pressure, while the second case is constituted of a capillary number above a critical value where the interface behavior is well-described by a viscous scenario. Their experiment also shows, at a high surfactant concentration, structural effects lead to the formation of patterns on the interface, which can be further used to trace the interface velocity, which yields direct confirmation of the boundary condition in the viscous regime (Huerre et al., 2015).

Apart from the aesthetics of the structures, the focus on this instability can be linked to its widespread applicability such as in porous media flows (Sandnes et al., 2011; Johnsen et al., 2006), flame propagation (Sato, Sakai, and Chiga, 1996), and bacterial colony formation (Ben-Jacob et al., 1994). The flow resistance decreases as a lower viscosity fluid replaces the more viscous fluid, causing instability; the inverse condition, when a highly viscous fluid is pushed into a cell filled with a weakly viscous fluid, is stable.

More recently, de Lózar et al. (Lozar and Hof, 2009), Pailha et al. (Pailha et al., 2012), and Hazel et al. (Hazel et al., 2013) examined two-phase flow via rectangular tubes, driven by the physiological difficulty of airway reopening with aspect ratio  $\alpha \gg 13$  that was partially occluded by axially uniform rectangular blocks occupying 50% and 33.3% of the tube height. Multiple stable modes of propagation were found in these geometries, including asymmetric modes, oscillatory modes, and the expected symmetric mode. These states are linked by a complicated bifurcation structure that is still unknown, owing to the fact that only stable modes could be found experimentally. Thompson, Juel, and Hazel (Franco-Gómez et al., 2016) modified McLean and Saffman's (McLean and Saffman, 1981) depth-averaged model to incorporate a specified depth profile and ran numerical simulations with a channel aspect ratio of  $\alpha = 10$  and relative obstacle width of  $\alpha_w = 0.25$ , but variable relative occlusion height  $\alpha_h$ . All experimentally observed states were anticipated by the model, according to the simulations. The bifurcation structure that resulted was qualitatively consistent with experimental data, but the nominal aspect ratio of  $\alpha = 10$  was thought to be too tiny for the model to give quantitative agreement. Despite this, Thompson et al. (Franco-Gómez et al., 2016) reduced the relative height of the occlusion from  $\alpha_h = 0.2$  to 0.01.

Morphological instability of a reactive fluid flowing in a soluble porous medium, which is also referred to as reaction-infiltration instability, is an important factor for many phenomena like weathering and diagenesis of rocks, melt extraction from the mantle, etc. Xu et al. (Xu et al., 2019), in their study, focused on experiments on dissolution finger growth in a radial geometry. They dissolved a plaster disk in a Hele-Shaw cell by withdrawing water from the center, thus creating the inward flow pattern,

and reported the reactive-infiltration instability and finger growth along the perimeter of the circular plaster sample that forms fracture walls with controlled injection rate and aperture. They also mentioned that the perimeter under consideration was sufficient to perform a statistical study of the reactive-infiltration instability and the dissolution of finger growth with time. Due to the strong competition between the growing fingers with the longest fingers, exponential growth can be seen in their experimental study, which is consistent with the theoretical and numerical predictions on the finger growth dynamics such as screening and selection between the fingers (Xu et al., 2019).

It is well known that Péclet number ( $Pe$ ), viscosity ratio ( $VR$ ), and Rayleigh number ( $Ra$ ) all these parameters are used to investigate instabilities due to injection rate, viscosity contrast, and gravitational field. It has been experimentally reported by Safari et al. (Hosseinalipoor et al., 2020) that as the Péclet number and viscosity ratio increase, more complex fingers can be seen, although sweep efficiency will be less. A new instability, known as Rayleigh–Taylor instability (Chandrasekhar, 2013) is encountered when the denser fluid, due to density contrast, moves into the lighter one in the presence of the gravitational field, and if the gravitational field is exerted by the rotating cell, this new instability will amplify the former fingers. These instabilities usually occur in environmental and technological processes such as filtration, hydrology, enhanced oil recovery, chromatography (Hosseinalipoor et al., 2020), etc.

Numerous studies (Paterson, 1981; Chen, 1989; Homsy, 1987) show viscous fingering (VF) with surfactants as capillary number increases, finger width decreases. But Nagtasu et al. (Tsuzuki et al., 2019), in their recent work, have shown that the nonlinear VF width in the surfactant system is independent of capillary numbers. An experimental investigation was performed (Suzuki et al., 2020b) on the effects of effective interfacial tension (EIT) on miscible VF by establishing two solution systems (both fluids are Newtonian) with different concentrations and the same viscosity contrast. A spinning drop tensiometer experiment is used to measure EIT for the glycerol–water system, which also demonstrates that the typical finger at high EIT is wider than that at low EIT (Suzuki et al., 2020b). This is an important study in establishing a well-controlled process for the understanding of viscous fingering dynamics in surfactant flooding, oil recovery, etc.

### 1.2.3 Analytical results

In recent times, pattern selection is a key issue that is related to the 2D Saffman–Taylor finger (Saffman and Taylor, 1958; McLean and Saffman, 1981). Saffman–Taylor dynamics control a variety of seemingly different physical phenomena, such as viscous fingering (Lindner and Wagner, 2009), directional solidification, or thermal plume (Zocchi, Tabeling, and Ben Amar, 1992). It is well known that the Saffman–Taylor finger results from the displacement of a viscous fluid by an immiscible, less viscous one in a Hele–Shaw cell. In this immiscible displacement problem, if the capillary number is sufficiently small, the interface in the gap consists of a nearly hemispherical meniscus, which completely spans the cell gap at the edges of the finger (Park and Homsy, 1985).



An increase in dimensionality affects the pattern selection rule (in 2D, significant work has already been done), which has attracted many to do further research. Lajeunesse et al. (Lajeunesse et al., 1997) studied the 3D instability of downward miscible displacement of one fluid by a less viscous one in a Hele-Shaw cell using the viscosity ratio and the flow velocity as control parameters. For sufficiently large flow velocity, mixing by diffusion is prevented in order to get a well-defined and sharp interface. If the value of control parameters is smaller than a critical value, the flow pattern will be 2D, and that leads to a tongue-shaped interface of the injected fluid spreading in the middle of the gap of the cell. However, above a threshold, in both the flow velocity and the viscosity ratio, a series of periodic 3D finger patterns can be developed (Lajeunesse et al., 1997).

The dynamics of a fluid bubble for a lifting plate in a Hele-Shaw cell (with time-dependent gap-width) have been studied by Shelly et al. (Shelley, Tian, and Wlodarski, 1997), which was identified through a basic version of Saffman-Taylor instability in a modified Darcy's law to account for the plate time dependence. Analytical conditions like existence, uniqueness, and regularity of solutions were established when the surface tension was zero as well as exact analytical solutions were constructed both with and without the presence of surface tension, which illustrate behaviors of the system such as cusp formation and bubble fission. The inclusion of surface tension gives some evidence of a topological singularity, although it is associated with the fission of a thin neck of fluid rather than with the collision of incipient cusps.

It is worth mentioning that pattern formation plays an important role in many hydrodynamics settings. The classical Saffman-Taylor problem is a widely studied example where a fluid-fluid interface evolves. Either a pressure gradient advancing the less viscous fluid against the more viscous one or gravity or a density difference between the fluids destabilizes the initially flat interface separating the two fluids. Due to the instability at the interface, first, it deforms, and different modes grow and compete dynamically, leading to undulated patterns. Though the first stage of interface instability is captured by linear stability analysis, however, after this initial linear behavior, the system evolves through a "weakly nonlinear" (Miranda and Widom, 1998) stage to a complex stage, which is characterized by the formation of fingers and bubbles where nonlinear effects dominate.

Casademunt (Casademunt and Magdaleno, 2000) has studied singular effects of surface tension in the dynamics of the finger competition in the Saffman-Taylor problem with channel geometry. First, they have done a detailed study of some relevant classes of exact solutions in the absence of surface tension and then compared them to finite surface tension. From there, they concluded that (nonsingular) zero-surface tension solutions are commonly nonphysical, and hence, they showed that the elementary two-finger competition process in the absence of surface tension is structurally unstable, and this fact is solely responsible for the lack of genuine finger competition. Second, they generalized solvability theory to study the selection of multi-finger configurations with finite surface tension, which gives a discrete set of nontrivial multi-finger solutions with stationary coexistence of distinct fingers and are selected by surface tension out of a continuum of solutions. While Casademunt (Casademunt and Magdaleno, 2000) has discussed the implications of dynamic solvability scenario in pattern selection, earlier Hong and Langer (Hong and Langer, 1986) linearized the integro-differential equation obtained by McLean and Saffman (McLean and

Saffman, 1981) around the family of solutions obtained for the zero-surface tension problem by considering the surface tension parameter as a singular perturbation to the problem in order to obtain an inhomogeneous integro-differential equation for finite surface tension and also constructed a necessary condition for the existence of solutions and computed it via WKB (Wentzel–Kramers–Brillouin) methods (Shraiman, 1986; Hong and Langer, 1986). Since solvability theory has proved to provide a very reasonable solution to the selection of the pattern in the isotropic problem with finite surface tension, later in their paper, they have extended such a theory to incorporate the effect of anisotropy (Hong and Langer, 1986).

Miranda et al. (Miranda and Widom, 1998) developed a mode-coupling theory to investigate the onset of non-linear effects in the viscous fingering problem in a rectangular Hele-Shaw cell, highlighting the link between interface asymmetry and viscosity contrast. Their analysis shows that symmetry breaking occurs through enhanced growth of sub-harmonic perturbations. Moreover, the absence of finger tip-splitting in the early flow stages was explained, and the onset of saturation effects, which moderates the exponential growth of the linear instability, was identified (Miranda and Widom, 1998).

A linear stability result was presented based on the three-dimensional Stokes equations for chemically reacting, propagating fronts giving rise to an unstable density stratification in a Hele-Shaw cell by Demuth et al. (Demuth and Meiburg, 2003). A growing discrepancy can be seen between linear stability results based on Darcy's and Stokes equations, respectively, as the Rayleigh number increased, and that motivated the authors to revisit the experiments in the paper of M. Böckmann and S.C. Müller (Böckmann and Müller, 2000), as well as with a corresponding linear stability analysis based on the Darcy equations that was performed in A. De Wit's paper in 2001 (De Wit, 2001). The results were in good agreement with the experiment for the relatively low value of Rayleigh number,  $Ra = 79$ , that shows Poiseuille-type flow behavior, and hence the Darcy equation is largely applicable (Demuth and Meiburg, 2003).

Ben Amar et al. (Amar and Bonn, 2005) studied the fingering instabilities that occur in the debonding of model adhesives and performed a linear analysis of the instability in the lifting Hele-Shaw cell that is relevant for the failure of soft adhesives. Though the analysis is done for a Newtonian fluid, it can be extended to shear-thinning fluids (non-Newtonian fluid). Significant differences are found between the linear theory and the experimental results when compared to the experiment, and hence, they discussed three-dimensional effects that improve the agreement; nevertheless, significant differences between theory and experiment still remain (Amar and Bonn, 2005). On the other hand, Goyal et al. (Goyal and Meiburg, 2006) were particularly interested in similarities and discrepancies between Stokes and Darcy results for the viscous fingering instability in the systematic linear stability analysis of miscible displacements in Hele-Shaw cells, based on the three-dimensional Stokes equations.

Earlier experiments and theory indicate that inertia has a significant influence on the system's behavior (Chevalier et al., 2006). In recent studies, Dias et al. (Dias and Miranda, 2011) employed a perturbative-mode-coupling method to examine how the stability and morphology of the viscosity-driven fingering patterns are affected by inertia in both rectangular and radial Hele-Shaw flow geometries. In the rectangular configuration, they have found that inertia has a stabilizing role at the linear stage and tends to widen the fingers at the weakly nonlinear regime. Whereas in radial

flow geometry, inertially induced, enhanced finger-tip splitting events at the onset of nonlinearities can be captured. Linder et al. (Nase, Derks, and Lindner, 2011) studied the dynamic evolution of fingering pattern formation in a Newtonian liquid during the lifting of a circular Hele–Shaw cell. They showed that the number of growing fingers depends only on the dimensionless surface tension and can be described by linear stability analysis. On the other hand, the finger amplitude and, consequently, the total number of fingers (growing and stagnant fingers) also depend on the cell confinement, though the finger amplitude has a distinct influence on the debonding force.

Housseiny et al. (Al-Housseiny and Stone, 2013) have considered two tapered Hele-Shaw geometries (rectilinear and radial), which have a constant depth gradient in the flow direction that show the presence of a depth gradient alters the stability of the interface that controls and tunes fingering instabilities. This implies the stability of the interface can be determined by both the viscosity contrast of the fluids and the ratio of the depth gradient to the capillary number of the system. A new prediction of wavelength selection in radial viscous fingering involving normal and tangential stresses was considered by Nagel et al. (Nagel and Gallaire, 2013) in a Hele-Shaw cell. They have used the so-called Brinkman equation to describe the flow field, which takes into account viscous stresses in the plane of the confining plates, in order to show that the in-plane stresses cannot always be neglected and that appeared naturally in the potential flow problem. The dispersion relation obtained with the Brinkman equation (Ho, Leiderman, and Olson, 2019; Nguyen, Olson, and Leiderman, 2019) complies with the experimental results in contrast to the classical linear stability analysis of radial fingering that uses Darcy’s law as a model for the fluid motion in Hele-Shaw cells (Nagel and Gallaire, 2013).

In contrast to previous investigations (Wooding, 1969; Goyal and Meiburg, 2006), Talon et al. (Talon, Goyal, and Meiburg, 2013) have been focused on analyzing the linear stability of variable density and viscosity, miscible displacements in a horizontal Hele-Shaw cell, where the influence of gravity on the base state and its linear stability is quite distinct from vertical cell (Talon, Goyal, and Meiburg, 2013). Beeson-jones (Beeson-Jones and Woods, 2015) examined the stability of a system with two radially spreading fronts in a Hele-Shaw cell in which the viscosity increases monotonically spreading in an annulus (that is, from the innermost to the outermost fluid) in order to discuss the application of this approach to a problem of injection of treatment fluid in an oil well (Beeson-Jones and Woods, 2015).

## 1.3 Non-Newtonian Saffman-Taylor instability

In this section, the focus will be on non-Newtonian flow instabilities and the various approaches used in understanding the instability in non-Newtonian fluids, like DNS, experiments, and stability analysis.

### 1.3.1 Computational results

In an earlier result of L. Kondic et al. (Kondic, Palffy-Muhoray, and Shelley, 1980), they used the generalized Darcy’s law to perform fully nonlinear simulations of a bubble expanding into a strongly shear-thinning liquid. Their simulations demonstrate

that shear-thinning significantly modifies the evolution of the interface, which has a dendritic appearance resembling those occurring in quasistatic solidification as tip splitting of fingers is suppressed. These results are consistent with experimental results. Moreover, the length scales under consideration from linear stability analysis are consistent with simulation results. Furthermore, they also give a morphological phase diagram in terms of flow and fluid parameters. In particular, they concluded from their simulations that the typical length-scale ( $l$ ) of the patterns scales with driving pressure ( $P_0$ ) as  $l \sim P_0^{-1/2}$  (Fast et al., 2001). In their analysis, they used the Johnson–Segalman – Oldroyd (JSO model) for a viscoelastic fluid that considerably simplifies the thin-gap limit  $\varepsilon = b/L \ll 1$ , where  $b$  is the gap between the plates, and  $L$  is the typical lateral dimension. In the  $\varepsilon$  leading order terms, they have found that the natural Weissenberg number of the flow is of  $O(1)$  in order to retain the shear-thinning property of the fluid. However, in this limit, elastic effects enter only through the definition of a Weissenberg number as the viscoelastic fluid is reduced to a generalized Newtonian fluid (Fast et al., 2001).

Singh et al. (Singh and Azaiez, 2001) have mentioned three types of instability mechanisms for Newtonian flow displacements that occurred at the fluid-fluid interface. These are shielding, coalescence, and fading. In addition to the patterns already known for purely Newtonian flow displacements, the authors introduced new mechanisms that are reported in the case of non-Newtonian flows. These new mechanisms are termed diagonal-fingering, side-branching, trailing-lobe detachment, and double-coalescence (Singh and Azaiez, 2001). It has become evident from their study that the presence of a non-Newtonian fluid in the flow leads to finger patterns, just like the case for Newtonian flow displacements, but that are richer and more complex than the usual Newtonian flow displacements. They (Singh and Azaiez, 2001) have used nonlinear pseudo-spectral numerical simulations based on the Hattley transform to examine the viscous fingering instability in miscible displacements involving shear-thinning fluids. A rectilinear Hele-Shaw cell has been used to study the instability, and the Carreau equation has been used to model the shear-thinning character of the fluids. Some of these new mechanisms that they have introduced here have also been reported in earlier studies in terms of the velocity-dependent mobility of the flow (Singh and Azaiez, 2001).

R.J.S. Booth (Booth, 2010) has observed that: “there is a close link between the growth rate of the mixing zone and a shape selection problem for Saffman-Taylor fingers”, and the author has noted this investigation in the paper (Booth, 2010) in 2010. It was long before observed that the most important property of viscous fingering instability is that the smallest wavelength disturbances generally grow fastest, whereas mechanisms such as diffusion or a diffused initial condition typically lead to the existence of a cut-off or least stable wavelength, leading to the expectation that small wavelength fingers will form. This suggests an ill-posed problem, as well as the Musket problem (Siegel, Caffisch, and Howison, 2004) with contrasting viscosity, which has been shown to develop singularities in the curvature of the interface between the two fluids.

A miscible displacement between the two fluids with molecular diffusion and a smoothly varying viscosity can be modeled by the well-posed equations:

$$\nabla \cdot u = 0 \tag{1.1}$$

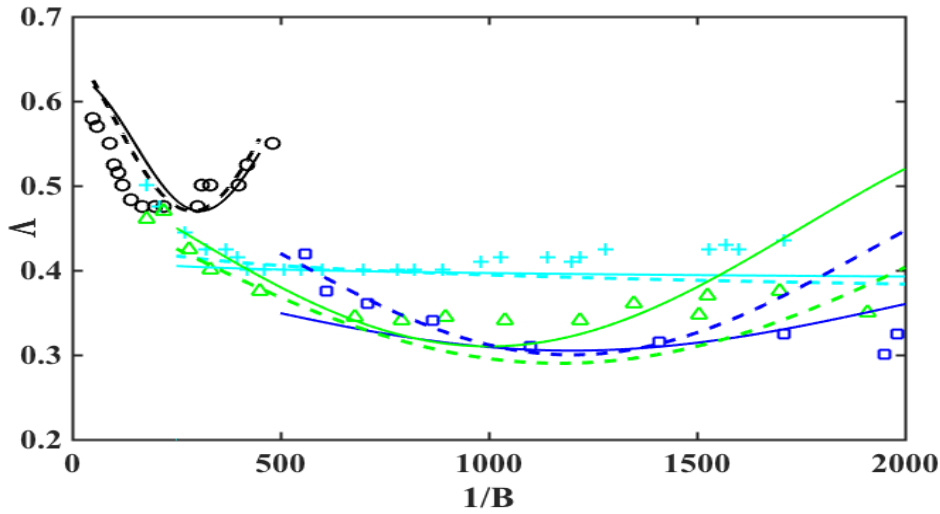


FIGURE 1.3: Numerical simulation of miscible viscous fingering (defined in equations (1.1)-(1.3)), with a constant flux of solvent (on left of image) into oil, and  $M$  (mobility ratio) = 5,  $Pe$  (Péclet number) = 3000. (Booth, 2010)

$$u = \frac{-k}{\mu(c)} \nabla p \quad (1.2)$$

$$\phi \frac{\partial c}{\partial t} + \nabla \cdot (uc) = D \nabla^2 c; \quad (1.3)$$

where  $u$  : total flux of the fluid per unit area,  $k$  : permeability of the medium,  $c$  : volume fraction of solvent,  $p$  : pressure,  $D$  : diffusion coefficient  $\mu(c)$  : viscosity of a homogeneous mixture of oil and solvent with a volume fraction  $c$  of solvent, which is taken (Koval, 1963) as equation (1.4)

$$\mu(c) = (\mu_s^{-1/4} c + \mu_0^{-1/4} (1 - c))^{-4} \quad (1.4)$$

$\mu_s, \mu_0$  are the viscosities of pure solvent and pure oil, respectively. For large Peclet number ( $Pe = UL/D \gg 1$ ), the Koval model supports numerical simulations of equation (1.1) to (1.3) (refer Figure-1.3). One of the most important features of this model is that, as a hyperbolic equation, it can predict the finite speed at which the mixing zone can encroach into the oil.

The important relationship between miscible viscous and density fingering is described by Wooding in 1969 (Wooding, 1969). When the viscosity ratio between the two fluids is close to 1, it is possible to show that, with a rescaling of diffusion, the two problems are equivalent (Manickam and Homsy, 1995). Furthermore, the growth rate of the mixing zone, as suggested by Koval for viscous fingering, agrees with the observations of Wooding (Wooding, 1969) of miscible density fingering in the Hele-Shaw cell. This agreement further provides support for the validation of the Koval model over a wide range of values of  $M$  (= mobility ratio =  $\mu_0/\mu_s$ ) (Booth, 2010). However, the model fails for the mean finger width, which does not vary over time.

The viscous fingering instability of miscible displacement involving a viscoelastic fluid is explored for the first time in the paper of Shokri et al. (Shokri, Kayhani, and

Norouzi, 2017) using both linear stability analysis and computational fluid dynamics. The constitutive equation of a viscoelastic fluid is the Oldroyd-B model. One of the displacing fluids or the displaced fluid is presumed to be viscoelastic in this case. The quasi-steady state approximation and the six-order shooting approach are used in linear stability analysis to anticipate the increasing rate of the disturbance in the flow. When the elasticity (Weissenberg number) of the displaced or displacing viscoelastic fluid is raised, the flow becomes more stable. The effect of the viscoelastic fluid on this instability was investigated in a nonlinear simulation utilizing the spectral method based on Hartley transforms and the fourth-order Adams-Bashforth technique. The elasticity has a substantial effect on the fingering instability, and the flow becomes more stable by raising the Weissenberg number, as measured by concentration contours, mixing length, sweep efficiency, and transversely average concentration (Shokri, Kayhani, and Norouzi, 2017).

### 1.3.2 Experimental results

Emphasizing the experimental approach to understanding instability in non-Newtonian fluids, viscous fingering, because of its unique features, has received considerable study. Nittmann et al. (Nittmann, Daccord, and Stanley, 1985) seminal work demonstrates that viscous fingering patterns created in non-Newtonian fluids differ significantly from those formed in Newtonian fluids. Fracture-like patterns have been discovered in clay slurries, colloidal fluids, and polymer solutions, for example (Nittmann, Daccord, and Stanley, 1985; Zhao and Maher, 1993). Due to non-Newtonian features such as shear thinning or thickening, viscoelasticity, yield stress, and so on, the physical genesis of the extremely varied structures is yet unknown.

Two types of phenomena can occur in the case of non-Newtonian fluids. These are as follows:

- Finger narrowing in shear-thinning fluids:

When performing experiments in a dilute solution of Xanthane, a strong modification of the selection process can be observed. Fingers are substantially narrower at high velocity than the traditional limit of  $\Lambda = 0.5$ . Qualitative behavior shows that the shear-thinning fluid is pushed by the finger in the Hele-Shaw cell. However, numerical simulations show that viscosity is not uniform throughout the cell; regions of high fluid velocity and, thus, high shear rate have a low viscosity. This is essentially the case in front of the (Fast et al., 2001) fingertip, and for that, the system becomes anisotropic, leading to finger narrowing.

For weak shear thinning ( $1 > n > 0.65$ ) (Lindner, Coussot, and Bonn, 2000; Lindner et al., 2002), they have shown (Lindner and Wagner, 2009) that by simply replacing the constant viscosity  $\eta$  in the control parameter  $1/B$  by a shear-dependent viscosity  $\eta(\dot{\gamma})$  allows rescaling the data onto the universal curve for Newtonian fluids, where, the shear rate  $\dot{\gamma}$  is the average shear rate in the cell. On the other hand, for strong shear-thinning ( $n < 0.65$ ), this rescaling fails, and deviations from the classical result toward smaller fingers are observed (refer Figure-1.4). Narrower fingers have also been documented by Rabaud et al. (Rabaud, Couder, and Gerard, 1988a).

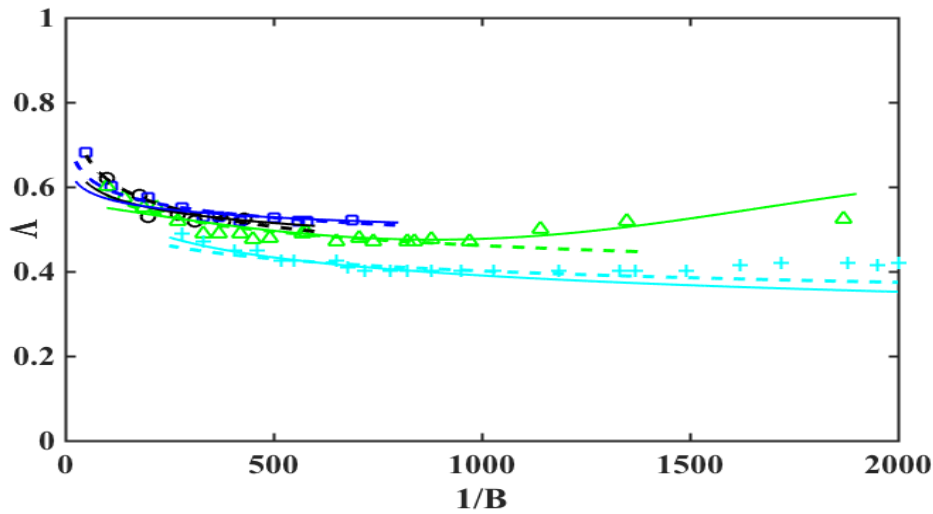


FIGURE 1.4: Shear-Thinning: Narrower fingers differs from the classical limit of  $\Lambda = 0.5$  (Lindner and Wagner, 2009)

Using a Hele-Shaw cell with engraved glass plates, they discovered viscous fingers with  $\Lambda$  substantially less than 0.5 for Newtonian fluids. The observation of such "anomalous" fingertips is explained by the engravings indicating a local perturbation at the fingertip. The traditional selection of the discrete set of solutions is disrupted by this disturbance. At high velocity, the continuum of solutions given by Saffman and Taylor's analytical result without surface tension becomes accessible; and can take values smaller than 0.5. Rabaud et al. (Rabaud, Couder, and Gerard, 1988a) demonstrated that for a given value of  $Ca$ , the shape predicted by Saffman and Taylor (Saffman and Taylor, 1958) is not the shape. A similar mechanism is responsible for the selection of the viscous finger in a shear-thinning fluid. When the shear-thinning character of the fluid is strong enough, anisotropy plays the role of the perturbation at the fingertip. The relation between  $\frac{\rho}{b}$  i.e. the dimensionless radius of curvature and  $\Lambda$  is dependent on the shear thinning character of the fluid and thus the shear thinning exponent  $n$ . So, knowledge of the relationship between  $\frac{\rho}{b}$  and  $\Lambda$  solves the selection problem, and hence one can now predict the finger width  $\Lambda$  from the rheological data. As a result of the presence of shear thinning, a whole other selection mechanism emerges, one that is more similar to what is seen in finger width, for example, and which may begin to play a role in this low viscosity fluid. The dimensionless radius of curvature at the tip  $\frac{\rho}{b}$  can be related to the finger width via the relation  $\rho = \frac{\Lambda^2 w}{\pi(1-\Lambda)}$ , which arises from finger dendritic growth and necessitates anisotropy in the system.

Corvera Poiré et al. (Corvera Poiré and Ben Amar, 1998) solved the problem for a power law fluid directly, and their results are in good accord with the experimental facts. At high velocities, the case may be that there is a saturation of the finger widths, resulting in a widening of the finger widths. This may be explained by inertial effects, which have been found to increase finger width (Chevalier et al., 2006) and may begin to play a role in this low-viscosity fluid.

- Finger widening due to Normal stresses :

In experiments, a completely different behavior is found using solutions of the flexible polymer PEO. Unlike with shear-thinning fluids, where finger narrowing occurs, in this situation (by comparing it to the Newtonian case), finger widening can be observed. Study shows the presence of normal stresses in the thin wetting layer might be responsible for the finger widening; one can attempt to account for this effect by adding a supplementary pressure to the system. In traditional theory, the radius of curvature determines the pressure jump at the interface between two liquids. Tabeling et al. (Tabeling and Libchaber, 1986) demonstrated that by correcting the surface tension in the control parameter, one can account for the influence of the wetting film's limited thickness. Using the same logic, the extra pressure caused by normal stress can be added to the surface tension term  $T^* = T + \frac{1}{2}N_1(\dot{\gamma})b$  in the control parameter. This enables the data to be rescaled into a single universal curve, which addresses the selection concerns for minor normal stresses yet again. For shear thickening, the viscosity in Darcy's law is unique, but the BVP can change from elliptical to hyperbolic (Kondic, Palfy-Muhoray, and Shelley, 1996; Fast et al., 2001).

Experiments have been conducted in recent years to untangle the influence of several non-Newtonian flow features on instability by using fluids with only one non-Newtonian property while other non-Newtonian effects have been ignored (Nagatsu et al., 2010). The relationship between viscous fingering and chemical reaction has recently been examined (Shukla and De Wit, 2020), with De Wit and Homsy (De Wit and Homsy, 1999b; De Wit and Homsy, 1999a) being the first to conceptually study the alterations of the fingering pattern caused by changes in the fluid's viscosity in the miscible system. Nagatsu et al. (Nagatsu et al., 2010) conducted studies on miscible viscous fingering, which involved changes in the viscosity of the displaced less-viscous liquid as a result of rapid interactions. They employed the dependence of viscosity of the PAA solution or the SPA solution on pH, as well as Nagatsu et al. (Nagatsu et al., 2010) studied to investigate the impact of changes in the viscosity of the displaced more-viscous liquid by instantaneous reactions on the fingering pattern. The PAA solution or the SPA solution was utilized as the less viscous liquid in this experiment. It was discovered that the shielding effect is decreased, and the fingers are broadened when the viscosity is increased. As a result of the response, the fingering pattern becomes denser. When the viscosity is reduced, however, the shielding effect is intensified, the fingers thin, and the fingering pattern becomes less dense as a result of the reaction. This research demonstrates that the effects of changes in viscosity caused by instantaneous reactions are unaffected by whether the changes occur in the displaced more viscous fluid or the displaced less viscous liquid.

The effects of reactant concentration in a more viscous liquid and bulk finger-advancement velocity on the current systems have also been studied (Nagatsu et al., 2010). In the system with increased viscosity, an increase in the reactant concentration  $c$  has a greater effect on the change in the fingering pattern as  $c_{m0,NaOH}$  increases up to a threshold value, but the effect on the change in the fingering pattern decreases as  $c_{m0,NaOH}$  increases above that threshold value. An increase in the reactant concentration  $c_{m0,HCl}$  causes a monotonic increase in the effect on the change in the fingering pattern, which is required in a system where the viscosity is reduced. They came to the conclusion that these tendencies are compatible with the correlations between



the polymer solution's shear viscosity and pH. In the current work, the change in the fingering pattern due to the reaction may be noticed under the experimental condition of bulk finger-advancement velocity, indicated by the Péclet number,  $Pe$ . All of the above findings are comparable to those of Nagatsu et al. (Nagatsu et al., 2010).

During the peeling of a thin layer of elastomer of a stiff substrate (Ghatak, 2006; Shull et al., 1998) or in probe-tak studies (Saintyves, Dauchot, and Bouchaud, 2013), where a semispherical probe in contact with the soft solid is dragged up at a constant speed, an elastic fingering instability has been reported. The crack line is observed to progress in most cases, and the instability settles on it. Saintyves et al. (Saintyves, Dauchot, and Bouchaud, 2013) demonstrated experimentally the existence of a purely elastic, nonviscous fingering instability that appears when air penetrates into an elastomer confined in a Hele-Shaw cell. As soon as a critical strain (independent of the elastic modulus) is exceeded, fingers appear and grow sequentially and propagate within the bulk of the material.

Ecke and Backhaus (Ecke and Backhaus, 2016) studied the mass-transport in multi-species porous media through molecular diffusion and plume dynamics. They studied a water and propylene-glycol system enclosed in a Hele-Shaw cell with variable permeability that represents a laboratory analog of the general properties of porous media convection. They observed a rapid decrease (and an approach to a constant steady value) of the critical wavenumber representing the plume pattern and validated their results for the plume velocities via the microscopic merger and the renucleation of the advancing interface. Through their study, one can find that the plume dynamics are closely related to the mass transport rate (Ecke and Backhaus, 2016).

Juel et al. (Franco-Gómez et al., 2016) in their paper, re-examine the channel geometry previously introduced by de Lózar et al. (Lozar and Hof, 2009) to probe the sensitivity of viscous fingering to a step change in channel depth as a function of channel aspect ratio  $\alpha$  by investigating the effects of centered, rectangular occlusions in Hele-Shaw channels. For large occlusions, when air displaces a more viscous fluid from within the channel, the geometry supports symmetric, asymmetric, and oscillatory propagation states. They have demonstrated that the depth-averaged model is in quantitative agreement with laboratory experimental results for  $\alpha \geq 40$ , provided that  $Ca \leq 0.012$ . They have shown that in the absence of the occlusion (the classical Saffman-Taylor viscous fingering problem (Saffman and Taylor, 1958; Saffman, 1959)), the multiplicity of solutions at finite occlusion heights arises through interactions of the single stable and multiple unstable solutions already present. They have also found that the height of occlusion required to observe bifurcations to asymmetric and oscillatory modes of propagation within the experimental range of  $Ca$  decreases with increasing aspect ratio. Hence, the system becomes more sensitive as the aspect ratio increases in the sense that multiple solutions are provoked for smaller relative depth changes. They estimated that the required depth changes have the same order as the typical roughnesses of the experimental system ( $1\mu m$ ) for aspect ratios  $\alpha > 155$ , which they conjectured that the sensitivity of Saffman-Taylor flow in large aspect ratio is an inevitable consequence of the roughness-induced stabilization of unstable solution branches in such Hele-Shaw channels (Franco-Gómez et al., 2016).

In contrast to classical Saffman-Taylor instability, it is revisited by Bihi et al. in 2016 (Bihi et al., 2016) for the inverse case of a viscous fluid displacing air when

partially wettable hydrophilic particles are present on the walls. Though the inverse situation is stable and it has been previously reported in the literature by Chan et al. (Chan and Liang, 1997) and then by Fernandez et al. (Fernandez, Krechetnikov, and Homsy, 2005), the authors showed that fingering instability still can be seen due to the presence of the particles at low capillary number ( $Ca$ ). They investigated that the destabilization of the interface (or the capillarity-driven instability) occurs due to interfacial energy minimization, provided all particles intersected by the meniscus are collected. In order to quantify this phenomenon, they have considered both axisymmetric and rectangular geometries.

Draga Pihler-Puzović et al. (Pihler-Puzović et al., 2018) have studied the viscous-fingering instability in a radial Hele-Shaw cell in which the top boundary has been replaced by a thin elastic sheet. In contrast to the previous study (Pihler-Puzović et al., 2012) where highly branched patterns were observed in rigid-walled cells, the presence of wall elasticity caused a delay in the onset of the fingering instability to much larger values of the injection flow rate, and hence, when the instability develops, the fingers that form on the expanding air-liquid interface are short and thick. From this experimental study, one can identify the various physical mechanisms causing the weakening of viscous fingering due to the presence of wall elasticity (Pihler-Puzović et al., 2018).

In order to examine the transition from the primary to the secondary acoustic instability, Lopez et al. (Veiga-López et al., 2019) experimentally studied the propagation of laminar premixed methane-air, propane-air, and DME (dimethyl ether) air flames inside a Hele-Shaw cell. Their experimental results revealed two distinct propagation regimes depending on the equivalence ratio of the mixture as a consequence of the coupling between the heat-release rate and the acoustic waves. Moreover, in the same year, Lee et al. (Hooshanginejad, Druecke, and Lee, 2019), has discussed the stabilizing mechanism through experiments and performed a linear stability analysis of the radial (time-dependent) suspension flow in a Hele-shaw cell of a non-colloidal particle (polyethylene) band on the fluid-fluid interface. Their main result models the coupling between the unstable miscible interface and the inherently stable immiscible interface, which produces a finite wavenumber of the particle band breaking (Hooshanginejad, Druecke, and Lee, 2019).

Petrolo et al. (Petrolo et al., 2020) have performed a set of experiments in a Hele-Shaw cell (a two-dimensional porous medium) saturated with a heated, non-Newtonian fluid, which is under a uniform horizontal pressure gradient. Their experimental results allow us to study flow patterns as functions of the Rayleigh number.

Discrepancies between theory and experiments (more relevant for the critical Rayleigh number) were accredited to a combination of factors such as the nonlinear phenomena, possible subcritical bifurcations, approximations in the rheological model, wall slip, aging, and degradation of the fluid properties. For partially miscible system, Suzuki et al. (Suzuki et al., 2020b; Suzuki et al., 2020a) experimentally discovered a new topological transition of VF instability that obtains a secondary instability such as multiple moving-droplets formation and is driven by thermodynamic instability like phase separation due to spinodal decomposition and Korteweg convection induced by compositional gradient during such phase separation by performing an experiment in a Hele-Shaw cell. Experimental results of coupling between hydrodynamics and chemical thermodynamics are in good agreement with the theoretical

findings.

Spatiotemporal analyses in viscoelastic flows are more recent and limited. An early experimental work of Vihinen (Vihinen, Honohan, and Lin, 1997) revealed absolute instability in viscoelastic liquid jets. Pipe (Pipe, 2005) found a stabilizing impact of polymer addition in his studies, which is offset by shear thinning and a transition from convective to absolute instability at greater polymer concentrations on viscoelastic cylindrical wakes. In contrast, a significant range of parameters where viscoelasticity was shown to be destabilizing (Bansal, Chauhan, and Sircar, 2022) was relayed by the linear analysis of dilute mixing layers (Ray and Zaki, 2014) and dilute jets (Ray and Zaki, 2015; Alhushaybar and Uddin, 2019; Alhushaybar and Uddin, 2020).

Contrary to the Saffman-Taylor instability for Newtonian fluid, a study on the impact of surfactant addition in a non-Newtonian fingering instability shows (due to surface tension anisotropy along the finger surface) that the surfactant concentration locally decreased the interfacial tension, leading to a reduction in viscosity, and an increased impact on the capillary number which led to the evolution of wider fingers (Ahmadikhamsi et al., 2020). However, the relative finger width of both non-Newtonian experiments with and without the surfactant converged asymptotically to the same value, caused by the decrease in surfactant concentration in the vicinity of the tip so that only the shear-thinning feature of polymer prevails at long times.

### 1.3.3 Analytical results

Bonn et al. and others (Hong and Langer, 1986; Bonn et al., 1995; Kondic, Palffy-Muhoray, and Shelley, 1996) had studied the Saffman Taylor instability of a non-Newtonian fluid in a Hele-Shaw cell. In this case, the viscosity is dependent on shear rate, and hence, a modified Darcy's law is used whose viscosity depends upon the square pressure gradient, which yields a natural non-linear boundary value for the pressure. They (Bonn et al., 1995) have also computed the exact non-Newtonian pressure for the circular expanding bubble in order to find

$$\nabla^2 p = \frac{-24\dot{R}\mu_0}{b^2 R D^2 (1 + (r/DR)^2)^2} (1 - \beta); \quad D = \frac{\tau \dot{R}}{b} \quad (1.5)$$

If  $\beta = 1$  (constant viscosity),  $\nabla^2 p = 0$ , this implies the pressure is harmonic. For shear-thinning fluids  $\beta \ll 1$ . For a circular bubble, if  $\nabla^2 p = 0$ , then that gives a relative error in the interface velocity (in a channel geometry, this error is negligible).

If  $We$  (Weissenberg number) number is small, a generalized Darcy's law can be obtained, governing the bulk fluid flow,

$$u = -\frac{\nabla_2 p}{\bar{\mu}} (We^2 |\nabla_2 p|^2); \quad \nabla \cdot u = 0 \quad (1.6)$$

where,  $u$  is the gap averaged longitudinal velocity,  $p$  = pressure of the fluid,  $We$ : Weissenberg number,  $\bar{\mu}$ : derived effective viscosity depending upon  $|\nabla_2 p|^2$ .

Equation (1.6) yields a non-linear, elliptic boundary value problem for the pressure in the driven fluid (Jha and Kadalbajoo, 2021). For a small  $We$  number, the non-linear BVP for the pressure can be simplified to a linear one, and hence, it can be solved exactly using linear stability analysis (Fast et al., 2001).

In the theoretical investigation of H. Pascal (Pascal, 1988), the approximate analytical solutions for the description of conditions required for the stability of non-Newtonian fluid interfaces in a porous medium have been studied, where the displacing and displaced fluids have been considered to be of power law behavior. Through this analysis, relevant results for an adequate understanding of the rheological effects of non-Newtonian behavior in oil displacement mechanisms have been obtained, where knowledge of possible performance in mobility control in enhanced oil recovery floods with non-Newtonian displacing fluids is required. The author has also mentioned in his paper that, in the absence of gravity, the oil displacement mechanism has led to the existence of a critical interface velocity for a linear flow geometry, for which the interface stability may be maintained, provided that fluids are of pseudo-plastic type (Pascal, 1988).

S. Mora et al. (Mora and Manna, 2010) have studied theoretically and experimentally the linear stability of an air front pushing on a viscoelastic upper convected Maxwell fluid inside a Hele-Shaw cell using a unique time-dependent control parameter  $\tilde{\lambda}$  (controls the elastic effects). In their theory, they have successfully described the transition between viscous to elastic instability.

The effect of shear-thinning on the onset condition of viscous fingering has been analyzed using the linear stability by M.C. Kim et al. (Kim and Choi, 2011). The shear-dependent viscosity of the fluid is described using the Carreau model. In the similar domain (Ben, Demekhin, and Chang, 2002; Pritchard, 2009), the new stability equations have been derived and solved analytically and hence compared the results numerically with and without the quasi-steady state approximation. Without the quasi-steady state approximation, it has been shown that initially, the present system is unconditionally stable, in contrast to the previous results where the system is initially unstable. With the quasi-steady state approximation, it has been shown that the flow where displacing fluid is a shear-thinning is always more unstable than the Newtonian counterpart, but the system is reversed for the case of a Newtonian fluid displacing a Newtonian one, the shear-thinning effect, in general, makes the system stable (Kim and Choi, 2011).

J. Avendano et al. (Avendano et al., 2013) has done an enhanced displacement of a liquid (Newtonian) pushed by different types of liquids, such as Newtonian, shear-thinning, viscoelastic fluids, that has slightly higher apparent viscosity. Their theoretical approach has confirmed that, when viscoelastic effects were absent, the interface between the two fluids becomes sharper at larger velocities, and hence, the thickness of the lateral film left behind increases with the flow rate and, on the contrary, in the case of viscoelastic fluid, the shape of the interface is velocity independent and hence the thickness of the lateral film is approximately constant. Furthermore, when the ratio of normal to tangential stresses increases, that is, normal stress differences increase, this thickness decreases (Avendano et al., 2013).

Analogous to the results of J. Avendano et al. (Avendano et al., 2013), Shokri et al. (Shokri, Kayhani, and Norouzi, 2017) in their paper have considered the viscous fingering instability of miscible displacement involving a viscoelastic fluid that has been investigated using both linear stability analysis and numerical approach. Here, they have assumed that one of the displacing fluids or the displaced one is viscoelastic. In linear stability analysis, it is shown that the flow is more stabilized when the elasticity (Weissenberg number) of the displaced or displacing viscoelastic fluid is

increased.

O. A. Fadoul et al. (Fadoul and Coussot, 2019) have compared the theoretical and experimental results of the Saffman-Taylor instability for yield stress fluids. Although the validity of this hypothesis has only been partially tested thus far, it is predicted from the theoretical analysis of this instability that fingering with a finite wavelength will occur at vanishing velocity, and that material will be deposited behind the front advance. Here, after reviewing the fundamental findings in that area, they have suggested a novel set of traction-based experiments to evaluate this fundamental theory's capacity for data prediction. They have conducted tests using various beginning material yield stresses, distances, and volumes. Additionally, a master curve is produced when plotting the finger number as a function of the yield stress times the sample volume divided by the square starting thickness over a wide range of these parameters, which is consistent with the theoretical prediction for the finger size. This, in particular, demonstrates that the material yield stress might be estimated using the traction test (Fadoul and Coussot, 2019).

## 1.4 Industrial applications of Saffman-Taylor flows

Hele-Shaw flow displacements in a porous material (Kambhammettu, Deshpande, and Chebolu, 2021) represent an important topic of research from both fundamental and practical points of view. Such flows are encountered in a wide variety of industrial applications, such as secondary and tertiary oil alteration, hydrology, fixed bed regeneration, chemical coating, electrodeposition, flooding, mixing of fluids, etc. Here, a few industrial applications are described point-wise :

- In recent times, a process called miscible flooding is frequently employed in the petroleum industry, in which a miscible solvent injected into oil-bearing rock formations displaces the oil towards the production well (Upchurch and Meiburg, 2008). Moreover, this flooding procedure can be used in the configuration of a vertically oriented gap for advanced oil production techniques via hydraulically induced fractures that can be extended several hundred feet away from the wellborn.
- In geological systems, dissolution plays an important role in the weathering and diagenesis of chemical erosion of salt deposits (Bekri, Thovert, and Adler, 1995; Steefel and Lasaga, 1994), Earth's rocks (Iyer et al., 2008; Ortoleva et al., 1987), and melt extraction from the mantle (Aharonov, Spiegelman, and Kelemen, 1997). It is also of fundamental importance in many engineering applications, including dam stability (Romanov, Gabrovšek, and Dreybrodt, 2003) and  $CO_2$  sequestration (Michael et al., 2010). The important applications in the oil industry include acidization of petroleum reservoirs (Fredd and Fogler, 1998) in order to enhance oil and gas production by increasing the permeability of the rock (Xu et al., 2019; Liang et al., 2007; Sudaryanto and Yortsos, 2001).
- The viscous fingering phenomenon finds its uses in oil spills and pollution control in oceans where dispersants are used to coagulate the oil particles.

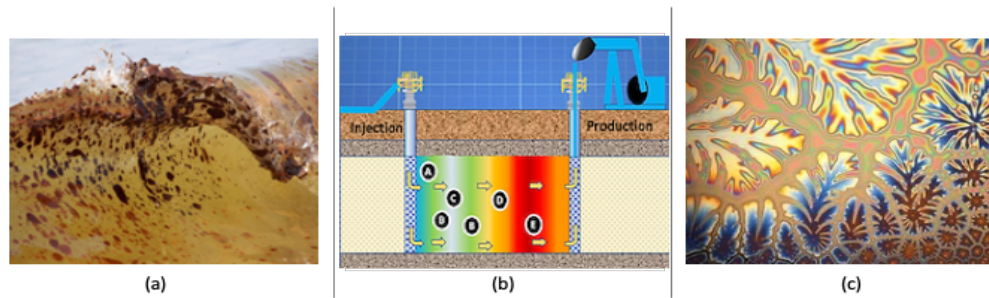


FIGURE 1.5: (a) Oil spill cleanup (b) Oil, gas recovery (c) Dendrite formation (Open source)

The dispersants are generally hydrophobic and oleophilic in nature, which, when distributed over the polluted seawater surface, helps in coagulating the oil particles, thus creating a jelly-like structure that can be easily removed from the water surface. The viscous fingering instability is used in the research for new biologically sustainable dispersants like *alcanivorax* bacteria and *fuso* bacteriota, which not only coagulates oil but also helps in the degradation of the oil particles known as bioremediation (Cogan, Gunn, and Wozniak, 2011).

- Flows involving an arbitrary number of interfaces (Using the idea of single-interface in viscous fingering flows (Saffman and Taylor, 1958)) arise during various flooding schemes in chemically enhanced oil recovery, a subject of intense current interest due to rising energy demands worldwide in a market of tight supply. To alleviate this situation, there is ongoing, much-needed research in the energy resources area. One such energy resource area is oil recovery. A fractional increase in the rate of oil recovery from an oil field using new oil recovery technology or even smarter use of existing technology will have a significant impact worldwide (Daripa and Ding, 2012).
- Water flooding, surfactant flooding, and, recently, polymer flooding are being used in the oil industry in order to recover oil from the earth's oil wells. These methods are called enhanced oil recovery (EOR) methods. In surfactant flooding, surfactants are effective in lowering the interfacial tension between oil and water to a level that promotes mobilization of trapped oil drops (Daripa and Ding, 2012; Reed, Healy, and Shah, 1977), whereas polymer flooding relies on reducing mobility contrast between displacing and displaced fluids (Daripa and Ding, 2012).
- The study of heat and mass transfer in porous media (Bernardi et al., 2023; Kambhammettu, Deshpande, and Chebolu, 2021) has a large number of applications in the areas of environmental geothermal, secondary and tertiary oil recovery, fixed bed regeneration in chemical processing, hydrology, and

filtration. Viscous fingering is an extremely important phenomenon in many applications of enhanced oil recovery, underground liquid waste disposal, and geothermal energy production (Islam and Saghir, 1999).

- Multiphase flow in porous media provides a wide range of applications: from the environmental understanding (aquifer, site-pollution) to industrial process improvements (oil production, waste management) (Pramanik, Kulukuru, and Mishra, 2012).
- During the production of heavy oil reservoirs, the movement of the fluids, namely oil and water, significantly affects the production rates. Viscous Fingering is the root cause of high water production rates. Studying and understanding this phenomenon is essential for comprehending the current challenges faced by oil and gas companies in producing heavy oil. This phenomenon has a direct impact on the assets managed by Enhanced Oil Recovery Techniques (EOR) (Pinilla, Asuaje, and Ratkovich, 2021).
- In a wide variety of situations, the formation of patterns results from a growth process. Such processes include viscous fingering, dendritic growth of crystals, electrodeposition, growth of bacterial colonies, propagation of flame fronts, fractures in brittle solids, dielectric breakdown, diffusion-limited aggregation, corrosion of solids, etc. These phenomena have been investigated not only for fundamental reasons but also for the need of its wide applications in industrial research such as in petroleum industry, oil recovery in porous media, chemical coating (Veeramani et al., 2023), dendritic growth in electrodeposition (the growth of dendritic fingers, are analogous to those associated with the instability of a solidification front (Barbieri, Hong, and Langer, 1987)), formation of lungs, etc.

This chapter has provided a brief summary of earlier research on Saffman-Taylor fluid instabilities for Newtonian and non-Newtonian fluids, as well as the technicalities and methodology involved in this study of fluid instability and the enormous industrial and practical implications connected with it. As the discussion continues, chapter 2 will provide a thorough review of the local instabilities in free shear flows. Chapter 3 will cover the numerical or mathematical method for comprehending fluid instabilities. In Chapter 4, the selection mechanism in non-Newtonian Saffman-Taylor fingers and the numerical approach for the same will be covered. The thesis is finally concluded in Chapter 5 by outlining the difficulties this study encountered and the potential for future work.

## Chapter 2

# Basics of spatiotemporal instability

### 2.1 Introductory remark

In several flows of consideration, throughout the streamwise direction, the mean velocity profile is nonuniform, and in order to differentiate between local and global spatiotemporal instability features, it is necessary first to assume that mean flow streamwise changes are non-stiff processes over a typical instability wavelength. The phrase "local" refers to the instability of the local velocity profile, whereas the phrase "global" refers to the entire flow field. This chapter aims to characterize the system's local impulse response at each streamwise position within the parallel-flow approximation.

To start with, it will be appropriate to briefly recall the classical hydrodynamic instability analysis of open flows. Many controlled studies have been done so far to test their sensitivity to different stimulation frequencies since some spatially evolving shear flows are known to be particularly sensitive to external noise. As a consequence, it has been common practice to depict the downstream development of vortical structures as a collection of spatially increasing instability waves of varying frequencies (see (Ho and Huerre, 1984) for a review of such studies applied to mixing layers). In other words, in general, the experimental data have been compared to the results of local spatial stability calculations (with a specified real frequency and an unknown complex wave number) done on the recorded time-averaged mean velocity profile at each streamwise position. In forced experiments, a similar deduction has been quite effective in elaborating the emergence of vortices. Crighton (1976) (Crighton and Gaster, 1976) and Gaster (1985) (Gaster, Kit, and Wygnanski, 1985), among many other similar research, are cited as instances of this kind of study. However, much of the work on hydrodynamic stability has been devoted to temporal theory (with a defined real wave number and unknown complex frequency), in which it is implicitly believed that the flow develops from some given initial state. The question then becomes, "What is the fundamental reason for adopting a spatial theory point of view in many open shear flows?" Local "absolute/convective" instability is said to provide a robust foundation for picking spatial theory in specific open flows such as homogeneous mixing layers, flat-plate wakes, uniform-density jets, and so on. More intriguingly, applying similar principles to other open flows, like in bluff-body wakes, hot jets, etc., leads to the conclusion that rigorous local spatial theory (i.e., real frequency) is not applicable. Both wave number and frequency must be regarded as complex, and a global temporal instability may occur, allowing the entire non-parallel mean flow to admit self-sustaining global modes with well-defined complex



frequencies.

The influence of such theories on the research of fluid-mechanical instability appears to be much more recent. Gaster et al. (Gaster, Kit, and Wynanski, 1985) developed an early spatiotemporal description of Tollmien-Schlichting wave packets in boundary layers, and a general formal methodology was proposed without explicitly introducing a definite distinction between the absolute or convective nature of the instability mechanism. Whereas the Briggs method (Briggs, 1964) has been used numerous times to investigate the receptivity of compressible shear flows to acoustic forcing. Thacker (Thacker, 1976) and Merkin (Merkin, 1977) found the transition from absolute to convective instability in a two-layer model of baroclinic instability in geophysical fluid dynamics. However, these concerns have only recently come to the forefront in the explanation of hydrodynamic instabilities in spatially developing shear flows. The distinction between absolute and convective instability appears to have been made for the first time in a broad context by Twiss (Twiss, 1952) and Landau (Landau and Lifshitz, 1959). It should be noted that plasma physicists have made significant and seminal contributions to the theoretical underpinnings behind these concepts, as well as applying them to the study of several plasma instabilities. Sturrock (Sturrock, 1958), Briggs (Briggs, 1964), and Lifshitz (Lifshitz and Pitaevskii, 1981) are recommended for methodical exploration of the main principles. Bers (Bers, 1983) comprehensive and straightforward overview is especially recommended for an up-to-date summary of theoretical work in the description of spatiotemporal plasma instabilities. Absolute and convective instabilities have made their way into the mainstream of plasma-physics literature, with presentations of the basic principles appearing in the book by Dougherty and Clemmow (Clemmow and Dougherty, 1969).

The concepts of local/global and absolute/convective instability give the theoretical framework required to identify distinct open shear flows based on the qualitative nature of their dynamic behavior. For example, if localized disturbances extend upstream and downstream, contaminating the entire parallel flow, the velocity profile is said to be locally totally unstable. Shear flows that are locally convectively unstable everywhere (e. g., mixing layers, flat-plate wakes) essentially exhibit extrinsic dynamics, as opposed to shear flows with a sufficiently large pocket of absolute instability (e. g., bluff-body wakes, hot or low-density jets), which exhibit intrinsic dynamics of the same type as in closed-flow systems. Fluid particles are still advected downstream, but there is a possibility of temporally developing global modes. These flows act like oscillators. The evolution of vortices is based on an increase in initial disturbances over time rather than the spatial amplification of external perturbations. In addition, the distribution of global modes is streamwise synchronized. This type of open flow lends itself particularly well to the nonlinear dynamical system methodology applied to closed systems. If deterministic chaos exists, it is likely to be clearly described in these systems: It is envisaged that a well-ordered sequence of bifurcations from a limit cycle (the global mode) to a low-dimensional odd attractor would definitely occur. On the contrary, the vulnerability of convectively unstable flows to external noise makes it significantly more challenging to distinguish between low-dimensional chaos emerging from the flow dynamics and spatially amplified random noise. Finally, there is a third class of marginally globally stable flows in which the local velocity profiles are, strictly speaking, locally convectively unstable throughout the

field, but absolute instability is incipient at one or more streamwise positions. Global modes are frequently weakly damped in time in such conditions, and they can be preferentially destabilized by applying external forcing near the global-mode frequency. For more details on this particular problem, an example is supplied in section 2.7.

This chapter is organized as follows: In sections 2.2, 2.3, and 2.4, the temporal instability, absolute and convective instability, and concepts of evanescent modes, have all been examined in that sequence. In sections 2.5 and 2.6, a fundamental understanding of the branch/pinch point, as well as the Cusp-Map diagram, are built to distinguish between these instabilities. The Briggs' Contour Integral Method, which is used to identify the flow-material features that lead to the aforementioned stability-instability regimes, is illustrated with an example in section 2.7.

## 2.2 Temporal instability

The traditional linear stability theory of parallel shear flows deals with the evolution of infinitesimal perturbations in space and time around a given fundamental flow  $U(y; Re)$ . Here,  $x$ ,  $y$ , and  $t$  represent the streamwise, cross-stream, and time directions, respectively, and the only component of the basic flow in the  $x$ -direction is given by  $U(y; Re)$ . It is now to be noted that as the fundamental state is parallel, it is considered to be independent of  $x$ . Typically, fluctuations are decomposed into elementary instability waves  $\phi(y; \alpha) \exp[i(\alpha x - \omega t)]$  with complex wave number  $\alpha$  and complex frequency  $\omega$ . The cross-stream distribution  $\phi(y; \alpha)$  is subsequently shown to satisfy an ordinary differential equation of the Orr-Sommerfeld type in most circumstances.

An eigenvalue problem arises, say,  $Y_1$  and  $Y_2$ , when proper boundary conditions are enforced. In this case, eigenfunctions  $\phi(y; \alpha)$  exist only if  $\alpha$  and  $\omega$  are required to meet a dispersion relation of the form

$$D[\alpha, \omega, \mathbf{M}] = 0. \quad (2.1)$$

where  $\mathbf{M}$  is the vector of material and fluid parameters. This relationship can be determined precisely for simple basic flows. It is generated by numerical integration of the Orr-Sommerfeld equation with more realistic velocity profiles. *Temporal modes*  $\omega(\alpha, Re)$  are circumstances in which the complex frequency  $\omega$  is determined as a function of the real wave number  $\alpha$ . *spatial branches*  $\alpha(\omega; Re)$ , on the other hand, are derived by solving for complex wave numbers  $\alpha$  when  $\omega$  is given real. Fluctuations in the cross-stream direction  $y$  have been purposefully disregarded in this section; instead, this focuses on the spatiotemporal evolution of instability waves in the  $(x, t)$ -plane. This projection considerably simplifies the explanation of the core principles while retaining all of the crucial features of the instability. As a result, a differential or integro-differential operator  $D[-i(\partial/\partial x), i(\partial/\partial t); \mathbf{M}]$  can be associated in physical space  $(x, t)$  to the dispersion relation (2.1) in spectral space  $(\mathbf{M}, \omega)$ , such that fluctuations  $u(x, t)$  satisfy

$$D \left[ -i \frac{\partial}{\partial x}, i \frac{\partial}{\partial t}; \mathbf{M} \right] u(x, t) = 0 \quad (2.2)$$

In order to solve the relevant receptivity problem for the preceding equation (2.2), one incorporates Green's function by defining the impulse response  $G(x, t)$  of the flow with  $\delta$  denoting the Dirac delta function, as

$$D \left[ -i \frac{\partial}{\partial x}, i \frac{\partial}{\partial t}; R \right] G(x, t) = \delta(x) \delta(t) \quad (2.3)$$

The basic flow is said to be linearly stable if

$$\lim_{t \rightarrow \infty} G(x, t) = 0 \text{ along all rays } x/t = \text{constant} \quad (2.4)$$

and it is linearly unstable if

$$\lim_{t \rightarrow \infty} G(x, t) = \infty \text{ along at least one ray } x/t = \text{constant}. \quad (2.5)$$

## 2.3 Absolute and Convective instability

In this section, a further differentiation between the two forms of impulse response among the linearly unstable flows has been discussed as follows:

The basic flow is known as absolutely unstable if

$$\lim_{t \rightarrow \infty} G(x, t) = \infty \text{ along the ray } x/t = 0, \quad (2.6)$$

and it is convectively unstable if

$$\lim_{t \rightarrow \infty} G(x, t) = 0 \text{ along the ray } x/t = 0 \quad (2.7)$$

as shown in Fig 2.1. The above definitions ((2.7), (2.6)) can possibly be demonstrated in the Ginzburg Landau linearized model. Hence, the operator  $D$  takes the form

$$D \left[ -i \frac{\partial}{\partial x}, i \frac{\partial}{\partial t}; \mathbf{M} \right] u(x, t) = \frac{\partial \psi}{\partial t} + V_g \frac{\partial \psi}{\partial x} - \frac{i}{2} V_{gg} \frac{\partial^2 \psi}{\partial x^2} + i V_{gr} (R \cdot R_e) \psi = 0 \quad (2.8)$$

where  $V_g$  is a real positive constant group velocity, and  $V_{gg}$  and  $V_{gr}$  are complex constants with  $V_{gg,i} < 0$ . This model is known to develop in many marginal-stability assessments of fluid-dynamical systems close to the onset (Newell and Whitehead, 1969; Stewartson and Stuart, 1971) when an adequate cubic nonlinearity is added.

Convectively unstable flows typically produce wave packets that migrate away from the source and eventually leave the medium undisturbed. In contrast, absolutely unstable flows are gradually contaminated everywhere by a point-source input. In order to differentiate between absolute and convective instabilities, it is important to investigate the long-time characteristic of the wave number  $\alpha_0$  noticed along the ray  $x/t = 0$  at a fixed spatial point using definitions (2.7) and (2.6). By definition, this complex  $\alpha_0$  has a zero group velocity, i.e.,

$$\frac{\partial \omega}{\partial \alpha}(\alpha_0) = 0, \quad (2.9)$$

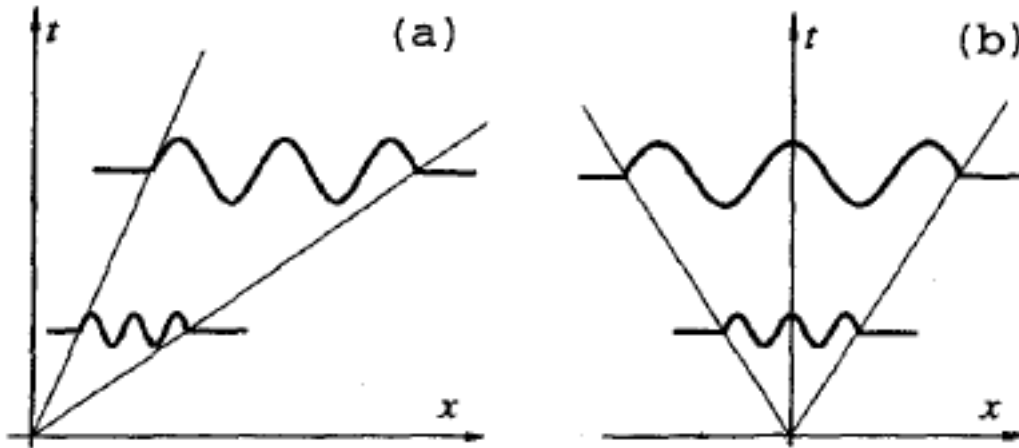


FIGURE 2.1: (a) Convective, (b) Absolute instability (Source (Schmid and Henningson, 2001))

and the corresponding  $\omega_0 = \omega(\alpha_0)$  is called the absolute frequency. Here, the absolute growth rate is expressed as  $\omega_{0,i} = \text{Imag}(\omega(\alpha_0))$ , and it can characterize the temporal evolution of the wave number  $\alpha_0$  observed at a fixed station in the limit  $t \rightarrow \infty$ . On the contrary, the previously defined maximum growth rate  $\omega_{i,max}$  is observed as the peak of the wave packet. The sign of  $\omega_{i,max}$  determines the unstable/stable nature of the flow, whereas in the same way, the sign of  $\omega_{0,i}$  determines its absolute/convective nature. Therefore, it leads us to the following criterion:

$$\begin{aligned} \omega_{0,i} > 0 & \quad \text{absolutely unstable flow,} \\ \omega_{0,i} < 0 & \quad \text{convectively unstable flow.} \end{aligned} \quad (2.10)$$

## 2.4 Notion of Evanescent modes

In general, a flow field regulated by the Navier-Stokes equations can support three forms of modal wave fields: acoustic, vorticity, and entropy waves (refer Pierce (Pierce, 1981)). Except at boundaries or maybe at direct resonances, these modal fields are uncoupled under the linear approximation. A direct resonance occurs when two (or more) wave modes coalesce in a physical system that enables more than one wave mode. The focus of this study will be on the coalescence of modes of the same wave type, specifically the coalescence of vorticity modes. Direct resonance can be a very powerful selection process resulting in algebraic development for short time frames or short distances if no or only very minor instabilities exist, and the corresponding potentially large amplitudes may initiate the nonlinear solution long before the exponentially developing mode does.

The idea of direct resonance appears to have important implications in the creation (on a weakly nonlinear theory) of waves by wind (Akylas, 1982) and in the stability of locally parallel shear flows (Benny and Gustavsson, 1981; Gustavsson and Hultgren, 1980; Gustavsson, 1981; Hultgren and Gustavsson, 1981; Akylas and Benney, 1980; Akylas and Benney, 1982). In the above-referred papers concerning the stability of parallel shear flows, the resonant forcing of the vertical vorticity (and hence the

horizontal velocity components) by the vertical velocity has been investigated with the intention of elucidating the laminar-turbulent transition process. This corresponds to the "Squire" mode, which is a direct resonance between an Orr-Sommerfeld and a vertical vorticity. The research on this so-called Benney-Gustavsson resonance mechanism is particularly promising and has been intensively pursued. The major goal of this thesis is to see: (i) if the flow can support a direct resonance between two Orr-Sommerfeld modes on their own, and if so, (ii) whether such a resonance mechanism is physically relevant. The nature of a direct resonance is determined by the type of singularity in the dispersion relation at the time of mode coalescence and it is frequently determined by the reaction to a point source in time and place. The "cut-off" phenomena, in a hard-walled duct, distinguishing propagating from evanescent acoustic waves belongs to this group of events in a linear neutrally stable system (Aranha, Yue, and Mei, 1982).

The associated singularity is of the double pole type if the two merging modes arise from waves traveling in the same direction, as in the case of a convectively unstable flow. According to linear theory, such a disturbance will eventually dissipate. A double pole is associated with short-term algebraic growth; on the other hand, it may play a crucial role in driving the system into a nonlinear state. The damping rate connected with the modal coalescence determines whether this is physically achievable. When the damping rate is high, such resonances are important in certain linear optimization problems (for example, the ducts with acoustically absorbent walls (Cremer, 1953)).

If the two coalescing modes originate from waves propagating in the same direction as in the case of a convectively unstable flow, the corresponding singularity is of the double pole type. Such a disturbance will decay ultimately according to linear

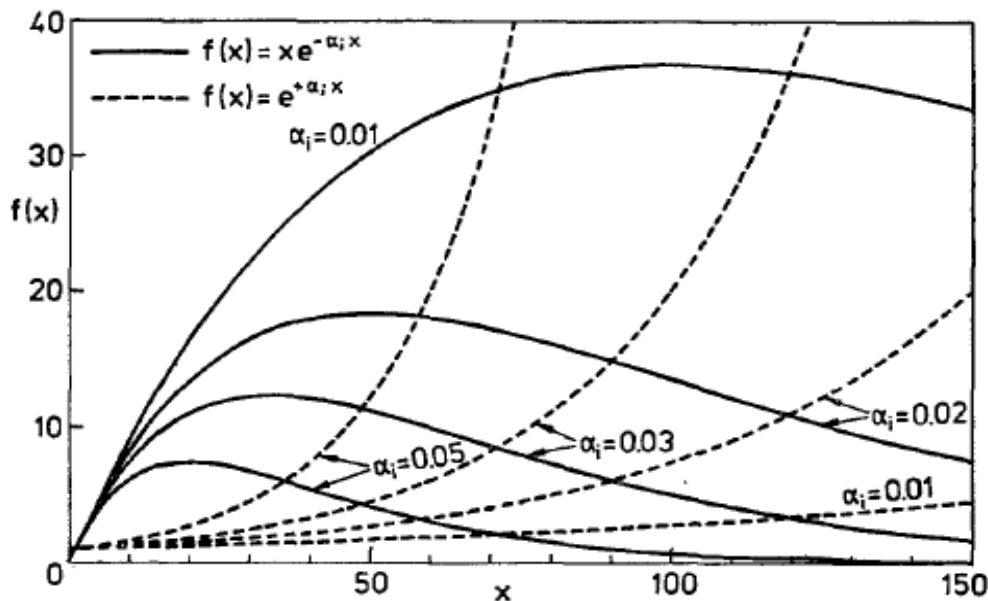


FIGURE 2.2: Effect of direct resonance on amplitude evolution  
(Source (Koch, 1986))

theory. However, the short-term algebraic growth associated with such a double pole may be decisive and carry the system into a nonlinear state. Whether this is physically

possible is determined by the damping rate associated with the modal coalescence. If the damping rate is large such resonances are of importance in certain linear optimization problems (an example is the (Cremer, 1953) for ducts with acoustically absorbing walls). If the coalescing modes are practically neutral, the related damping rates are very low, and algebraic growth may locally outnumber exponential decay. This is the case handled by Benny in 1981 (Benny and Gustavsson, 1981) as well as the current exploration of plane Poiseuille and boundary-layer type mean flows (both represent the convectively unstable flow).

In order to have an understanding of the concept of evanescent mode, an example of a function, given by  $f(x) = \exp(-\alpha_i x)$  has been considered here. It is illustrated in Fig. 2.2 by plotting the functions  $x \exp(\alpha_i x)$  and  $\exp(-\alpha_i x)$  for various  $\alpha_i = \text{Im}(\alpha)$ . Now, for large  $\alpha_i$ , high amplitudes  $f(x)$  are rapidly reached by the exponentially growing mode  $\exp(\alpha_i x)$ . However, notice that if  $\alpha_i$  is very small, the growth is very slow, and therefore, a direct resonance generating  $x \exp(-\alpha_i x)$  can produce large amplitudes much faster. According to linear theory, although these modes ultimately decay, the locally high amplitudes may initiate the nonlinear state. To determine if this is possible for a given flow, one needs to ascertain (i) under which conditions direct resonances exist and (ii) how large the corresponding damping rates are.

## 2.5 Pinch points and Branch points

A pinch point in the  $\alpha$ -plane and a branch point in the  $w$ -plane simultaneously occur, and it can be illustrated as follows:

A pinch point, denoted as  $\alpha^{pinch}$ , in the complex  $\alpha$ -plane, can be identified as a special kind of saddle point that fulfills the relation given by the following equations:

$$D(\alpha^{pinch}, \omega^{cusp}) = 0; \quad \frac{\partial D}{\partial \alpha}(\alpha^{pinch}, \omega^{cusp}) = 0; \quad \frac{\partial^2 D}{\partial \alpha^2}(\alpha^{pinch}, \omega^{cusp}) \neq 0 \quad (2.11)$$

A Taylor series expansion of the dispersion relation in the neighborhood of the singularity  $(\alpha^{pinch}, \omega^{cusp})$  then leads to

$$0 = \frac{\partial D}{\partial \omega} \Big|_0 (\omega - \omega^{cusp}) + \frac{1}{2} \frac{\partial^2 D}{\partial \alpha^2} \Big|_0 (\alpha - \alpha^{pinch})^2 + \mathcal{O} \left( (\omega - \omega^{cusp})^2, (\alpha - \alpha^{pinch})^3 \right) \quad (2.12)$$

This expression gives a relation between the neighborhood of  $\omega^{cusp}$  in the  $w$ -plane and the neighborhood of  $\alpha^{pinch}$  in the  $\alpha$ -plane. Because of the quadratic nature of the local map between the  $\alpha$  and  $w$ -planes, a square root singularity will occur between the local maps of  $w$  and  $\alpha$ -planes.

If the contour deformation process produces a pinch point in the  $\alpha$ -plane, the accompanying branch point in the  $w$ -plane sits above the imaginary  $w$ -axis, indicating an absolute instability. Absolute instability is defined as the presence of an unstable wave with zero group velocity. The group velocity,  $V_g$ , is obtained at an unstable pinch or branch point, such that,

$$V_g = \frac{\partial \omega}{\partial \alpha} = \frac{\partial D}{\partial \alpha} / \frac{\partial D}{\partial \omega} = 0. \quad (2.13)$$

## 2.6 The Cusp map

Till now, it can be noticed that the asymptotic space-time evolution of a linear instability is determined by the placement of pinch points in the complex  $\alpha$ -plane, which can be identified by analytically extending the Laplace inversion contour into the lower half of the  $w$ -plane. Solving the dispersion relation for the spatial wavenumber  $\alpha$  as a function of frequency  $w$  is required for this technique. This seems to be extremely undesirable because computing  $w$  as a function of  $\alpha$  is usually much simpler. The purpose of this section is to present a method for finding absolute instabilities that are based simply on a mapping from the  $\alpha$ -plane to the  $w$ -plane. This technique was developed by Kupfer (1987) (Kupfer, Bers, and Ram, 1987), who referred to it as the "cusp map" in the complex-frequency plane.

So, to begin, let's look at the mapping from the  $\alpha$ -plane to the  $w$ -plane. Dispersion relations, in general, are higher order polynomials (or transcendental) in the wave number  $\alpha$ , and hence the mapping of the  $F$ -contour into the  $w$ -plane is multivalued. The image of  $F$  in the  $w$ -plane is denoted as  $w(F)$ . In the dispersion relation, the inverse mapping of  $w(F)$  back into the  $\alpha$ -plane will result in  $n$  branches  $\alpha_k(w(F))$  with  $n$  as the highest order of  $\alpha$ . Nonetheless, from one of the  $n$  branches, the original  $F$ -contour can be recovered. Now, by supplying the  $n$  Riemann sheets in the complex  $w$ -plane and then by associating the  $n$  contours in the multi-sheeted  $w$ -plane with the  $n$  branches  $\alpha_k(w(F))$  in the  $\alpha$ -plane, the mapping of the  $F$ -contour into the  $w$ -plane can be made single-valued. It is well-known that the dispersion relation is a relation between the wavenumber ( $\alpha$ ) and frequency ( $\omega$ ) of a wave, and hence, the mapping between the  $w$  and  $\alpha$ -plane is governed by the dispersion relation  $D(\alpha, w) = 0$ . Moreover, the additional constraints for a pinch point in the complex  $\alpha$ -plane, given by the equations

$$\frac{\partial D(\alpha, \omega)}{\partial \alpha} = 0 \quad \frac{\partial^2 D(\alpha, \omega)}{\partial \alpha^2} \neq 0 \quad (2.14)$$

A point  $w_0$  that satisfies these conditions in the complex  $w$ -plane for a corresponding  $\alpha_0$ , has only  $n1$  image points in the complex  $\alpha_0$  plane. In other words, at this specific point  $w_0$ , it can be stated that the two sheets in the  $w$ -plane connect to each other. Now careful attention will be given to these two sheets, and for that, a vertical ray is introduced that connects the contour  $L$  in each of the two sheets to the point  $w_0$  (refer Fig. 2.3). These rays are denoted as  $R_1$  and  $R_2$ , and they can eventually help to determine whether the point  $w_0$  in the  $w$ -plane corresponds to a pinch point  $\alpha_0$  in the  $\alpha$ -plane.

If and only if the images of the rays  $R_1$  and  $R_2$  in the complex  $\alpha$ -plane, i.e.,  $\alpha(R_1)$  and  $\alpha(R_2)$  in Fig. 2.3, originate on two different sides of  $F$ , the branch point at  $w = w_0$  corresponds to a pinch point in the  $\alpha$ -plane. On the other hand, if the images  $\alpha(R_1)$  and  $\alpha(R_2)$  originate on different sides of  $F$  but connect at one single point  $\alpha_0$ , which is not on  $F$ , then a conclusion can be drawn that at least one of these images

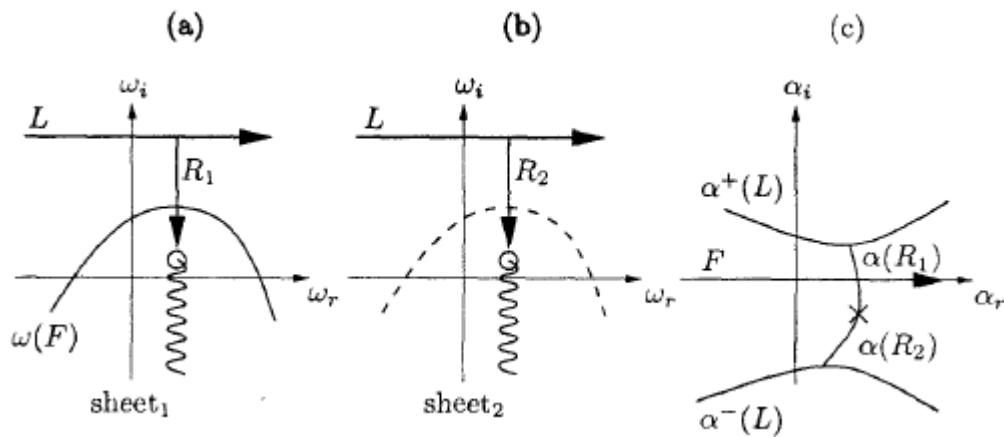


FIGURE 2.3: Sketch illustrating the cusp map method (Source (Kupfer, Bers, and Ram, 1987)).

crosses  $F$ . But, if more than one crossing occurs, the total number of crossings by both images must be odd.

This criterion indeed forms the basis of the cusp map method. One can determine whether the branch point  $w_0$  corresponds to a pinch point in the  $\alpha$ -plane by simply counting the number of times that each vertical ray,  $R_1$  and  $R_2$  intersects the contour  $w_k(F)$ . The above approach, which is entirely universal, can be used in conjunction with the following procedure to establish the stability properties of any dispersion relation. The process entails mapping a piece of the  $\alpha$ -plane into a region indicated beneath  $w(F)$ . The  $w$ -plane is mapped by a series of vertical rays spanning the range of unstable wave numbers. These parallel rays in the  $\alpha$ -plane may have pictures that meet, indicating a branch point. The angle-doubling property of the local map identifies the singularity. This is seen in The process that entails mapping a piece of the  $\alpha$ -plane into a region indicated beneath  $w(F)$ . The  $w$ -plane is mapped by a series of vertical rays spanning the range of unstable wave numbers. These parallel rays in the  $\alpha$ -plane may have pictures that meet, indicating a branch point. The angle-doubling property of the local map identifies the singularity. This is seen in Fig. 2.4, where the branch point is nested at the edge of a cusp-like trajectory. One obtains a mapping consistent with the multi-sheeted structure implied by the contour  $w(F)$  if a branch cut is taken downward from the singularity, and in that case, the branch point is covered only once by  $w(F)$  and thus corresponds to a pinch point. In many cases, replacing the vertical rays depicted in Fig. 2.4 with a series of horizontal contours representing deformations of the Fourier integral path is simpler. These contours will proceed downhill from  $w(F)$  in the  $w$ -plane and form a cusp as they approach the singularity; see Fig. 2.4. The angle-doubling (or angle-tripling, etc.) characteristic of the branch point's local map is used to locate it once more. A similar method can be applied to dispersion relations with several unstable branches.



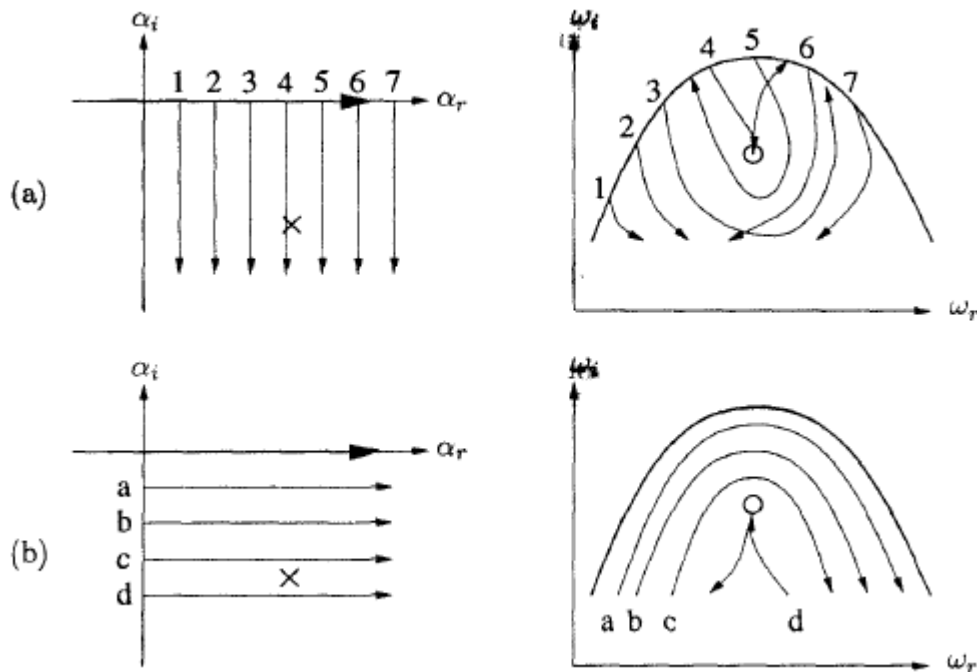


FIGURE 2.4: Outline of the numerical procedure for detecting branch points in the  $w$ -plane used in the cusp map method (Source (Kupfer, Bers, and Ram, 1987)).

## 2.7 Briggs' method

In this section, general mathematical criteria based on the singularity structure of the dispersion relation in the complex  $w$  and  $\alpha$ -planes have been discussed to categorize instabilities as convective or absolute. Locating pinch points in the complex  $\alpha$ -plane is an important step in discovering absolute instability. In 1964, Briggs' (Briggs, 1964) proposed a systematic method for accomplishing this, in which one needs to repeatedly solve for the spatial branches of the dispersion relation for frequencies  $w$  provided along specified pathways in the complex  $w$ -plane. To keep things simple, one can consider straight lines that are parallel to the imaginary  $w$ -axis. Mapping points along these  $w$  pathways into the  $\alpha$ -plane traces out spatial branches of the dispersion relation corresponding with the given temporal branches in the  $w$ -plane. One can gradually visualize the map of the  $w$ -plane into the  $\alpha$ -plane by altering the real component of the  $w$  lines under the dispersion relation  $D(\alpha, w) = 0$ . It should then be rather simple to locate saddle points in the  $\alpha$ -plane. Another key consideration is that the saddle point must be composed of spatial branches that start in various half-spaces. As the  $w$  lines are modified, a saddle point clearly forms in the  $\alpha$ -plane. Furthermore, the two spatial branches that comprise the saddle point originate in two distinct half-spaces. According to Briggs' criterion, the appropriate branch point in the  $w$ -plane, denoted by a circle along the third ray (see Fig. 2.5), sits below the real  $w$ -axis and so does not constitute an absolute instability.

Now, let's begin with the solution to the stability problem in Fourier-Laplace space. The use of Fourier- and Laplace-transform Eqn. (2.3) and formally reverting back to physical space can provide

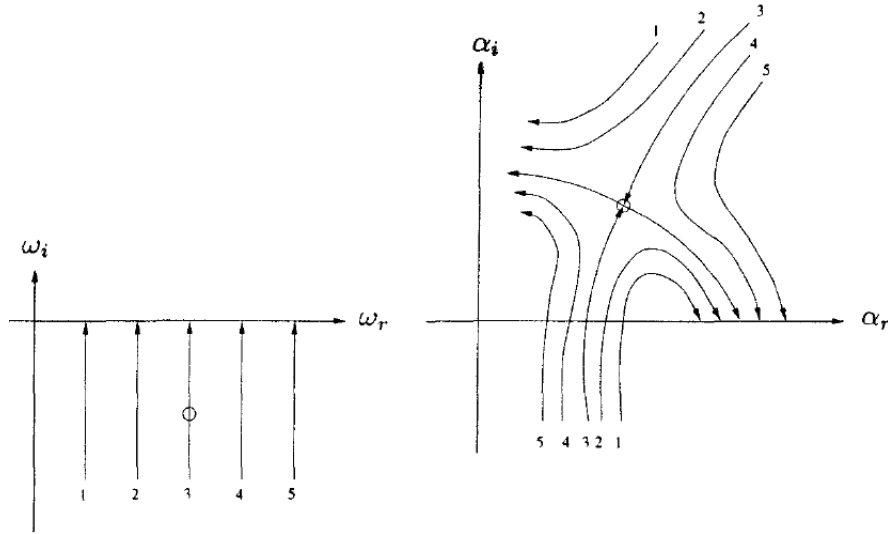


FIGURE 2.5: Illustration of the numerical procedure for detecting saddle points in the  $\alpha$ -plane used in the Briggs' method (Source (Schmid and Henningson, 2001)).

$$G(x, t) = \frac{1}{4\pi^2} \int_L \int_F \frac{\exp[i(\alpha x - \omega t)]}{D(\alpha, \omega, \mathbf{M})} d\alpha d\omega \quad (2.15)$$

where  $L$  and  $F$  denote the inversion contour in the Laplace- $w$ -plane and the Fourier  $\alpha$ -plane, respectively. Even though the Fourier-Laplace integral (2.15) could be calculated for all  $x$  and  $t$ , the dispersion relation's complexity suggests a time-asymptotic solution of the integral. Furthermore, the notion of convective and absolute instability as a limit process for a large duration necessitates an asymptotic approach to calculating the Fourier-Laplace integral (2.15). The modification of the integration contours in the complex  $\alpha$  and  $w$ -planes will be required for the time-asymptotic assessment of the integral expression for the Green's function. The method of steepest descent can be utilized to evaluate the time-asymptotic behavior by deforming the integration path through a saddle point in the  $\alpha$ -plane. According to the definition, if this evaluation yields a divergent integral, the flow under consideration is regarded as utterly unstable. The flow will be convectively unstable if the asymptotic limit results in a convergent integral (in fact, in a zero integral). However, special care has to be taken when applying the method of steepest descent. This topic will be revisited later. By introducing Briggs' method, the time-asymptotic behavior of the Fourier-Laplace integral (2.15) can be carefully evaluated. In Briggs' method (Briggs, 1964), the wave number integral is chosen first,

$$\tilde{G}(x, \omega) = \frac{1}{2\pi} \int_F \frac{\exp[i\alpha x]}{D(\alpha, \omega, \mathbf{M})} d\alpha \quad (2.16)$$

which is followed by the  $w$ -inversion

$$G(x, t) = \frac{1}{2\pi} \int_L \tilde{G}(x, \omega) \exp[-i\omega t] d\omega \quad (2.17)$$

The analytic continuation method is used to deflect the initial  $L$ -contour in an attempt to decrease it below the real  $w$ -axis (see Fig. 2.6). If this is accomplished,

the exponent in the  $w$ -inversion integral (2.17) causes the integrand to vanish as  $t \rightarrow \infty$ ; otherwise, the time-asymptotic discrete response is guided by the highest discrete singularity in the  $w$ -plane. Lowering the  $w$ -contour may fail if a singularity is encountered above the true  $w$ -axis. This singularity in the  $w$ -plane will have an associated singularity in the  $\alpha$ -plane due to the link via the dispersion relation.

To begin, let's select the real  $\alpha$ -axis as the inversion contour for the spatial component. This integration path, indicated by  $w(F)$ , maps through the dispersion relation to a curve in the  $w$ -plane. To satisfy causality, the temporal inversion contour must sit above this curve: The integration route for  $t < 0$ , which involves closure in the upper half-plane, cannot encircle any singularities; that is, the integrand of the  $w$  integral (2.17) must be analytic in the  $w$ -half-space:  $0 > \max \text{Im}(w(F))$ . The temporal contour  $L$  can also be mapped back into the  $\alpha$ -plane, yielding the  $\alpha^+(L)$  and  $\alpha^-(L)$  branches. The dynamics downstream of the origin are related to the spatial branch above the real axis, whereas the perturbation behavior upstream of the source is governed by the branch below the real  $\alpha$ -axis. Now, try to lower the  $w$  inversion contour below the real axis via analytic continuation. As the  $w$ -contour starts to distort, the picture in the  $\alpha$ -plane deforms as well. The original  $\alpha$ -contour will eventually be squashed between the two branches, necessitating deformation of the original  $\alpha$ -contour as well. This, in turn, will change the  $w$ -contour. The crossing of singularities can be avoided by constantly modifying the inversion contours and their maps into the related plane. If this happens, the temporal inversion contour cannot be decreased anymore because a branch point forms in the  $w$ -plane.

When the  $L$  contour is distorted onto the actual  $\alpha$ -axis, convectively unstable modes are produced by  $\alpha$ -roots that end up in a different half of the  $\alpha$ -plane from the one from which they originated. They are distinguished from evanescent modes by the crossing of the real  $\alpha$ -axis. Bers (Bers, 1983) provides a more detailed description of the theory. The merging of two eigenmodes results in an absolute instability eigenmode. As a result, its existence can be seen intuitively as a type of resonance between the modes; a resonance that leads to growth because the merged eigenmode has  $w_i > 0$ . The modal interaction associated with merging occurs physically over the source of the perturbation. This is due to the participating modes coming from the upstream ( $x_1 < 0$ ) and downstream ( $x_1 > 0$ ) sides of the source. As a result, the instability is localized with respect to the source's position and gradually wraps an ever-increasing neighborhood of the disturbance source. A shear flow with a large pocket of absolute instability may exhibit the dynamics of a closed-flow (compact) system. These instabilities behave like oscillators. A convectively unstable mode, on the other hand, has been linked to a sinusoidal wave that grows in amplitude as it moves away from the source and receives its frequency. A driven mode is essentially a convectively unstable mode. When the driving source is switched off, it decays to zero over time; however, a completely unstable mode is more analogous to a self-sustaining temporal mode and has been labeled as such by Bers (Bers, 1983).

A probable absolute instability is detected when  $(w_0)_i > 0$ . However, it is still important to confirm that the intersection results from roots originating in opposing halves of the  $\alpha$ -plane. At least one of the  $\alpha$ -roots must cross the  $\alpha_r$ -axis of the  $\alpha$ -plane at least once for such an intersection to be possible. An even number of crossings returns a  $\alpha$ -root to its original half of the  $\alpha$ -plane, while an odd number returns it to the opposite half. For a genuine pinch point, the total number of crossings

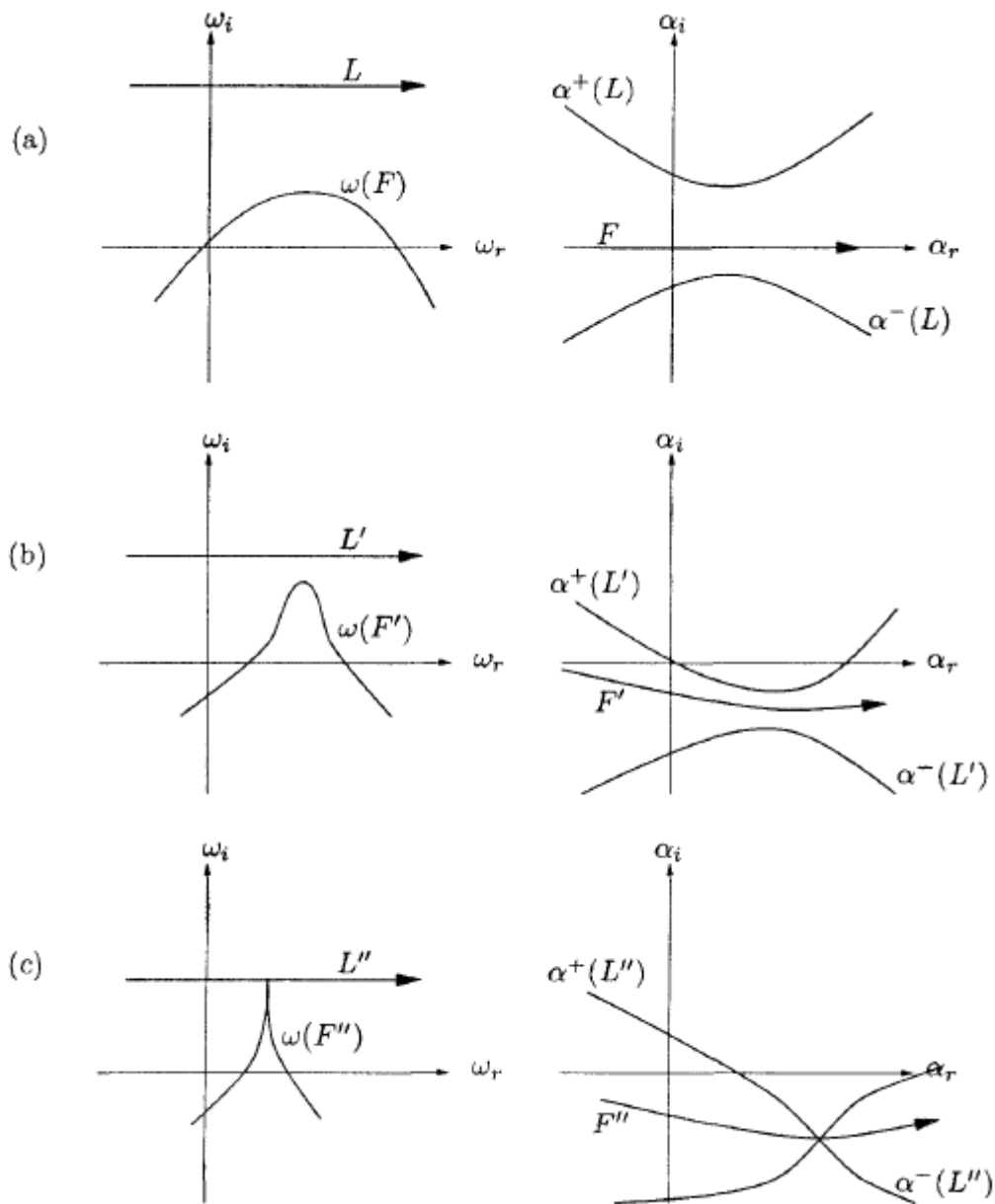


FIGURE 2.6: Sketch of contour deformation procedure for Briggs' method. Left: complex  $w$ -plane, right: complex  $\alpha$ -plane (Source (Schmid and Henningson, 2001)).

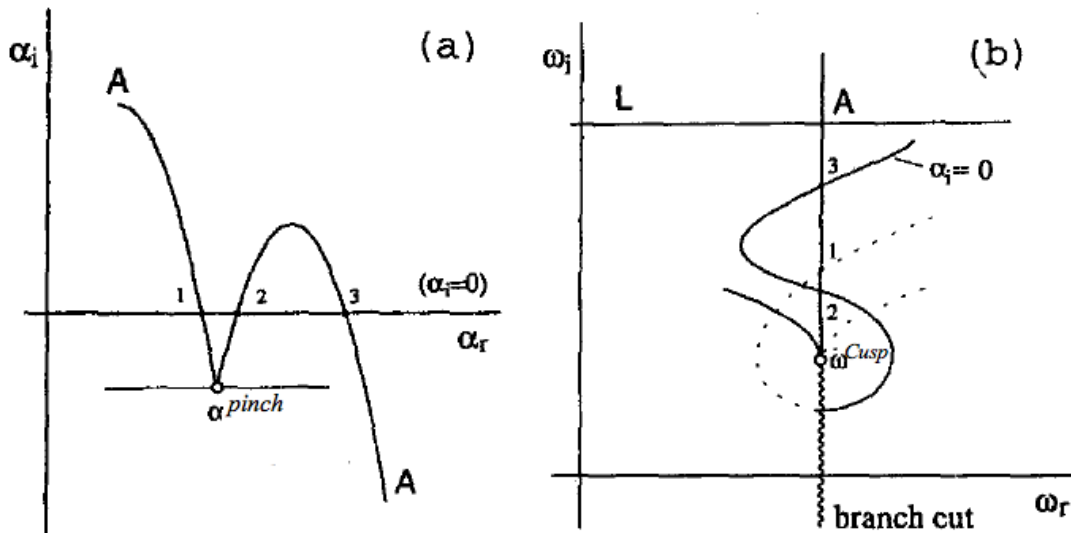


FIGURE 2.7: An example in the schematic of an absolute instability created by the intersection of two  $\alpha$ -roots with three crossing of the  $\alpha_r$ -axis ( $\alpha_i = 0$ ). The vertical ray from  $w_0$  cuts the  $\alpha_i = 0$  contour in the three places in the double-sheeted  $w$ -plane (Source (Yeo, Khoo, and Zhao, 1996)).

must be an odd number. This criteria can be met by drawing a straight ray vertically upward ( $w_r = \text{constant}$ ) from the suspected cusp point and counting the number of times this ray crosses the image of the  $\alpha_r$ -axis ( $\alpha_i = 0$ ) in the  $w$ -plane (a double or multisheeted Riemann surface). This phenomenon is happening due to the fact that every crossing of the  $\alpha_r$ -axis in the  $\alpha$ -plane by the  $\alpha$ -roots (as the  $w_i$  is varied with the lowering of the  $L$  contour) is reflected by a corresponding crossing of the image of the  $\alpha_r$ -axis ( $\alpha_i = 0$ ) in the  $w$ -plane by the vertical ray (which represents variation in  $w_i$ ) in one of the Riemann sheets of the co-plane. Figure 2.7 shows a simplified application of this criterion to a situation in which the crossing pair of  $\alpha$ -roots crosses the  $\alpha_r$ -axis three times. In this scenario, the upward vertical ray emerging from the cusp point cuts the image of the  $\alpha_r$ -axis on the two Riemann sheets three times. When the Riemann sheets of the branch point  $w^{cusp}$  correspond to spatial branches in the same  $\alpha$ -plane for large enough  $L$ , there is no pinching of  $F$  as  $L$  is reduced. The absolute growth rate is unrelated to the associated branch point in the  $w$ -plane. To detect branch-point singularities belonging to spatial branches originating from distinct sides of the  $\alpha$ -plane, care must be taken. The vertical-ray criterion can also be used to differentiate between true convective instabilities and evanescent modes.

Now, let's aim to summarize Briggs' contour integral method as follows: The vanishing characteristic of the group velocity,  $v_g$ , at the saddle point in the  $\alpha$ -plane or the branch point in the  $\omega$ -plane is a required (but not sufficient) condition for the presence of absolute instability ( $v_g = \frac{\partial \omega}{\partial \alpha} = \frac{(\frac{\partial D}{\partial \alpha})}{(\frac{\partial D}{\partial \omega})} = 0$  such that  $\omega = D(\alpha)$ ). However, the group velocity is zero at every saddle point, especially when the two  $\alpha$  branches meet, regardless of whether the branches originate from the same half of the  $\alpha$ -plane (i.e. when evanescent modes are identified). Briggs' (Briggs, 1964) devised the idea of analytic continuation to overcome this inadequacy, in which the Laplace contour  $L$ , in equation (2.15), is deformed towards the  $\omega_r$  axis of the complex  $\omega$ -plane, with the simultaneous adjustment of the Fourier contour  $F$  in the  $\alpha$ -plane

to maintain the separation of the  $\alpha$ -branches; those which originate from the top half (the upstream modes with  $\alpha_i > 0$ ) from those which originate from the bottom half of the  $\alpha$ -plane (or the downstream modes).

The deformation of the  $F$  contour is prevented (while preserving causality) when the paths of the two  $\alpha$ -branches originating from the opposite halves of the  $\alpha$ -plane intersect, resulting in the appearance of saddle points, which are the *pinch point* and the  $\alpha^{pinch}$ . The concurrent branch point appearance in the  $\omega$ -plane is the *cusp point*,  $\omega^{cusp}$  (i. e.,  $D(\alpha^{pinch}, \omega^{cusp}) = \frac{\partial D(\alpha^{pinch}, \omega^{cusp})}{\partial \alpha} = 0$  but  $\frac{\partial^2 D(\alpha^{pinch}, \omega^{cusp})}{\partial \alpha^2} \neq 0$ ). Kupfer (Kupfer, Bers, and Ram, 1987) conceptualized the stability features of this branch point and used a local mapping approach. A local Taylor expansion near a "reasonably close" neighborhood of the pinch point yields a dispersion relation with a second-order algebraic form in the  $\omega$ -plane (and a first-order saddle point in the  $\alpha$ -plane), i.e.,  $(\omega - \omega^{cusp}) \sim (\alpha - \alpha^{pinch})^2$ . Because of the map's period-doubling property, the  $\alpha_i$ -contours "rotate" around the  $\omega^{cusp}$ , forming a cusp. In the  $\omega$ -plane, draw a ray parallel to the  $\omega_i$ -axis from the cusp point and count the number of intersections with the image of the  $F$ -contour (or  $\alpha_i = 0$  curve) and consequently, count the number of times both  $\alpha$ -branches cross the  $\alpha_r$ -axis before forming a pinch point in the  $\alpha$ -plane, as shown in Figure 2.7. If the ray traced from the cusp point intersects the image of the  $F$ -contour in the  $\omega$ -plane an even number of times (or if either one or both  $\alpha$ -branches cross the  $\alpha_r$ -axis), the flow dynamics correspond to an evanescent mode. Otherwise, in the case of odd intersections, the observed cusp point is genuine, leading to either an absolutely unstable (upper half of the  $\omega$ -plane) or a convectively unstable (lower half of the  $\omega$ -plane) system, provided the system is temporally unstable (Bansal, Ghosh, and Sircar, 2021).

To demonstrate this crucial method further, a sample dispersion relation (adapted from (Kupfer, Bers, and Ram, 1987)) is presented, and Briggs' method is also used here. The dispersion relation is a mathematical relationship that is only utilized for illustration purposes in this case. Because of its simplicity, it provides explicit solutions for pinch point and branch point positions. Now, consider

$$D(\omega, \alpha) = \omega - \left[ \frac{1}{3}(\alpha - i)^3 + i - \alpha V \right] \quad (2.18)$$

where a parameter,  $V$ , is introduced here.

By solving  $dw/d\alpha = 0$ , the pinch points and branch points can be found, which yields

$$\alpha_{1,2} = i \pm \sqrt{V} \quad (2.19)$$

for the pinch points and

$$\omega_{1,2} = (1 - V)i \mp \frac{2}{3}V\sqrt{V} \quad (2.20)$$

for the associated branch points in the  $w$ -plane.

To proceed with the Briggs' method as outlined earlier, first set  $V = 0.75$  and then map lines of constant  $w$  into the complex  $\alpha$ -plane by solving the cubic dispersion relation (2.18).

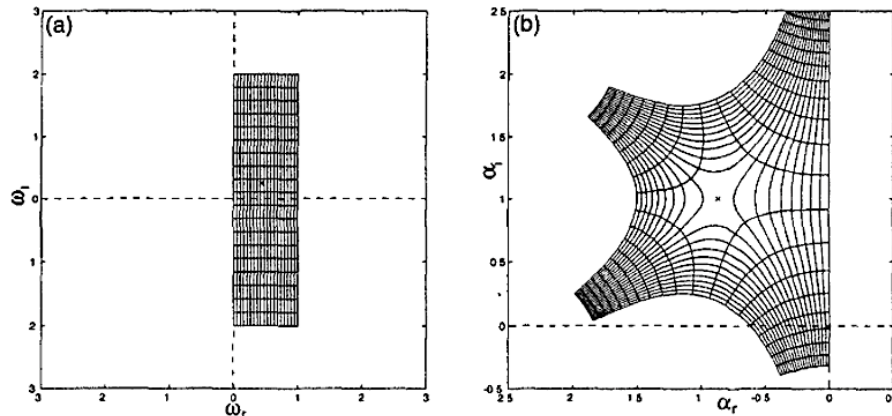


FIGURE 2.8: Map of the complex  $w$ -plane into the complex  $\alpha$ -plane under the dispersion relation (2.18) (Source (Schmid and Henningson, 2001)).

A saddle point clearly forms in the complex  $\alpha$ -plane, which is denoted by a symbol and corresponds to the solution of equation (2.19) for  $V = 0.75$  (refer to Fig. 2.8). Its branches emerge from several half-spaces of the  $\alpha$ -plane. In the  $w$ -plane, the relevant branch point is also marked. The branch point is clearly above the actual  $w$ -axis, indicating the presence of an absolute instability. To be sure, this is a very simplified example. Nonetheless, it highlights the utility of Briggs' method for detecting absolute instability. More sophisticated dispersion relations can be created to test the readers' understanding of analytic function theory.

The approach just described for calculating absolute and convective stability characteristics is closely linked to the steepest descent method. The steepest descent approach makes no distinction between branches that originate in the same or different half-spaces. Additional examination of the global topology of the phase function is required to focus on the certain category of saddle points in the  $\alpha$ -plane. The integral representation of Green's function solution, in fact, advises looking for saddle points of the phase function and evaluating the integral asymptotically using traditional approaches. It is also necessary to evaluate the global topology of the phase function; not all points with  $\frac{dw}{d\alpha} = 0$  are connected with absolute instabilities. Failure to incorporate the global topology of the phase function may result in inaccurate calculations and false conclusions concerning the absolute or convective character of the instability, according to Huerre (Huerre and Monkewitz, 1990). The reader is referred to Lingwood, 1997 for a more complete approach, including numerical examples.

## 2.8 Concluding remark

This chapter discusses the fundamentals of temporal and spatiotemporal stability characterization of confined and open flows using progressive moving of isocontours in the complex frequency ( $\omega$ ) and wavenumber ( $\alpha$ ) planes. Based on the singularity structure of the dispersion relation in the complex  $\omega$  and  $\alpha$ -planes, the principles of Briggs' technique are used to construct general mathematical criteria for defining instabilities as convective or absolute. Locating pinch points in the complex  $\alpha$ -plane

is a key step in detecting absolute instability, which is known as the "cusp map" in the complex-frequency plane (Kupfer, Bers, and Ram, 1987). Furthermore, this chapter attempts to highlight absolute instabilities (perturbations that grow exponentially in time at the point of excitation), convective instabilities (disturbances that are swept downstream from the source and decay at any fixed position in space), and evanescent modes (non-propagating modes or false modes) (Patne and Shankar, 2017). While convectively unstable flows act as spatial amplifiers of incoming interface perturbations, absolutely unstable flows exhibit intrinsic self-sustained dynamics or global modes (Huerre and Monkewitz, 1990). As a result, studying the transition from convective to absolute instability is crucial; however, this study is complicated by the presence of evanescent modes (stable modes) arising from the direct resonance of two coalescing modes originating from waves propagating in the same direction (Koch, 1986).



## Chapter 3

# An analytical approach to the WKB approximation method

### 3.1 Introductory remark

Injecting a fluid into a more viscous fluid in a thin linear channel (or the Hele-Shaw cell) triggers a two-dimensional viscous fingering pattern which is characterized by increasingly long fingers undergoing tip splitting and branching events, also known as the Saffman-Taylor instability (STI) (Saffman and Taylor, 1958). These complex structures are considered to be a paradigm for interfacial pattern formation and have continued to receive prolonged interest in theoretical and experimental studies (Ben-simon et al., 1986; Couder, 2000) as well as due to its practical applicability in crude oil recovery (Homsy, 1987), surface coating (Grillet, Lee, and Shaqfeh, 1999) and electrodeposition (Schröder et al., 2002).

The classical (or Newtonian) STI was outlined by Saffman and Taylor (Saffman and Taylor, 1958), however, the finger selection mechanism in their experiments remained an enigma for several decades. Omitting surface tension, they found a continuous family of solutions with the shape of the interface in the  $x - y$  plane, given by the expression,

$$x = \frac{w(1 - \Lambda)}{2\pi} \ln \left[ \frac{1}{2} \left( 1 + \cos \frac{2\pi y}{\Lambda w} \right) \right], \quad 0 < \Lambda < 1.0. \quad (3.1)$$

Although their analytical expression for the shape of the finger matched well with their experimental observations, the treatment did not explain the specific selection of the relative finger width or  $\Lambda = 0.5$  ( $\Lambda$  is defined as the ratio of the width of the protruding interface to the cell width,  $w$ ). The significance of the surface tension on the shape selection procedure was analytically highlighted much later by Hong (Hong and Langer, 1986), Shraiman (Shraiman, 1986) and Combescot (Combescot et al., 1986), who showed that the surface tension represented a singular perturbation leading to a solvability condition at the finger tip, thereby isolating a particular value from the continuum of solutions proposed by Saffman (which is  $\Lambda = 0.5$ ).

Experiments of viscous fluids pushing a dilute solution of a shear-thinning polymeric liquid (xanthate gum) reveal a strong modification of the finger selection process, in particular, fingers were found to be narrower than the classical limit (Lindner, Bonn, and Meunier, 2000). Numerical simulations of shear thinning fluids (Kondic, Palfy-Muhoray, and Shelley, 1996; Kondic, Palfy-Muhoray, and Shelley, 1980; Fast et al., 2001) divulge that the viscosity is not uniform throughout the cell; regions

of high fluid velocity (thus high shear rate) have low viscosity, especially in front of the fingertip, which leads to an anisotropic system. For weakly shear thinning case (with the viscosity exponent  $0.65 < n < 1$  in Ostwald-de Waele fluids (Ostwald, 1925; Waele, 1923)), Lindner (Lindner, Bonn, and Meunier, 2000) showed that simply replacing the constant viscosity by a shear dependent viscosity, in the control parameter, allows for the rescaling of the data for the relative finger width onto the same, universal curve for Newtonian fluids. Whereas for stronger shear-thinning fluids (dilute solution of polyethylene oxide or PEO, a shear thickening liquid and  $n < 0.65$ ), this rescaling fails, and deviations from the classical limit result towards smaller fingers (Lindner et al., 2002). The experiments of a finger widening phenomena (compared with the Newtonian case) show that the presence of normal stresses in the thin wetting layer was held accountable for the finger widening (Tabeling and Libchaber, 1986). For moderate normal stresses, this allows for the rescaling of the data onto the universal curve for Newtonian fluids and again resolves the finger selection problem.

Despite the fact that the aforementioned investigations have been partially effective in describing the finger widening and thinning phenomena in non-Newtonian fluids empirically, an analytical expression generated via a single, unified theory explaining both of these aspects has yet to be discovered. This chapter seeks to derive such an expression and contrast the findings with the *in vitro* and *in silico* data that are already accessible. It also provides a mathematical method for forecasting the finger width of a straightforward fluid driving a non-Newtonian (power-law) fluid. The Wentzel-Kramers-Brillouin (WKB) technique approximation has been used to characterize the departure from Newtonian viscosity as a singular perturbation in a parameter, leading to a solvability condition at the fingertip, which chooses a unique finger width from the family of solutions. Here, in the limit of small  $\nu$ , one can discover that the relationship between the dimensionless finger width  $\Lambda$  and the dimensionless group of parameters containing the viscosity and surface tension,  $\nu$ , has the form:  $\Lambda \sim \frac{1}{2} - \mathcal{O}(\nu^{-1/2})$  for shear thinning case, and  $\Lambda \sim \frac{1}{2} + \mathcal{O}(\nu^{2/(4-n)})$  for shear thickening case. Finally, a comparison made between the theoretical and experimental finger width data using the linearized model is found to arrive at an excellent agreement near to the power-law exponent,  $n = 1$ .

This chapter is organized as follows: the mathematical model, along with the assumptions, are delineated in 3.2. 3.3 outlines the main result and it also includes the re-calculated cusp function to include all nonlinear terms at the level of the WKB approximation rather than just the leading order term. 3.4 presents the numerical and experimental validation of the analytical results with *in silico* and *in vitro* data collected from the available literature, and the conclusions follow in 3.5.

## 3.2 Mathematical model

The starting point of our analysis is the model proposed by Palffy-Muhoray and co-workers (Kondic, Palffy-Muhoray, and Shelley, 1996), of the slow, two-dimensional flow of an incompressible, non-Newtonian (driven) fluid inside the Hele-Shaw cell,

governed by the (shear-rate) modified Darcy's law,

$$\mathbf{u} = -\frac{b^2}{12\mu(\dot{\gamma})}\nabla p, \quad \nabla \cdot \mathbf{u} = 0, \quad (3.2)$$

where  $b$ ,  $\mathbf{u} = (u_x, u_y)$ ,  $p$ ,  $\mu$ ,  $\dot{\gamma}$  are the cell gap, the gap averaged velocity vector, pressure, viscosity of the non-Newtonian fluid and the shear-rate, respectively.  $(x, y, z)$  denote the flow direction, the direction parallel to the channel width, and the direction along the cell gap, respectively. The adjective 'lateral' will be applied to variations in the  $x - y$  plane, whereas the adjective 'transverse' will be applied to changes across the gap in the  $z$  direction. The other parameters utilized in the model are  $U$ , the velocity of the fingertip,  $w$ , the half-width of the channel (such that  $b/w \ll 1$ ),  $T$ , the interfacial tension between the driven (outside finger) and driving fluids and  $\tilde{\theta}$  is the angle between the tangent to the interface and the flow direction (figure 3.1). The boundary conditions are,

$$\left. \begin{aligned} \mathbf{n} \cdot \mathbf{u} &= U \sin \tilde{\theta} \\ p_0 - p &= \frac{T}{R} \end{aligned} \right\} \text{ on the advancing finger}$$

$$u_y = 0 \quad \text{on the walls: } y = \pm w$$

$$u_x = U\Lambda, u_y = 0 \quad \text{as } x \rightarrow \infty, -w < y < w,$$

$$u_x = u_y = 0 \quad \text{as } x \rightarrow -\infty, w\Lambda < |y| < w. \quad (3.3)$$

where  $p_0$  is the constant pressure inside the finger (assumed zero),  $\mathbf{n}$  is the unit normal to the interface, and  $R$  is the lateral radius of curvature. The underlying assumptions in the model are as follows:

1. In congruence with the in vitro (Lindner, Coussot, and Bonn, 2000; Lindner et al., 2002) and in silico (Kondic, Palfy-Muhoray, and Shelley, 1980; Fast et al., 2001) experiments, it is assumed that the viscosity of the driving (Newtonian) fluid as well as the buoyancy forces are negligible.
2. The driving fluid completely expels the driven fluid. In experimental setups (Tabeling and Libchaber, 1986), this assumption is generally not true since a thin film of the driven fluid is left adhering to the plates. The presence of this finite, spatially varying, wetting film, controls the shape of the advancing interface.
3. The steady, gap-averaged velocity of the fluid,  $\mathbf{u}$ , is low such that the inertial terms in the Navier-Stokes equation may be neglected (i. e., the Stokes-Darcy hypothesis).
4. Palfy-Muhoray and co-workers have argued that the pressure,  $p$ , is essentially harmonic (Kondic, Palfy-Muhoray, and Shelley, 1996), since applying the divergence free condition to equation (3.2) leads to,

$$\mu \nabla^2 p - \mu' \nabla(\mathbf{u} \cdot \mathbf{u}) \cdot \nabla p = 0.$$

Since  $\nabla(\mathbf{u} \cdot \mathbf{u})$  scales like the convective derivative in the Navier-Stokes equation, in the limit of zero Reynolds number, this term may be neglected. Thus,

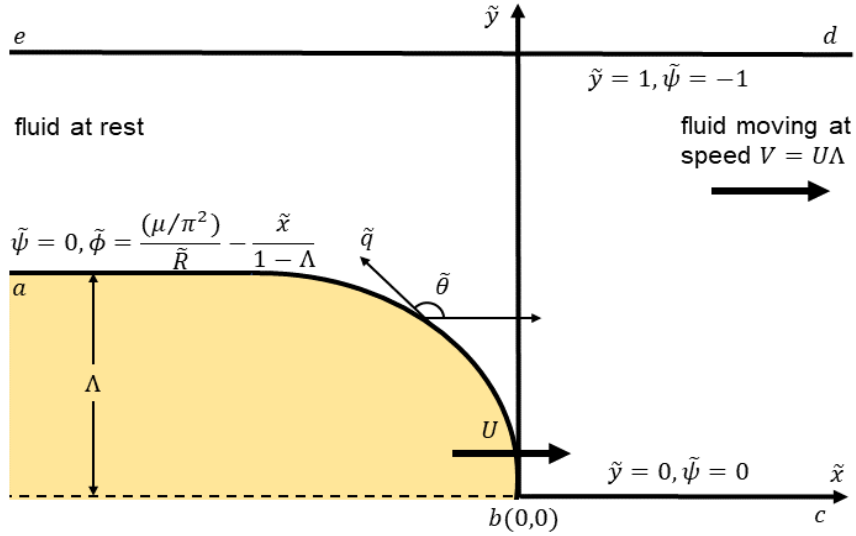


FIGURE 3.1: Schematic diagram of a Saffman-Taylor finger in the laboratory frame, assumed symmetric about the  $\tilde{x}$ -axis.

from equation (3.2) and the harmonicity of  $p$ , an inference can be drawn that,

$$p = -\frac{12\mu}{b^2}\phi, \quad (3.4)$$

where  $\phi$  is the velocity potential. Later, the stream function,  $\psi$  has also been introduced, which is the harmonic conjugate of  $\phi$ , such that  $\mathcal{F} = \phi + i\psi$  is a complex analytic function of  $(x, y)$ .

5. This work is primarily focused on the shear-thinning feature (thereby neglecting the effects of elasticity), and utilize the Ostwald-de Waele (Ostwald, 1925; Waele, 1923) power-law model, representing the viscosity of the non-Newtonian fluid,

$$\mu(\dot{\gamma}) = \mu_0 \dot{\gamma}^{n-1}, \quad (3.5)$$

where,  $\mu_0, n$ , are considered constants. When  $n = 1$  (or  $\mu = \mu_0$ ), the Newtonian fluid is recovered. If  $n < 1$ , the fluid is said to be “pseudoplastic” or “shear thinning” and if  $n > 1$ , the fluid is “dilatant” or “shear thickening”. In reality, both  $\mu_0, n$ , are temperature dependent, and in particular,  $\mu_0$  decreases rapidly with increasing temperature.

6. Finally, in the absence of elastic effects and in the Darcy regime, the flow is assumed to be symmetric about the centerline.

Based on the assumptions listed above, the equations for the steady two-dimensional non-Newtonian flow produced by a finger inside a channel with surface tension effects due to the inclusion of lateral curvature has been derived. Utilizing equations (3.3), the corresponding boundary conditions on the velocity potential,  $\phi$  and the pressure,

$p$  are,

$$\begin{aligned} \frac{\partial \phi}{\partial n} = U \sin \tilde{\theta}, \quad p_0 - p = \frac{T}{R} \quad \text{on the finger} \\ \phi \rightarrow U\Lambda x \quad \text{as } x \rightarrow \infty, -w < y < w, \\ \phi \rightarrow 0 \quad \text{as } x \rightarrow -\infty, w\Lambda < |y| < w. \end{aligned} \quad (3.6)$$

Next, a frame of reference moving with the interface (say, located at  $\zeta_0$ ) with origin at the finger-tip is chosen and the dimensionless variables,  $w$  and  $(1 - \Lambda)U$  as length and velocity scales are also introduced, respectively,

$$\begin{aligned} \tilde{x} = (x - \zeta_0)/w, \quad \tilde{y} = y/w, \quad \tilde{R} = R/w, \\ \tilde{\phi} = \frac{\phi - Ux}{(1 - \Lambda)Uw}, \quad \tilde{\psi} = \frac{\psi - Uy}{(1 - \Lambda)Uw}. \end{aligned} \quad (3.7)$$

Symmetry about the centre-line of the channel has been assumed. The center-line and the interface is the streamline,  $\tilde{\psi} = 0$ , while the wall,  $\tilde{y} = 1$  is the streamline,  $\tilde{\psi} = -1$  (figure 3.1). Thus, the region inside the channel maps onto an infinite strip in the potential plane  $-\infty < \tilde{\phi} < \infty, -1 < \tilde{\psi} < 0$  and our goal is to study the analytic function  $-\log \tilde{q} + i\tilde{\theta}$ , where  $\tilde{u} - i\tilde{v} = \tilde{q}e^{i\tilde{\theta}}$  is the (dimensionless) complex velocity relative to the finger, in terms of the complex potential,  $\tilde{\mathcal{F}} = \tilde{\phi} + i\tilde{\psi}$ .

Now, it can be inferred that the interface (characterized by the arclength,  $s$ ) evolves with time,  $t$ , and in order to describe this evolution more precisely, a complex conformal map,  $\sigma(s, t)$ , is introduced, such that

$$\sigma = s + it = e^{-(\tilde{\mathcal{F}} - \tilde{\phi}_0)\pi}, \quad (3.8)$$

mapping the potential plane onto the upper half of the  $\sigma$ -plane, with the upper wall ( $de$ ) mapped into  $-\infty < s < 0$ , the interface ( $ab$ ) into  $0 \leq s \leq 1$ , the centerline ( $bc$ ) into  $1 < s < \infty$  (refer figure 3.1 for a diagrammatic description).  $\tilde{\phi}_0$  is a (constant) reference potential. If  $\tilde{S}$  denotes the dimensionless arclength along the interface from the finger-tip, then the radius of curvature takes a simple form,

$$\frac{1}{\tilde{R}} = \frac{d\tilde{\theta}}{d\tilde{S}} = \frac{\partial \tilde{\theta}}{\partial \tilde{\phi}} \frac{\partial \tilde{\phi}}{\partial \tilde{S}} = \tilde{q} \frac{\partial \tilde{\theta}}{\partial \tilde{\phi}}. \quad (3.9)$$

Using Cauchy's integral theorem, the speed,  $\tilde{q}$ , on the interface ( $ab$ ) is related to the direction,  $\tilde{\theta}$ , by the Cauchy's principle value integral,

$$\log(\tilde{q}) = -\frac{1}{\pi} \mathcal{P} \int_0^1 \frac{\tilde{\theta} - \pi}{s' - s} ds', \quad (3.10)$$

where the constants are fixed by the requirement that  $\tilde{q} \rightarrow 1$  as  $\phi \rightarrow -\infty$ . Equation (3.10) is found solely from kinematic considerations. However, the dynamics is introduced through equations (3.6, 3.7) and (3.9), which gives,

$$\frac{Tb^2}{12\mu U w^2} \frac{\tilde{q}}{(1 - \Lambda)} \frac{\partial \tilde{\theta}}{\partial \tilde{\phi}} - \frac{\tilde{x}}{1 - \Lambda} = \tilde{\phi}, \quad \tilde{\phi}_0 < \tilde{\phi} < \infty. \quad (3.11)$$

Using  $s$  as the independent variable and the relations,

$$\cos \tilde{\theta} = \frac{d\tilde{x}}{d\tilde{S}}, \quad \frac{d\tilde{\phi}}{d\tilde{S}} = \tilde{q}, \quad \frac{d\tilde{\phi}}{ds} = -\frac{1}{\pi s}, \quad (3.12)$$

now differentiate (3.11) along the interface to obtain the second relation between  $\tilde{q}$  and  $\tilde{\theta}$  (the first relation is equation (3.10)),

$$\frac{Tb^2\pi^2}{12Uw^2}\tilde{q}s\frac{d}{ds}\left(\frac{\tilde{q}s}{\mu}\frac{d\tilde{\theta}}{ds}\right) - (1-\Lambda)\tilde{q} = \cos \tilde{\theta}, \quad 0 < s < 1, \quad (3.13)$$

along with the appropriate boundary conditions,

$$\begin{aligned} \tilde{\theta}(0) &= \pi, & \tilde{q}(0) &= 1/(1-\Lambda), \\ \tilde{\theta}(1) &= \pi/2, & \tilde{q}(1) &= 0, \end{aligned} \quad (3.14)$$

where  $s = 1$  denote the finger-tip. Next, notice that the main shear in the Hele-Shaw cell occurs in the transverse direction, and thus, one may estimate the shear rate,  $\dot{\gamma} \approx \tilde{q}/b$  in the power law model (3.5). Further, note that at  $s = 0$ , equation (3.10) reduces to

$$\log(1-\Lambda) = \frac{1}{\pi} \int_0^1 \frac{\tilde{\theta} - \pi}{s'} ds', \quad (3.15)$$

Utilizing equation (3.15), and introducing a set of new variables,

$$\theta = \tilde{\theta} - \pi, \quad q = (1-\Lambda)\tilde{q}, \quad (3.16)$$

leads us to rewrite the equations (3.10, 3.13),

$$\begin{aligned} v_0 \left\{ \frac{1}{b(1-\Lambda)} \right\}^{(1-n)} q s \frac{d}{ds} \left( q^{(2-n)} s \frac{d\theta}{ds} \right) &= q - \cos \theta, \\ \log q &= -\frac{s}{\pi} \mathcal{P} \int_0^1 \frac{\theta(s')}{s'(s'-s)} ds', \quad s \in [0, 1], \end{aligned} \quad (3.17)$$

alongwith the boundary conditions,

$$\theta(0) = 0, \quad q(0) = 1, \quad \theta(1) = -\pi/2, \quad q(1) = 0, \quad (3.18)$$

where  $v_0 = \frac{Tb^2\pi^2}{12\mu_0Uw^2(1-\Lambda)^2}$ .

### 3.3 Main results

A crucial feature of the integro-differential equations (3.17) is the fact that  $v_0$  appears in the equation as a singular perturbation parameter. It multiplies the highest derivative and, therefore, completely changes the mathematical structure of the problem. When  $v_0 = 0$ , equations (3.17) can be solved explicitly to yield,

$$q_0 = \cos \theta_0 = \left[ \frac{1-s}{1+\alpha s} \right]^{\frac{1}{2}}, \quad (3.19)$$

where  $\alpha = (2\Lambda - 1)/(\Lambda - 1)^2$ . McLean (McLean, 1980) showed that the equation (3.19) satisfies the family of solutions (3.1) proposed by Saffman. Equation (3.19) is automatically consistent with the boundary conditions (3.18) for any  $\Lambda$ , and thus this solution fails to selectively determine a unique value of  $\Lambda$ . Hence, our main result (obtained by Dipa Ghosh, the author of this thesis) (Bansal, Ghosh, and Sircar, 2023) is the following proposition, providing us with a unique solution for the system of equations (3.17), (3.18) in the limit  $v_0 \rightarrow 0$  (but  $v_0 \neq 0$ ).

In the limit  $v_0 \rightarrow 0$ ,  $(q, \theta)$  satisfying equations (3.17) along with the boundary conditions (3.18) has a unique solution provided  $\Lambda$  satisfies the following relation (accurate unto the leading order in  $v_0$ ),

$$\Lambda \sim \begin{cases} \frac{1}{2} - \mathcal{O}(v_0^{-1/2}), & n < 1 \\ \frac{1}{2} + \mathcal{O}(v_0^{2/(4-n)}). & n \geq 1. \end{cases} \quad (3.20)$$

Let us now begin the proof of the above statement by first stating the following trivial (but vital) result, which gives us the necessary condition for the existence of a unique solution.

Consider  $\Theta \in C^\infty(\mathbb{R})$  and a differential operator  $\mathcal{L}$  such that,

$$\mathcal{L}\Theta = \bar{R},$$

where  $\bar{R} \in L^1(\mathbb{R})$ . Let  $\Theta_0$  be the null eigenvector of the adjoint of  $\mathcal{L}$ , or  $\Theta_0 \in \mathcal{N}(\mathcal{L}^\dagger)$ . Further, define the cusp function,  $\mathcal{C} \in L^1(\mathbb{R})$ , such that

$$\mathcal{C} = \int_{-\infty}^{\infty} d\eta \Theta_0 \bar{R}(\eta). \quad (3.21)$$

If  $\Theta$  exists uniquely, then  $\mathcal{C} \equiv 0$ .

The proof of the above result follows from the observation that

$$\int_{-\infty}^{\infty} d\eta \Theta_0 \mathcal{L}(\Theta) = \int_{-\infty}^{\infty} d\eta \Theta_0 \bar{R}(\eta) = \int_{-\infty}^{\infty} d\eta \Theta_0 \mathcal{L}^\dagger(\Theta_0) = 0,$$

provided that  $\Theta$  is sufficiently well behaved such that the above integral is convergent.

Next, let us linearize around the zero-surface tension solution by defining  $\theta_1$  through,

$$\theta(s) = \theta_0(s) + v_0 \theta_1, \quad (3.22)$$

where the perturbation  $\theta_1$  satisfies the boundary conditions  $\theta_1(0) = \theta_1(1) = 0$ . Similarly, as a consequence of equation (3.17), the perturbation in  $q$  takes the form,

$$\ln q_1(s) = -\frac{s}{\pi} \mathcal{P} \int_0^1 \frac{\theta_1(s')}{s'(s'-s)} ds' = -\frac{1}{\pi} \mathcal{P} \int_0^1 \frac{\theta_1(s')}{(s'-s)} ds', \quad (3.23)$$

where the second equality in equation (3.23) holds via a direct application of the Cauchy residue theorem and the fact that  $\theta_1(0) = 0$ . From equations (3.22) and (3.23),

it can be inferred that,

$$\begin{aligned} q &\approx q_0(1 + \nu_0 \ln q_1) \\ \cos \theta_0 &\approx q_0 - \nu_0 \theta_1 \sin \theta_0. \end{aligned} \quad (3.24)$$

Next, a singular perturbation expansion is carried out in which, the terms which are quadratic and higher order in  $\nu_0$  are neglected, to arrive at the following form of equation (3.17), substitute the relations (3.24) in equations (3.17), to get,

$$\begin{aligned} \nu_0(q_0 + \nu_0 q_0 \ln q_1) s \frac{d}{ds} \left[ \{b(1 - \Lambda)\}^{(n-1)} (q_0 + \nu_0 q_0 \ln q_1)^{(2-n)} s \frac{d}{ds} (\theta_0 + \nu_0 \theta_1) \right] \\ = q_0(1 + \nu_0 \ln q_1) - \cos(\theta_0 + \nu_0 \theta_1). \end{aligned}$$

But  $\cos(\theta_0 + \nu_0 \theta_1) \approx q_0 - \nu_0 \theta_1 \sin \theta_0$ . This implies,

$$\begin{aligned} \nu_0(q_0 + \nu_0 q_0 \ln q_1) s \frac{d}{ds} \left[ \{b(1 - \Lambda)\}^{(n-1)} (q_0 + \nu_0 q_0 \ln q_1)^{(2-n)} s \left( \frac{d\theta_0}{ds} + \nu_0 \frac{d\theta_1}{ds} \right) \right] \\ = q_0 + \nu_0 q_0 \ln q_1 - q_0 + \nu_0 \theta_1 \sin \theta_0 \\ = \nu_0(q_0 \ln q_1 + \theta_1 \sin \theta_0), \end{aligned}$$

or

$$\begin{aligned} \{b(1 - \Lambda)\}^{(n-1)} (\nu_0 q_0 s + \nu_0^2 q_0 s \ln q_1) \frac{d}{ds} \left[ (q_0 + \nu_0 q_0 \ln q_1)^{(2-n)} s \left( \frac{d\theta_0}{ds} + \nu_0 \frac{d\theta_1}{ds} \right) \right] \\ = \nu_0(q_0 \ln q_1 + \theta_1 \sin \theta_0). \end{aligned}$$

Next, using the binomial expansion of  $(1 + x)^{-n}$ , it can be found that,

$$\begin{aligned} q_0^{(2-n)} (1 + \nu_0 \ln q_1)^2 (1 + \nu_0 \ln q_1)^{-n} &= q_0^{(2-n)} (1 + \nu_0^2 (\ln q_1)^2 + 2\nu_0 \ln q_1) \\ (1 - n\nu_0 \ln q_1 + \frac{n(n+1)}{2!} (\nu_0 \ln q_1)^2 + \dots) &= q_0^{(2-n)} (1 + 2\nu_0 \ln q_1) (1 - n\nu_0 \ln q_1). \end{aligned}$$

Now, using the above binomial expansion and neglecting terms involving  $\nu_0^2$  and higher powers of  $\nu_0$  simplifies the above equation and provides the following relation for  $\theta_1$ ,

$$\begin{aligned} \{b(1 - \Lambda)\}^{(n-1)} (q_0 s) \frac{d}{ds} \left[ (q_0)^{(2-n)} s \frac{d\theta_0}{ds} \right] + \nu_0 \{b(1 - \Lambda)\}^{(n-1)} (q_0 s) \frac{d}{ds} \left[ (q_0)^{(2-n)} s \frac{d\theta_1}{ds} \right] \\ = q_0 \ln q_1 + \theta_1 \sin \theta_0. \end{aligned}$$

Dividing the above equation throughout by  $\{b(1 - \Lambda)\}^{(n-1)}$  and rearranging the terms, the following equation (3.25) is arrived at.



$$v_0 \frac{d^2 \theta_1}{ds^2} + \frac{1}{q_0^{(2-n)} s} v_0 \left\{ s \frac{d}{ds} (q_0^{(2-n)}) + q_0^{(2-n)} \right\} \frac{d\theta_1}{ds} - \left\{ \frac{1}{(b(1-\Lambda))^{(n-1)}} \frac{1}{q_0^{(3-n)} s^2} \sin \theta_0 \right\} \theta_1 - \frac{1}{(b(1-\Lambda))^{(n-1)}} \frac{1}{q_0^{(2-n)} s} \ln q_1 = - \frac{1}{q_0^{(2-n)} s} \frac{d}{ds} \left( q_0^{(2-n)} s \frac{d\theta_0}{ds} \right). \quad (3.25)$$

Alternatively, the equation (3.25) can be written in a concise form as follows,

$$v_0 \frac{d^2 \theta_1(s)}{ds^2} + v_0 P(s) \frac{d\theta_1(s)}{ds} + Q(s) \theta_1(s) + H(s) \mathcal{P} \int_0^1 ds' \frac{\theta_1(s')}{(s' - s)} = R(s), \quad (3.26)$$

where

$$\begin{aligned} P(s) &= \frac{1}{s} + \frac{1}{q_0^{(2-n)}} \frac{d}{ds} (q_0^{(2-n)}) = \frac{1}{s} - \left( \frac{2-n}{2} \right) \frac{(1+\alpha)}{(1-s)(1+\alpha s)} \\ Q(s) &= - \frac{1}{\{b(1-\Lambda)\}^{(n-1)}} \frac{1}{q_0^{(3-n)} s^2} \sin \theta_0 = \frac{1}{\{b(1-\Lambda)\}^{(n-1)}} \frac{(1+\alpha)^{\frac{1}{2}} (1+\alpha s)^{\left(\frac{2-n}{2}\right)}}{(1-s)^{\left(\frac{3-n}{2}\right)} s^{\frac{3}{2}}} \\ H(s) &= \frac{1}{\pi} \frac{1}{\{b(1-\Lambda)\}^{(n-1)}} \frac{1}{q_0^{(2-n)} s^2} = \frac{1}{\pi} \frac{1}{\{b(1-\Lambda)\}^{(n-1)}} \frac{(1+\alpha s)^{\left(\frac{2-n}{2}\right)}}{s^2 (1-s)^{\left(\frac{2-n}{2}\right)}} \\ R(s) &= - \frac{1}{q_0^{(2-n)} s} \frac{d}{ds} \left( q_0^{(2-n)} s \frac{d\theta_0}{ds} \right) \\ &= \frac{(1+\alpha)^{\frac{1}{2}}}{2s^{\frac{1}{2}} (1-s)^{\frac{1}{2}} (1+\alpha s)} \left[ \frac{1}{2s} - \left( \frac{1-n}{2} \right) \frac{1}{(1-s)} - \left( \frac{4-n}{2} \right) \frac{\alpha}{1+\alpha s} \right], \end{aligned} \quad (3.27)$$

where the second equality in each of the above expressions follows from equation (3.19). Next, the following change of variable is made,

$$\eta = \left[ \frac{1-s}{(1+\alpha)s} \right]^{\frac{1}{2}}. \quad (3.28)$$

In terms of Cartesian coordinates,  $\eta$  is the slope which varies from  $-\infty$  to  $\infty$  as one traverses the finger arc-length through  $\eta = 0$  at the finger tip, i. e.,  $s = 1$  (equivalently,  $\eta = \tan(\pi/2 + \theta_0) = -\cot \theta_0 = \left( \frac{1-s}{(1+\alpha)s} \right)^{\frac{1}{2}}$ ). Now, equation (3.28) is used to rewrite equation (3.26), that is given as follows,

$$v_0 \frac{d^2 \theta_1(\eta)}{d\eta^2} + v_0 \left[ \frac{d^2 \eta}{ds^2} + P \frac{d\eta}{ds} \right] \frac{1}{\left( \frac{d\eta}{ds} \right)^2} \frac{d\theta_1(\eta)}{d\eta} + \frac{Q}{\left( \frac{d\eta}{ds} \right)^2} \theta_1(\eta) + \frac{H}{\left( \frac{d\eta}{ds} \right)^2} I = \frac{R}{\left( \frac{d\eta}{ds} \right)^2}, \quad (3.29)$$

where  $I$  is defined as the integral in equation (3.26). Here, a change of variable is made in order to eliminate the first derivative. This is done by introducing the variable  $\Theta(\eta)$ , and defining  $\theta_1(\eta) = g(\eta)\Theta(\eta)$ , where  $g(\eta)$  is chosen in such a way

that the coefficient of the first derivative vanishes in equation (3.29). Thus, ignoring the non-singular terms of order  $v_0$  and considering only terms consistent with the first approximation can give us the following form,

$$v_0 \frac{d^2 \Theta}{d\eta^2} + v_0 \left( 2 \frac{g'}{g} + \frac{\frac{d^2 \eta}{ds^2} + P \frac{d\eta}{ds}}{(d\eta/ds)^2} \right) \frac{d\Theta}{d\eta} + \frac{Q}{\left(\frac{d\eta}{ds}\right)^2} \Theta(\eta) + \frac{H}{g \left(\frac{d\eta}{ds}\right)^2} I = \frac{R}{g \left(\frac{d\eta}{ds}\right)^2}. \quad (3.30)$$

In order to eliminate the first derivative, the function  $g$  should satisfy the following equation,

$$\ln g = \ln(k) - \frac{1}{2} \int \frac{\frac{d^2 \eta}{ds^2} + P \frac{d\eta}{ds}}{(d\eta/ds)^2} d\eta. \quad (3.31)$$

Using equation (3.28) to find the derivatives,

$$\begin{aligned} \eta' &= -\frac{1}{2s^{3/2}(1-s)^{1/2}(1+\alpha)^{1/2}}, \\ \eta'' &= -\frac{1}{2s^{3/2}(1-s)^{1/2}(1+\alpha)^{1/2}} \left[ \frac{1}{2(1-s)} - \frac{3}{2s} \right], \end{aligned} \quad (3.32)$$

the following form of  $g(s)$  is obtained,

$$g = \frac{s^{1/4}(1-s)^{(n-1)/4}}{(1+\alpha)^{1/4}(1+\alpha s)^{(n-2)/4}}, \quad (3.33)$$

where the scale  $k$  in equation (3.31) is chosen as  $k = 1$ .  $()'$  denotes the derivative with respect to  $s$ . The function  $g$  can be written in terms of the new variable  $\eta$  as follows,

$$g = \frac{\eta^{(n-1)/2}(1+\eta^2)^{(2-n)/4}}{(1+\beta^2\eta^2)^{1/2}}, \quad (3.34)$$

such that,

$$\Theta = \frac{(1+\beta^2\eta^2)^{1/2}}{\eta^{(n-1)/2}(1+\eta^2)^{(2-n)/4}} \theta_1. \quad (3.35)$$

The parameter  $\beta = (1+\alpha)^{1/2} = \frac{\Lambda}{1-\Lambda}$  is introduced in equations (3.34), (3.35). The coefficients of (3.30) should be computed in terms of  $\eta$ . To do that, let us first see that the integral  $I$  is,

$$I = -2 \int_{\infty}^0 d\eta' \frac{\eta'^{(n+1)/2}(1+\eta'^2)^{(2-n)/4}}{(\eta'^2 - \eta'^2)} \frac{1+\beta^2\eta'^2}{(1+\beta^2\eta'^2)^{3/2}} \Theta(\eta'). \quad (3.36)$$

The integral term  $\bar{H} = \frac{H}{g \left(\frac{d\eta}{ds}\right)^2} I$  can be written as,

$$\bar{H} = \frac{4\beta^4 \eta^{(n+1)/2} (1+\eta^2)^{\frac{2-n}{4}}}{\pi \{b(1-\Lambda)\}^{(n-1)} (1+\beta^2\eta^2)^{1/2}} \int_{\infty}^0 \frac{(\eta'^2 + 1)^{(2-n)/4} (\eta'^2)^{(n-1)/4}}{(1+\beta^2\eta'^2)^{3/2}} \left( \frac{1}{\eta + \eta'} - \frac{1}{\eta - \eta'} \right) \Theta(\eta') d\eta' \quad (3.37)$$

Now, by substituting  $\eta' \rightarrow -\eta'$  in equation (3.37) and considering  $\Theta(-\eta') = -\Theta(\eta')$ ,  $\bar{H}$  can be written as,

$$\bar{H} = \frac{4\beta^4 \eta^{(n+1)/2} (1 + \eta^2)^{\frac{2-n}{4}}}{\pi \{b(1 - \Lambda)\}^{(n-1)} (1 + \beta^2 \eta^2)^{1/2}} \left[ \mathcal{P} \int_{-\infty}^{\infty} \frac{(\eta'^2)^{(n-1)/4} (\eta'^2 + 1)^{(2-n)/4} \Theta(\eta')}{(1 + \beta^2 \eta'^2)^{3/2}} \frac{\Theta(\eta')}{\eta - \eta'} d\eta' \right]. \quad (3.38)$$

The extension of the range of  $\eta$  to include the negative real axis is allowed since only symmetric fingers are considered. Hence  $\theta_1$  and therefore  $\Theta$  are antisymmetric functions of their arguments. Similarly, the coefficients of the linear term and the inhomogeneous term on the right-hand side of equation (3.30) are redefined as  $\bar{Q}_1 = Q/(d\eta/ds)^2$  and  $\bar{R} = R/g(d\eta/ds)^2$ . Hence, equations (3.17) have been transformed into

$$v_0 \frac{d^2 \Theta(\eta)}{d\eta^2} + \bar{Q}_1(\eta) \Theta(\eta) + \frac{1}{\pi} \mathcal{P} \int_{-\infty}^{\infty} d\eta' \frac{\bar{Q}_2(\eta, \eta') \Theta(\eta')}{\eta - \eta'} = \bar{R}(\eta), \quad (3.39)$$

where,

$$\begin{aligned} \bar{Q}_1(\eta) &= \frac{4}{\{b(1 - \Lambda)\}^{(n-1)}} \left[ \frac{(1 + \eta^2)^{\frac{2-n}{2}}}{\eta^{1-n}} \frac{\beta^4}{(1 + \beta^2 \eta^2)^2} \right] \\ \bar{Q}_2(\eta, \eta') &= \frac{4\beta^4 \eta^{(n+1)/2} (1 + \eta^2)^{\frac{2-n}{4}}}{\{b(1 - \Lambda)\}^{(n-1)} (1 + \beta^2 \eta^2)^{1/2}} \left[ \frac{\eta'^{(n-1)/2} (\eta'^2 + 1)^{(2-n)/4}}{(1 + \beta^2 \eta'^2)^{3/2}} \right] \\ \bar{R}(\eta) &= \frac{\eta^{\frac{3-n}{2}}}{(1 + \beta^2 \eta^2)^{1/2} (1 + \eta^2)^{\frac{10-n}{4}}} \left[ \beta^2 (1 + \eta^2) - (1 - n) \frac{(1 + \eta^2)}{\eta^2} - (4 - n)(\beta^2 - 1) \right]. \end{aligned} \quad (3.40)$$

Now, utilize equation (3.21) to find the null eigenvector of the adjoint operator,  $\mathcal{L}^\dagger$ , in equation (3.39). Multiplying by  $\Theta_0$  and integrating, the left hand side of equation (3.25) is,

$$\begin{aligned} \int_0^\infty d\eta \Theta_0(\eta) \mathcal{L} \Theta(\eta) &= \int_0^\infty d\eta \Theta_0(\eta) v_0 \frac{d^2 \Theta(\eta)}{d\eta^2} + \int_0^\infty d\eta \Theta_0(\eta) \bar{Q}_1(\eta) \Theta(\eta) + \\ &\int_0^\infty d\eta \Theta_0(\eta) \frac{1}{\pi} \left\{ \mathcal{P} \int_{-\infty}^0 d\eta' \frac{\bar{Q}_2(\eta, \eta') \Theta(\eta')}{\eta - \eta'} + \mathcal{P} \int_0^\infty d\eta' \frac{\bar{Q}_2(\eta, \eta') \Theta(\eta')}{\eta - \eta'} \right\} \end{aligned} \quad (3.41)$$

Integrating by parts, the first term on the right-hand side of (3.41) can be written as

$$\int_0^\infty d\eta \Theta_0(\eta) v_0 \frac{d^2 \Theta(\eta)}{d\eta^2} = [\Theta_0 v_0 \Theta' - \Theta_0' v_0 \Theta] \Big|_0^\infty + \int_0^\infty d\eta \Theta(\eta) v_0 \frac{d^2 \Theta_0(\eta)}{d\eta^2}. \quad (3.42)$$

First, the term in the square bracket on the right-hand side of equation (3.42) is analyzed. It was shown that this term is at the side of the finger for which  $\eta = \infty$  vanishes (Hong and Langer, 1986). The later discussion is centered around the value of this term at the fingertip for which  $\eta = 0$ . The explicit form of  $\Theta$  is unknown, but as the equation (3.35) relates  $\Theta$  to the angle at the tip of the finger, this problem is resolved. So, from equation (3.35), it can be found that when  $\eta = 0$ ,  $\Theta|_{\text{tip}} = \theta_1|_{\text{tip}}$ .

Further, the derivative of equation (3.35) with respect to  $\eta$  reveals that at the tip of the finger,  $\Theta'|_{\text{tip}} = \theta'_1|_{\text{tip}}$ . Furthermore, it can be seen that  $\frac{d\theta_1}{d\eta}|_{\text{tip}} = \frac{d\theta_1}{ds}|_{\text{tip}} \frac{ds}{d\eta}|_{\text{tip}}$ , but  $\frac{ds}{d\eta}|_{\text{tip}} = 0$ , so the first term in the square bracket on the right-hand side of (3.42) vanishes. For physical solutions, the term  $\theta_1|_{\text{tip}}$  is required to vanish (or  $\theta_1(0) = 0$ ) and therefore consequently the second term in the square bracket also vanishes.

Next, by changing  $\eta' \rightarrow -\eta'$  and  $\eta \rightarrow -\eta$ , the third term on the right hand side of equation (3.41) modifies to,

$$\begin{aligned} \int_0^\infty d\eta \Theta_0(\eta) \frac{1}{\pi} \mathcal{P} \int_{-\infty}^0 d\eta' \frac{\bar{Q}_2(\eta, \eta') \Theta(\eta')}{\eta - \eta'} &= \int_{-\infty}^0 -d\eta' \Theta(-\eta') \frac{1}{\pi} \mathcal{P} \int_0^{-\infty} -d\eta \frac{\bar{Q}_2(-\eta, -\eta') \Theta_0(-\eta)}{\eta' - \eta} \\ &= \int_{-\infty}^0 d\eta' \Theta(\eta') \frac{1}{\pi} \mathcal{P} \int_0^{-\infty} d\eta \frac{\bar{Q}_2(\eta, \eta') \Theta_0(\eta)}{\eta - \eta'} \\ &= \int_0^\infty d\eta' \Theta(\eta') \frac{1}{\pi} \mathcal{P} \int_{-\infty}^0 d\eta \frac{\bar{Q}_2(\eta, \eta') \Theta_0(\eta)}{\eta - \eta'} \\ &= \int_0^\infty d\eta \Theta(\eta) \frac{1}{\pi} \mathcal{P} \int_{-\infty}^0 d\eta' \frac{\bar{Q}_2(\eta', \eta) \Theta_0(\eta')}{\eta' - \eta}. \end{aligned} \quad (3.43)$$

In the above implication, the symmetries  $\bar{Q}_2(-\eta, -\eta') = -\bar{Q}_2(\eta, \eta')$  and  $\Theta(-\eta') = -\Theta(\eta')$  are utilized in order to find a  $\Theta_0(\eta)$  such that  $\Theta_0(-\eta) = -\Theta_0(\eta)$ . Further,  $\eta'$  and  $\eta$  has been changed to  $\eta$  and  $\eta'$ , respectively, to write the last equality in equation (3.43). Similarly, changing  $\eta' \rightarrow \eta$  and  $\eta \rightarrow \eta'$ , the fourth term in the right-hand side of equation (3.41) is rewritten as

$$\int_0^\infty d\eta \Theta_0(\eta) \frac{1}{\pi} \mathcal{P} \int_0^\infty d\eta' \frac{\bar{Q}_2(\eta, \eta') \Theta(\eta')}{\eta - \eta'} = \int_0^\infty d\eta \Theta(\eta) \frac{1}{\pi} \mathcal{P} \int_0^\infty d\eta' \frac{\bar{Q}_2(\eta', \eta) \Theta_0(\eta')}{\eta' - \eta}. \quad (3.44)$$

Using relations (3.42, 3.43, 3.44), the equation (3.41) can be rewritten as,

$$\begin{aligned} \int_0^\infty d\eta \Theta_0(\eta) \mathcal{L} \Theta(\eta) &= \int_0^\infty d\eta \Theta(\eta) v_0 \frac{d^2 \Theta_0(\eta)}{d\eta^2} + \int_0^\infty d\eta \Theta(\eta) \bar{Q}_1(\eta) \Theta_0(\eta) + \\ &\quad \int_0^\infty d\eta \Theta(\eta) \frac{1}{\pi} \left\{ \mathcal{P} \int_{-\infty}^\infty d\eta' \frac{\bar{Q}_2(\eta', \eta) \Theta_0(\eta')}{\eta' - \eta} \right\}. \end{aligned} \quad (3.45)$$

From equation (3.45), the adjoint operator  $\mathcal{L}^\dagger$  can be defined as,

$$\mathcal{L}^\dagger \Theta_0 \equiv v_0 \frac{d^2 \Theta_0(\eta)}{d\eta^2} + \bar{Q}_1(\eta) \Theta_0(\eta) + \frac{1}{\pi} \mathcal{P} \int_{-\infty}^\infty d\eta' \frac{\bar{Q}_2(\eta', \eta) \Theta_0(\eta')}{\eta' - \eta} \quad (3.46)$$

From (3.21), a conclusion can be drawn that if a solution to the equation  $\mathcal{L}^\dagger \Theta_0 = 0$ , is found, with  $\Theta_0(-\eta) = -\Theta_0(\eta)$ , then the right-hand side of equation (3.45) as well as the cusp function vanishes (see equation (3.21)).

Suppose  $\Theta_0$  has the WKB form  $e^{\frac{S}{\sqrt{v_0}}}$ , where the real part of  $S < 0$ , and  $S$  has points of stationary phase (i.e. points  $\bar{\eta}$  where  $S'(\bar{\eta}) = 0$ ). Then, in the limit of  $v_0 \rightarrow 0$ , the following integral can be evaluated by expanding the exponent around

the point of the stationary phase,

$$\mathcal{P} \int_{-\infty}^{\infty} d\eta' \frac{\bar{Q}_2(\eta', \eta) \Theta_0(\eta')}{\eta' - \eta} \simeq e^{\frac{S(\eta)}{\sqrt{v_0}}} \mathcal{P} \int_{-\infty}^{\infty} d\eta' \frac{\bar{Q}_2(\eta', \eta) e^{\frac{S'(\eta)(\eta' - \eta)^2}{2i\sqrt{v_0}}}}{\eta' - \eta}. \quad (3.47)$$

The only contribution to the integral that is not exponentially small comes from the pole at  $\eta' = \eta$ , hence,

$$\mathcal{P} \int_{-\infty}^{\infty} d\eta' \frac{\bar{Q}_2(\eta', \eta) \Theta_0(\eta')}{\eta' - \eta} = \pi i e^{\frac{S(\eta)}{\sqrt{v_0}}} e^{\frac{S'(\eta)(\eta - \eta)^2}{2i\sqrt{v_0}}} \bar{Q}_2(\eta, \eta) = \pi i \bar{Q}_2(\eta, \eta) \Theta_0(\eta), \quad (3.48)$$

and defining  $\bar{Q} = \bar{Q}_1 + i\bar{Q}_2(\eta, \eta)$ , the equation for the null eigenvector of  $\mathcal{L}^\dagger$  becomes

$$v \frac{d^2 \Theta_0(\eta)}{d\eta^2} + \bar{Q} \Theta_0(\eta) = 0, \quad (3.49)$$

where

$$\bar{Q}(\eta) = \frac{4\beta^4}{\{b(1 - \Lambda)\}^{(n-1)} \eta^{(1-n)}} \left[ \frac{(1 + i\eta)^{\frac{4-n}{2}} (1 - i\eta)^{\frac{2-n}{2}}}{(1 + \beta^2 \eta^2)^2} \right]. \quad (3.50)$$

Now, a solution of the equation (3.49) is searched, which is of the form  $\Theta_0 \sim \exp(S/\sqrt{v_0})$ , where  $S$  can be expanded in powers of  $\sqrt{v_0}$ ,

$$S = \sum_{n=0}^{\infty} S_n v^{\frac{n}{2}}. \quad (3.51)$$

In this section, the first two terms of this expansion are retained and also the method is extended in  $n^{th}$  order to include all terms. Thus,  $\Theta_0$  can be written as,

$$\Theta_0 = e^{\frac{S_0}{\sqrt{v_0}} + S_1}, \quad (3.52)$$

$$\frac{d\Theta_0}{d\eta} = \left( \frac{S'_0}{\sqrt{v_0}} + S'_1 \right) e^{\frac{S_0}{\sqrt{v_0}} + S_1}, \quad (3.53)$$

and

$$\frac{d^2 \Theta_0}{d\eta^2} = \left( \frac{S''_0}{\sqrt{v_0}} + S''_1 \right) e^{\frac{S_0}{\sqrt{v_0}} + S_1} + \left( \frac{S'_0}{\sqrt{v_0}} + S'_1 \right)^2 e^{\frac{S_0}{\sqrt{v_0}} + S_1}. \quad (3.54)$$

Substituting equations (3.52), (3.53) and (3.54) into equation (3.49), equation (3.55) is obtained as,

$$v_0 \left( \frac{S''_0}{\sqrt{v_0}} + S''_1 + \frac{S_0'^2}{v_0} + 2 \frac{S'_0 S'_1}{\sqrt{v_0}} + S_1'^2 \right) + \bar{Q} = 0. \quad (3.55)$$

From equation (3.55), the leading and the first order terms  $v_0$  can be written, as follows,

$$S_0'^2 + \bar{Q} = 0, \quad (3.56a)$$

$$S_0'' + 2S'_0 S'_1 = 0, \quad (3.56b)$$

which gives a set of equations for  $S_0$  and  $S_1$ . From equation (3.56a),  $S_0$  has the form,

$$S_0 = i \int_0^\eta d\eta \bar{Q}^{1/2}, \quad (3.57)$$

and from equation (3.56b),  $S_1$  has the form,

$$S_1 = \ln \bar{Q}^{-1/4}, \quad (3.58)$$

Equations (3.57) and (3.58) implies that,

$$\Theta_0 = \frac{e^{S_0/\sqrt{v_0}}}{\bar{Q}^{1/4}}. \quad (3.59)$$

Using equation (3.50),  $S_0$  can be written as,

$$S_0 = \frac{2\beta^2 i}{\{b(1-\Lambda)\}^{(n-1)/2}} \int_0^\eta d\eta' \left[ \frac{(1+i\eta')^{(4-n)/4} (1-i\eta')^{(2-n)/4}}{\eta'^{(1-n)/2} (1+\beta^2\eta'^2)} \right]. \quad (3.60)$$

Since the complex conjugate of  $\Theta_0$  is also a solution of equation (3.49). So, the appropriate antisymmetric combination of the solution is given by

$$\frac{1}{2i} [\Theta_0 - \Theta_0^*] = \text{Im}\Theta_0, \quad (3.61)$$

implying that the cusp function (3.21) is

$$\mathcal{C}(\Lambda, v_0) = \int_{-\infty}^{\infty} d\eta \text{Im}\Theta_0 \bar{R}(\eta) = \int_{-\infty}^{\infty} d\eta \mathcal{F}(\eta) e^{S_0/\sqrt{v_0}}, \quad (3.62)$$

where  $\mathcal{F}$  can be written from equation (3.40) and (3.50), as follows,

$$\begin{aligned} \mathcal{F} &= \frac{\bar{R}}{i\bar{Q}^{1/4}} \\ &= \frac{-i\{b(1-\Lambda)\}^{(n-1)/4}}{\sqrt{2\beta}\eta^{\frac{3n+1}{4}}(1+\eta^2)^{\frac{23-3n}{8}}} \left[ (n-1) + \eta^2(3 + \beta^2(\eta^2 + n - 3)) \right] \left( \frac{1-i\eta}{1+i\eta} \right)^{\frac{1}{8}}. \end{aligned} \quad (3.63)$$

From equation (3.60), it is seen that  $\eta = i$  is the point of stationary phase while  $\eta = \eta_b = \frac{i}{\beta}$  is a logarithmic branch point of the integral in equation (3.62). There are two qualitatively different situations, as can be seen in fig 3.2.

- Case I:  $\beta < 1$  (or  $\Lambda < 1/2$ )

In this case, the branch point,  $\eta_b$ , lies out of the contour of integration for evaluating  $\mathcal{C}$  (fig 3.2a), which implies that it can be integrated by expanding  $S_0(\eta)$  around the point of stationary phase,  $\eta = i$ . Introducing a variable  $\omega$

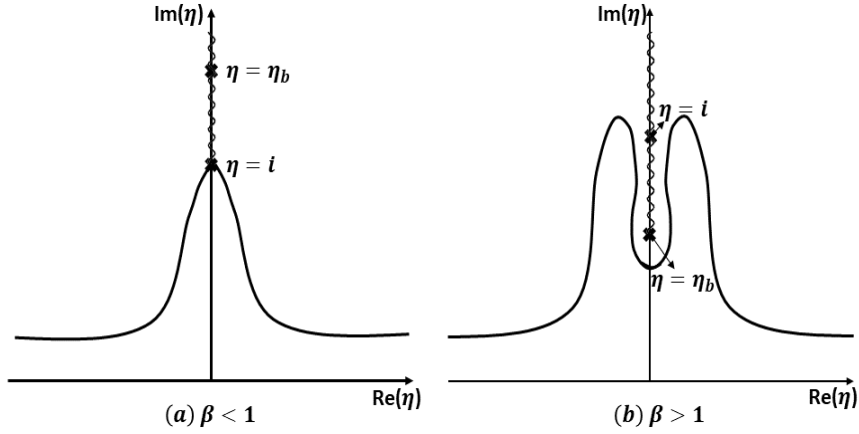


FIGURE 3.2: Contours of integration for the evaluation of the cusp function,  $\mathcal{C}$  (3.21):Cusp

such that  $\eta = i + \omega$ ,  $S_0$  can be written as,

$$S_0 = \frac{2\beta^2 i}{\{b(1-\Lambda)\}^{(n-1)/2}} \int_0^i d\eta' \left[ \frac{(1+i\eta')^{(4-n)/4} (1-i\eta')^{(2-n)/4}}{\eta'^{(1-n)/2} (1+\beta^2 \eta'^2)} \right] \\ + \frac{2\beta^2 i}{\{b(1-\Lambda)\}^{(n-1)/2}} \int_i^{i+\omega} d\eta' \left[ \frac{(1+i\eta')^{(4-n)/4} (1-i\eta')^{(2-n)/4}}{\eta'^{(1-n)/2} (1+\beta^2 \eta'^2)} \right]. \quad (3.64)$$

In the first integral on the right-hand side of equation (3.64), a change of variable  $u = -i\eta'$  is made, and the resultant integral is,

$$I_1(\Lambda) = \left[ -\frac{2\beta^2}{\{b(1-\Lambda)\}^{(n-1)/2}} \int_0^1 \frac{(1-u)^{4-n/4} (1+u)^{2-n/4}}{(1-\beta^2 u^2) u^{1-n/2}} du \right] i^{n-1} \\ \approx \underbrace{\frac{-2\Lambda^2}{\{b(1-\Lambda)\}^{(n-1)/2} (1-2\Lambda)} \mathcal{B}\left(\frac{n+1}{2}, \frac{8-n}{4}\right) {}_2F_1\left(\frac{n-2}{4}, \frac{n+1}{2}; \frac{n+10}{4}; -1\right)}_{= A_1 \text{ (to be used in equation (3.69))}} i^{n-1}, \quad (3.65)$$

where  $\mathcal{B}(\cdot, \cdot)$  and  ${}_2F_1(\cdot, \cdot, \cdot, \cdot)$  are the Beta function and the Hypergeometric function, respectively. For the second integral in equation (3.64), approximating it for small  $\omega$  can reduce the integral to

$$I_2(\Lambda) = \frac{2^{14-n} i^{6+n}}{(8-n) \{b(1-\Lambda)\}^{n-1} (1-2\Lambda)} \Lambda^2 \omega^{8-n}. \quad (3.66) \\ = A \text{ (to be used in equation (3.68))}$$

The details of the expressions are found in equation (3.65) and (3.66). Thus,  $S_0(\eta) = I_1(\Lambda) + I_2(\Lambda)$ , in the neighborhood of the point of stationary phase.

For consistency,  $\mathcal{F}(\eta)$  is expanded in the neighbourhood of  $\eta = i$  (i. e., substituting  $\eta = i + \omega$  in equation (3.63)), leading to,

$$\mathcal{F}(\omega) = \underbrace{\{b(1-\Lambda)\}^{(n-1)/4} \frac{(4-n)}{2^{27-3n/8}} \frac{(1-2\Lambda)}{\Lambda(1-\Lambda)} 2^{1/8} i^{14-3n/8} \omega^{3n-24/8}}_{= B \text{ (to be used in equation (3.68))}}. \quad (3.67)$$

Finally, the cusp function is,

$$\begin{aligned} \mathcal{C} &= \int_{-\infty}^{\infty} \mathcal{F}(\eta) e^{\frac{S_0}{\sqrt{v_0}} \eta} d\eta = \int_{-\infty}^{\infty} \mathcal{F}(\omega) e^{\frac{S_0}{\sqrt{v_0}} \omega} d\omega \\ &= B e^{\frac{I_1(\Lambda)}{\sqrt{v_0}}} \int_{-\infty}^{\infty} \omega^{3n-24/8} e^{\frac{A}{\sqrt{v_0}} \omega^{8-n/4}} d\omega. \end{aligned} \quad (3.68)$$

Substituting,  $x = \frac{A}{\sqrt{v_0}} \omega^{8-n/4}$  in equation (3.68), it is found that,

$$\begin{aligned} \mathcal{C} &= \frac{4}{8-n} B e^{\frac{I_1(\Lambda)}{\sqrt{v_0}}} \left( \frac{\sqrt{v_0}}{A} \right)^{\frac{3n-16}{16-2n}} \int_{-\infty}^{\infty} x^{\frac{5n-32}{16-2n}} e^x dx \\ &= B e^{\frac{I_1(\Lambda)}{\sqrt{v_0}}} 2\pi i \left( \frac{4}{8-n} \right) \left( \frac{\sqrt{v_0}}{A} \right)^{\frac{3n-16}{16-2n}} \frac{1}{\Gamma\left(\frac{32-5n}{16-2n}\right)} \\ &= \frac{(4-n)\pi 2^{\frac{26-4n}{8-n}}}{b^{\frac{(n-1)(n-4)}{16-2n}} (8-n)^{\frac{32-5n}{16-2n}} \Gamma\left(\frac{32-5n}{16-2n}\right) (1-\Lambda)^{\frac{12+3n-n^2}{16-2n}} v_0^{\frac{16-3n}{32-4n}}} \frac{(1-2\Lambda)^{\frac{n}{16-2n}} \Lambda^{\frac{8-2n}{8-n}}}{i^{\frac{34-6n}{8-n}} e^{\frac{A_1 i^{\frac{i-1}{2}}}{\sqrt{v_0}}}} \\ &\quad = N \\ &= N e^{\frac{A_1(\Lambda)}{\sqrt{v_0}} \cos\left(\frac{n-1}{2} \frac{\pi}{2}\right)} e^{i \left[ \left( \frac{34-6n}{8-n} \frac{\pi}{2} \right) + \left( \frac{A_1(\Lambda)}{\sqrt{v_0}} \sin \frac{(n-1)\pi}{4} \right) \right]}. \end{aligned} \quad (3.69)$$

Since the cusp function is real-valued, it can be concluded that,

$$\mathcal{C} = N e^{\frac{A_1(\Lambda)}{\sqrt{v_0}} \cos\left(\frac{n-1}{2} \frac{\pi}{2}\right)} \cos \left[ \left( \frac{34-6n}{8-n} \frac{\pi}{2} \right) + \left( \frac{A_1(\Lambda)}{\sqrt{v_0}} \sin \frac{(n-1)\pi}{4} \right) \right]. \quad (3.70)$$

Equation (3.70) illustrates the singular nature of the surface tension parameter,  $v_0$ :  $\mathcal{C}$  has no regular series expansion in powers of  $v_0$ . From equation (3.70), it can also be deduced that the cusp function will vanish at each zero of the cosine term. For the Newtonian fluid, it has been proven that only the solution coming from the first zero of the cosine is linearly stable (Hong and Langer, 1986). This solution corresponds to the branch having the thinner finger. This idea is intuitively correct since wider fingers have curvatures at the tip that are smaller, and they can be subject to the same type of instabilities that made the fiat interface unstable in the first place. Consequently, from equation (3.69), the following expression is obtained,

$$\left( \frac{34-6n}{8-n} \frac{\pi}{2} \right) + \left( \frac{A_1(\Lambda)}{\sqrt{v_0}} \sin \frac{(n-1)\pi}{4} \right) = \frac{\pi}{2} \quad (3.71)$$



Substituting  $A_1$  from equation (3.65), it is found that

$$\Lambda - \frac{1}{2} = \underbrace{\frac{\left[ \sin \frac{(n-1)\pi}{4} \right] \frac{1}{4} \mathcal{B} \left( \frac{n+1}{2}, \frac{8-n}{4} \right) {}_2F_1 \left( \frac{n-2}{4}, \frac{n+1}{2}; \frac{n+10}{4}; (-1) \right)}{\left( \frac{26-5n}{8-n} \frac{\pi}{2} \right) b^{\frac{n-1}{2}} (1-\Lambda)^{\frac{n-1}{2}}} v_0^{-\frac{1}{2}} \quad (3.72)$$

Now, from the above equation (3.72), it can be noticed that for  $n > 1$  (and in the vicinity of  $n = 1$ ), the constant  $C_0 > 0$  leads to a contradictory conclusion that  $\Lambda > \frac{1}{2}$  (or  $\beta > 1$ ). Hence, the power-law exponent  $n < 1$  in this case.

• Case II:  $\beta > 1$  (or  $\Lambda > 1/2$ )

In this case, the integral in  $S_0$  (equation (3.60)) has a pole at  $\eta_b (< i)$ , and the contour of integration for the cusp function must deform around this pole (see fig 3.2b). Consequently, the evaluation of  $S_0$  is divided into 3 integrals,

$$S_0 = \left\{ \int_0^{i-\delta} + \int_{i-\delta}^{i+\delta} + \int_{i+\delta}^{i+\omega} \right\} d\eta' \underbrace{\frac{2\beta^2 i}{\{b(1-\Lambda)\}^{(n-1)/2}} \left[ \frac{(1+i\eta')^{\frac{4-n}{4}} (1-i\eta')^{\frac{2-n}{4}}}{\eta'^{\frac{1-n}{2}} (1+\beta^2 \eta'^2)} \right]}_{\psi(\eta) \text{ to be used in equation (3.74)}}, \quad (3.73)$$

where  $\delta (\lim \delta \rightarrow 0)$  is large enough in the second integral in equation (3.73) such that the contour of integration includes the pole. The evaluation of the first and the third integral in equation (3.73) follows an identical process as in the evaluation of the first and the second integral in case I (respectively) and hence omitted for brevity. For the second integral,  $J_2$ , the Cauchy's residue theorem is used in equation (3.73),

$$J_2 = \lim_{\delta \rightarrow 0} [\psi(i+\delta) - \psi(i-\delta)] = 2\pi \frac{(2\Lambda-1)^{\frac{4-n}{4}}}{b^{\frac{n-1}{2}} (1-\Lambda)} i^{\frac{n+1}{2}}. \quad (3.74)$$

Using the expressions for  $I_1(\Lambda), I_2(\Lambda), \mathcal{F}(\eta)$  from equations (3.65), (3.66), and (3.67), the cusp function is evaluated as follows,

$$\begin{aligned} \mathcal{C} &= \int_{-\infty}^{\infty} \mathcal{F}(\eta) e^{\frac{S_0}{\sqrt{v_0}}} d\eta \\ &= B e^{\frac{I_1}{\sqrt{v_0}}} e^{\frac{I_2}{\sqrt{v_0}}} \int_{-\infty}^{\infty} \omega^{\frac{3n-24}{8}} e^{\frac{A}{\sqrt{v_0}} \omega^{\frac{8-n}{4}}} d\omega \\ &= N e \left\{ \frac{A_1}{\sqrt{v_0}} \cos \left( \frac{(n-1)\pi}{4} \right) + \frac{2\pi(2\Lambda-1)^{\frac{4-n}{4}}}{b^{\frac{n-1}{2}} (1-\Lambda)\sqrt{v_0}} \cos \left( \frac{(n+1)\pi}{4} \right) \right\} \\ &\quad e^{i \left\{ -\frac{34-6n}{8-n} \frac{\pi}{2} + \frac{A_1}{\sqrt{v_0}} \sin \frac{(1-n)\pi}{4} + \frac{2\pi(2\Lambda-1)^{\frac{4-n}{4}}}{b^{\frac{n-1}{2}} (1-\Lambda)\sqrt{v_0}} \sin \frac{(n+1)\pi}{4} \right\}}. \end{aligned} \quad (3.75)$$

In order to find the first zero of the (real-valued) cusp, the condition must be,

$$\frac{6n-34}{8-n} \frac{\pi}{2} + \frac{A_1}{\sqrt{v_0}} \sin \frac{(1-n)\pi}{4} + \frac{2\pi(2\Lambda-1)^{\frac{4-n}{4}}}{b^{\frac{n-1}{2}}(1-\Lambda)\sqrt{v_0}} \sin \frac{(n+1)\pi}{4} = \frac{\pi}{2}, \quad (3.76)$$

and utilizing the expression for  $A_1$  from equation (3.65), and the fact that  $\frac{-2\Lambda^2}{1-2\Lambda} > 1$  for  $\Lambda > 1/2$ , the following relation is obtained,

$$\Lambda - \frac{1}{2} = \left[ \frac{\frac{42-7n}{8-n} \frac{\pi}{2} - \frac{\mathcal{B}(\frac{n+1}{2}, \frac{8-n}{4}) {}_2F_1(\frac{n-2}{4}, \frac{n+1}{2}, \frac{n+10}{4}; -1)}{(b/2)^{(n-1)/2} \sqrt{v_0}} \sin \frac{(1-n)\pi}{4}}{b^{\frac{1-n}{2}} 2^{\frac{12-n}{4}} \pi \sin(\frac{(n+1)\pi}{4})} \right]^{\frac{4}{4-n}} (v_0)^{\frac{2}{4-n}}. \quad (3.77)$$

In expression (3.77),  $n = 1$  leads to the familiar Newtonian limit,  $\Lambda - \frac{1}{2} \sim \mathcal{O}(v^{2/3})$  (Combescot et al., 1986; Hong and Langer, 1986; Shraiman, 1986). However, in the limit  $v_0 \rightarrow 0$ , it is seen that  $n < 1$  (such that  $n \approx 1$ ) leads to a contradiction,  $\beta < 1$ . Hence, the conclusion is that in this case,  $n \geq 1$ .

Hence, equations (3.72) and (3.77) completes the proof of our proposition.

Now, while evaluating terms for  $m \geq 2$

$$\Theta_0 = e^{\frac{S_0}{\sqrt{v_0}}} \sum_{m=0}^{\infty} g_m v_0^{\frac{m}{2}} \quad (3.78)$$

$$\begin{aligned} & (S_0'^2 + Q)g_0 + \left[ (S_0'^2 + Q)g_1 + (2S_0'g_0' + S_0''g_0) \right] v_0^{\frac{1}{2}} \\ & + \sum_{m=0}^{\infty} \left[ g_m'' + (S_0'^2 + Q)g_{m+2} + (2S_0'g_{m+1}' + S_0''g_{m+1}) \right] v_0^{m/2+1} = 0 \end{aligned}$$

Equating same power in  $v_0$ , the following is obtained,

$$(a) (S_0'^2 + Q)g_0 = 0 \Rightarrow g_0 \neq 0,$$

$$S_0 = i \int_0^\eta Q^{1/2} d\eta \quad (3.79)$$

$$(b) (S_0'^2 + Q)g_1 + (2S_0'g_0' + S_0''g_0) = 0$$

$$\Rightarrow g_0' + \frac{S_0''}{2S_0'} g_0 = 0$$

$$(c) g_m'' + (S_0'^2 + Q)g_{m+2} + (2S_0'g_{m+1}' + S_0''g_{m+1}) = 0$$

$$\Rightarrow g_m'' + 2S_0'g_{m+1}' + S_0''g_{m+1} = 0$$

$$\Rightarrow g_{m+1}' + \frac{S_0''}{2S_0'} g_{m+1} = -\frac{1}{2S_0'} g_m''$$

Around the point of stationary phase  $\eta = i$ , let us consider  $\eta = i + \omega$ .

$$\text{Now, } \bar{Q} = \frac{4\beta^4}{\{b(1-\Lambda)\}^{n-1} \eta^{1-n}} \frac{(1+i\eta)^{(4-n)/2} (1-i\eta)^{(2-n)/2}}{(1+\beta^2\eta^2)^2}$$

$$\begin{aligned}
&= \frac{4\beta^4}{\{b(1-\Lambda)\}^{n-1}} \frac{1}{i^{1-n}} \frac{i^{(4-n)/2} \omega^{(4-n)/2} 2^{(2-n)/2}}{(1-\beta^2)^2} \\
&= \frac{2^{(6-n)/2} i^{(n+2)/2}}{\{b(1-\Lambda)\}^{n-1}} \left( \frac{\Lambda^2}{1-2\Lambda} \right)^2 \omega^{\frac{4-n}{2}} \\
&\Rightarrow \bar{Q} = a \omega^{\frac{4-n}{2}} \quad \text{where, } a = \frac{2^{(6-n)/2} i^{(n+2)/2}}{\{b(1-\Lambda)\}^{n-1}} \left( \frac{\Lambda^2}{1-2\Lambda} \right)^2 \quad (3.80)
\end{aligned}$$

$$\text{Now, } \frac{S_0''}{2S_0'} = \frac{Q'}{4Q} \equiv \left( \frac{4-n}{8} \right) \omega^{-1} \quad (3.81)$$

$$\text{Also, } 2S_0' = 2iQ^{1/2} = 2ia^{1/2} \omega^{\frac{4-n}{4}}$$

$$\text{Now, the expression of (b) can be written as, } g_0' + \frac{S_0''}{2S_0'} g_0 = 0 \Rightarrow g_0' + \left( \frac{4-n}{8} \right) \omega^{-1} g_0 = 0$$

$$\Rightarrow g_0 = a_0 \omega^{\frac{n-4}{8}} \quad \text{where, } a_0 = \text{constant}$$

$$\text{And (c) implies } g_{m+1}' + \left( \frac{4-n}{8} \right) \omega^{-1} g_{m+1} = -\frac{1}{2ia^{1/2} \omega^{\frac{4-n}{4}}} g_m''$$

$$\text{Using } g' + Fg = G \Rightarrow g = g_h \int \frac{G}{g_h} d\omega \quad \text{where, } g_h = e^{-\int d\omega F}$$

$$\text{Now, one can get, } g_{m+1} = \omega^{-A} B \int d\omega \omega^{A-\frac{4-n}{4}} g_m'' \quad \text{where, } A = \frac{4-n}{8} \text{ and } B = \frac{-1}{2ia^{1/2}}$$

Suppose,  $g_m$  has the form:  $g_m = a_m \omega^{-A_m}$ . Then  $g_m$  will have the same form, and hence the form can be obtained recursively.

$$\begin{aligned}
g_m &= a_m \omega^{-A_m} \\
\Rightarrow g_m' &= -A_m a_m \omega^{-A_m-1} \\
\Rightarrow g_m'' &= A_m(A_m+1) a_m \omega^{-A_m-2}
\end{aligned}$$

$$\begin{aligned}
\text{So, } g_{m+1} &= \omega^{-A} B \int \omega^{A_1-\frac{4-n}{4}} a_m A_m(A_m+1) \omega^{-A_m-2} d\omega \\
&= \frac{\omega^{-A} B a_m A_m(A_m+1)}{A - A_m - \frac{4-n}{4} - 1} \omega^{A-A_m-\frac{4-n}{4}-1} \\
&\Rightarrow g_{m+1} = a_{m+1} \omega^{-A_{m+1}} \quad (3.82)
\end{aligned}$$

$$\begin{aligned}
\text{where, } a_{m+1} &= \frac{B a_m A_m(A_m+1)}{A - A_m + \frac{n-8}{4}} \\
\text{and } A_{m+1} &= A_m + \frac{8-n}{4} \quad (3.83)
\end{aligned}$$

$$\begin{aligned}
\text{So, } A_1 &= A_0 + \frac{8-n}{4} \\
A_2 &= A_1 + \frac{8-n}{4} = A_0 + 2\frac{8-n}{4} \\
&\dots \quad \dots \quad \dots \\
&\dots \quad \dots \quad \dots \\
&\dots \quad \dots \quad \dots \\
&\dots \quad \dots \quad \dots \\
&\dots \quad \dots \quad \dots \\
A_m &= A_0 + m\frac{8-n}{4}
\end{aligned}$$

Thus, the form that is recursively obtained is,

$$A_{m+1} = A_0 + (m+1)\frac{8-n}{4} \quad (3.84)$$

Comparing the multiplicative coefficients determines  $a_m$

$$a_m = \left[ -\left(\frac{8-n}{4}\right) \right]^m B^m \frac{\Gamma(m + \frac{4-n}{16-2n})\Gamma(m + \frac{12-n}{16-2n})}{\Gamma(\frac{4-n}{16-2n})\Gamma(\frac{12-n}{16-2n})\Gamma(m+1)} \quad (3.85)$$

For consistency,  $e^{\frac{S_0}{\sqrt{V_0}}}$  and  $\bar{R}$  are expanded around the point of stationary phase  $\bar{\eta}$ . So,  $S_0$  can be approximated from (3.64) and (3.79) as,

$$\begin{aligned}
S_0 &\approx I_1(\lambda) + I_2 \\
S_0 &\approx A_1(\Lambda)i^{\frac{n-1}{2}} + M\omega^{\frac{8-n}{4}} \quad (M = A \text{ from } \beta < 1 \text{ case})
\end{aligned} \quad (3.86)$$

where,  $\omega = \eta - i$  and therefore it can be written as,

$$e^{\frac{S_0}{\sqrt{V_0}}} = e^{\frac{I_1}{\sqrt{V_0}}} e^{\frac{I_2}{\sqrt{V_0}}} = e^{\frac{A_1(\Lambda)i^{\frac{n-1}{2}}}{\sqrt{V_0}}} e^{\frac{M}{\sqrt{V_0}}\omega^{\frac{8-n}{4}}}$$

With the above results (3.78) becomes,

$$\Theta_0 = e^{\frac{A_1(\Lambda)i^{\frac{n-1}{2}}}{\sqrt{V_0}}} \sum_{m=0}^{\infty} \left[ a_m V_0^{\frac{m}{2}} \omega^{-\frac{8-n}{4}m - \frac{4-n}{8}} e^{\frac{M}{\sqrt{V_0}}\omega^{\frac{8-n}{4}}} \right] \quad (3.87)$$

$$\bar{R}(\eta) = \frac{\eta^{\frac{3-n}{2}}}{(1 + \beta^2 \eta^2)^{1/2} (1 + \eta^2)^{\frac{10-n}{4}}} \left[ \beta^2 (1 + \eta^2) - (1-n) \frac{(1 + \eta^2)}{\eta^2} - (4-n)(\beta^2 - 1) \right]$$

For,  $\eta = i + \omega$ ,

$$\begin{aligned}
&= \frac{(i + \omega)^{\frac{3-n}{2}}}{(1 + \beta^2 (i + \omega)^2)^{1/2} (1 + (i + \omega)^2)^{\frac{10-n}{4}}} \left[ \beta^2 (1 + (i + \omega)^2) - (1-n) \frac{(1 + (i + \omega)^2)}{(i + \omega)^2} \right. \\
&\quad \left. - (4-n)(\beta^2 - 1) \right]
\end{aligned}$$

$$\Rightarrow \bar{R}(\omega) = \frac{(4-n)(1-\beta^2)^{\frac{1}{2}}}{2^{\frac{10-n}{4}} i^{\frac{n+4}{4}}} \omega^{-\frac{10-n}{4}}$$

$$\text{So, } \bar{R}(\omega) = b_1 \omega^{-\frac{10-n}{4}} \quad \text{where, } b_1 = \frac{(4-n)(1-\beta^2)^{\frac{1}{2}}}{2^{\frac{10-n}{4}} i^{\frac{n+4}{4}}}$$

Now, the cusp function can be written as

$$\mathcal{C} = \int_{-\infty}^{\infty} d\omega \text{Im}\Theta_0(\omega) \bar{R}(\omega) = \frac{1}{i} b_1 e^{\frac{I_1}{\sqrt{v_0}}} \sum_{m=0}^{\infty} a_m v_0^{\frac{m}{2}} I_m \quad (3.88)$$

where,  $I_m$  is defined as

$$I_m = \int_{-\infty}^{\infty} \omega^{-\frac{8-n}{4}m - \frac{24-3n}{8}} e^{\frac{M}{\sqrt{v_0}} \omega^{\frac{8-n}{4}}} d\omega$$

$$= \left(\frac{4}{8-n}\right) \left(\frac{M}{\sqrt{v_0}}\right)^{m + \frac{16-3n}{16-2n}} \int_{-\infty}^{\infty} e^x x^{\frac{5n-32}{16-2n} - m} dx$$

$$\Rightarrow I_m = \left(\frac{8\pi i}{8-n}\right) \left(\frac{M}{\sqrt{v_0}}\right)^{m + \frac{16-3n}{16-2n}} \frac{1}{\Gamma(m - \frac{5n-32}{16-2n})}$$

The Cusp function then can be written as:

$$\mathcal{C} = \left[ \frac{8\pi}{8-n} a_0 b_1 M^{\left(\frac{16-3n}{16-2n}\right)} \frac{1}{v_0^{\frac{16-3n}{32-4n}}} \right] e^{\frac{A_1}{\sqrt{v_0}} i^{\left(\frac{n-1}{2}\right)}} \Delta \quad (3.89)$$

Where,

$$\Delta = \frac{1}{a_0} \sum_{m=0}^{\infty} M^m \frac{v_0^{\frac{m}{2}}}{v_0^{\frac{m}{2}}} a_m \frac{1}{\Gamma(m + \frac{32-5n}{16-2n})}$$

$$= \frac{1}{a_0} \sum_{m=0}^{\infty} M^m \left[ -\left(\frac{8-n}{4}\right) \right]^m B^m \frac{\Gamma(m + \frac{4-n}{16-2n}) \Gamma(m + \frac{12-n}{16-2n}) a_0}{\Gamma(\frac{4-n}{16-2n}) \Gamma(\frac{12-n}{16-2n}) \Gamma(m+1)} \frac{1}{\Gamma(m + \frac{32-5n}{16-2n})}$$

$$\text{Now, } M = \left(\frac{8}{8-n}\right) \frac{2^{\frac{2-n}{4}} i^{\frac{6+n}{4}}}{\{b(1-\Lambda)\}^{\frac{n-1}{2}}} \left(\frac{\Lambda^2}{1-2\Lambda}\right)$$

$$\text{So, } M^m = \left(\frac{8}{8-n}\right)^m \frac{2^{\frac{2-n}{4}m} i^{\frac{6+n}{4}m}}{\{b(1-\Lambda)\}^{m(\frac{n-1}{2})}} \left(\frac{\Lambda^2}{1-2\Lambda}\right)^m$$

$$\text{and } B = \frac{-1}{2ia^{1/2}} \Rightarrow B^m = \frac{(-1)^m}{2^m i^m a^{m/2}}$$

$$\text{But, } a = \frac{4i^{\frac{2+n}{2}} 2^{\frac{2-n}{2}}}{\{b(1-\Lambda)\}^{n-1}} \left(\frac{\Lambda^2}{1-2\Lambda}\right)^2$$

$$\Rightarrow a^{\frac{m}{2}} = \frac{2^m i^{\frac{2+n}{4}m} 2^{\frac{2-n}{4}m}}{\{b(1-\Lambda)\}^{\frac{n-1}{2}m}} \left(\frac{\Lambda^2}{1-2\Lambda}\right)^m$$

$$\text{Thus, } M^m B^m \left[ -\left(\frac{8-n}{4}\right) \right]^m = \left[ \frac{1}{2} \right]^m$$

Hence,  $\Delta$  can be expressed as,

$$\Delta = \frac{1}{\Gamma\left(\frac{4-n}{16-2n}\right)\Gamma\left(\frac{12-n}{16-2n}\right)} \sum_{m=0}^{\infty} \left[ \frac{1}{2} \right]^m \frac{\Gamma\left(m + \frac{4-n}{16-2n}\right)\Gamma\left(m + \frac{12-n}{16-2n}\right)}{\Gamma(m+1)\Gamma\left(m + \frac{32-5n}{16-2n}\right)} \quad (3.90)$$

There is an overall constant which is irrelevant since what is uniquely determined is the normalized cusp function.

To compare with the original calculation,  $a_0$  is to be set to agree with the results of (3.70) when only the term  $m = 0$  in (3.90) is considered.

Thus  $\mathcal{C}$  has the form,

$$\mathcal{C} = N e^{\frac{A_1(\Lambda)}{\sqrt{v_0}} \cos\left(\frac{n-1}{2}\pi\right)} \cos \left[ \left(\frac{34-6n}{8-n}\right) \frac{\pi}{2} + \frac{A_1(\Lambda)}{\sqrt{v_0}} \sin\left(\frac{(n-1)\pi}{4}\right) \right] \Delta \Gamma\left(\frac{32-5n}{16-2n}\right) \quad (3.91)$$

$$\begin{aligned} \text{where, } N &= \frac{(4-n)\pi 2^{\frac{26-4n}{8-n}}}{b^{\frac{(n-1)(n-4)}{16-2n}} (8-n)^{\frac{32-5n}{16-2n}} \Gamma\left(\frac{32-5n}{16-2n}\right)} \frac{(1-2\Lambda)^{\frac{n}{16-2n}} \Lambda^{\frac{8-2n}{8-n}}}{(1-\Lambda)^{\frac{12+3n-n^2}{16-2n}} v_0^{\frac{16-3n}{32-4n}}} \\ &= N_1 \frac{(1-2\Lambda)^{\frac{n}{16-2n}} \Lambda^{\frac{8-2n}{8-n}}}{(1-\Lambda)^{\frac{12+3n-n^2}{16-2n}} v_0^{\frac{16-3n}{32-4n}}} \\ \text{here, } N_1 &= \frac{(4-n)\pi 2^{\frac{26-4n}{8-n}}}{b^{\frac{(n-1)(n-4)}{16-2n}} (8-n)^{\frac{32-5n}{16-2n}} \Gamma\left(\frac{32-5n}{16-2n}\right)} \end{aligned}$$

Hence, the quantity  $\Delta \Gamma\left(\frac{32-5n}{16-2n}\right)$  gives a multiplicative factor which tells us how different this result is from the result where only two terms in (3.51) are kept. So, when setting  $m = 0$ ,  $\Delta \Gamma\left(\frac{32-5n}{16-2n}\right) = 1$ , the result of (3.70) is recovered.

The general form of  $N_1$  is given as follows,

$$\begin{aligned} N_1 &= \frac{(4-n)\pi 2^{\frac{26-4n}{8-n}}}{b^{\frac{(n-1)(n-4)}{16-2n}} (8-n)^{\frac{32-5n}{16-2n}} \Gamma\left(\frac{32-5n}{16-2n}\right)} \\ \text{At } n=1, \quad N_1 &= \frac{3\pi 2^{\frac{22}{7}}}{7^{\frac{27}{14}} \Gamma\left(\frac{27}{14}\right)} = 2.008 \end{aligned}$$

Therefore, the result of D.C. Hong and J.S. Langer (for  $n = 1$ ) are recovered.

### 3.4 Experimental and numerical validation

The competition between the viscous and the capillary forces on the advancing front leads to the emergence of a characteristic length scale that determines the relative

finger width,  $\Lambda_{\text{Temp}}$  and the same can be calculated using the linear stability analysis. This physical reasoning has been made rigorous by deriving a dispersion relation relating the growth-rate,  $\omega$  of the instability to the wavenumber  $\alpha$ , assuming a normal mode expansion of the disturbance,  $e^{i(\alpha x - \omega t)}$  and by choosing real wavenumbers,  $\alpha \in \mathbb{R}$ , and allowing for complex frequencies,  $\omega \in \mathbb{C}$ , or the so-called temporal stability analysis (Huerre and Monkewitz, 1985). Following the analysis by Chuoke (Chuoke, Van Meurs, and Poel, 1959), the dispersion relation has been derived in a rectilinear channel for the power law fluids. From equation (3.2), it is found that the Darcy flow inside (outside) the finger, denoted by subscript ‘1’ (and ‘2’), is given by

$$\begin{aligned}\bar{\mathbf{u}}_1 &= -\frac{b^2}{12\mu_1}\nabla p_1, \\ \bar{\mathbf{u}}_2 &= -\frac{b^{n+1}}{12\mu_2}\nabla p_2,\end{aligned}\quad (3.92)$$

where the assumption is made that the flow inside (outside) the finger is Newtonian (non-Newtonian) and  $\mu_2$  is given by the power-law (3.5). For the moving interface,  $\zeta_0$ , the nonlinear interface conditions are

$$\frac{\partial \zeta}{\partial t} + \bar{\mathbf{u}}_j \cdot \mathbf{e}_y \frac{\partial \zeta}{\partial y} = \bar{\mathbf{u}}_j \cdot \mathbf{e}_x, \quad j = 1, 2 \quad (3.93)$$

and

$$p_2 - p_1 = T \frac{\left(\frac{\partial^2 \zeta}{\partial y^2}\right)}{\underbrace{\left[1 + \left(\frac{\partial \zeta}{\partial y}\right)^2\right]^{3/2}}_{\text{interface curvature}}}. \quad (3.94)$$

Let us proceed to the stability analysis of a plane front propagating at constant velocity  $U\mathbf{e}_x$ . The mean pressure field for fluids 1 and 2 is obtained by integrating (3.92) and choosing the pressure to be zero on the interface located at  $x = \zeta_0 = Ut$ , it can be found that,

$$\begin{aligned}P_1 &= -\left(\frac{12\mu_1}{b^2}\right)U(x - Ut), \\ P_2 &= -\left(\frac{12\mu_0}{b^{(n+1)}}\right)U^n(x - Ut).\end{aligned}\quad (3.95)$$

Next, a linearization of the variables is considered with  $p = P + \varepsilon p'$ ,  $\mathbf{u} = U\mathbf{e}_x + \varepsilon \mathbf{u}'$  and  $\eta = Ut + \varepsilon \eta'$  ( $\varepsilon \ll 1$ ). Now, at the interface, notice that,

$$p_2 - p_1 \approx T \left(\frac{\partial^2 \eta}{\partial y^2}\right). \quad (3.96)$$

From equation (3.92), linearized Darcy's law for both the fluids is given by,

$$\begin{aligned}\bar{\mathbf{u}}'_1 &= -\frac{b^2}{12\mu_1}\nabla p'_1, \\ \bar{\mathbf{u}}'_2 &= \frac{-\left[\frac{b^{(n+1)}U^{(1-n)}}{12\mu_0}\nabla p'_2\right]}{\left[1 + \frac{b^{(n+1)}}{6\mu_0U^n}\nabla P_2\right]},\end{aligned}\quad (3.97)$$

Also, the linearized interface equation is,

$$\frac{\partial \eta'}{\partial t} = \bar{\mathbf{u}}'_j \cdot \mathbf{e}_x \quad (3.98)$$

Considering the independent fate of each wavenumber  $\alpha$  chosen to be real positive in the  $y$  direction (without loss of generality), it is natural to look for a normal mode expansion  $p'_i = \hat{p}_i \exp(i(\alpha y - \omega t))$  and  $\eta' = C \exp(i(\alpha y - \omega t))$  suggested by the invariance of the base flow solution with respect to  $y$ . Imposing far-field boundary conditions in each fluid yields

$$\hat{p}_1 = A_1 \exp(kx), \quad \hat{p}_2 = A_2 \exp(-kx). \quad (3.99)$$

Using equations (3.97) and (3.98), the following equations can be obtained at the interface,

$$\begin{aligned}-i\omega C &= -\frac{b^2}{12\mu_1}\alpha A_1 \exp(\alpha Ut) \\ -i\omega C &= \frac{b^{(n+1)}U^{(1-n)}}{12\mu_0}\alpha A_2 \exp(-\alpha Ut),\end{aligned}\quad (3.100)$$

Now, by using equations (3.96) and (3.100), it can be found that,

$$-\frac{12U}{b^2}C \left[ \frac{\mu_2 U^{(n-1)}}{b^{(n-1)}} - \mu_1 \right] + A_2 \exp(-\alpha Ut) - A_1 \exp(\alpha Ut) = -T\alpha^2 C \quad (3.101)$$

Finally, using equations (3.100) and (3.101), the system of equations governing the solution vector,  $[A_1 \ A_2 \ C]^T$  can be obtained and it is given by,

$$\begin{bmatrix} -\frac{b^2}{12\mu_1}k \exp(kUt) & 0 & i\omega \\ 0 & \frac{b^{(n+1)}U^{(1-n)}}{12\mu_2}k \exp(-kUt) & i\omega \\ -\exp(kUt) & \exp(-kUt) & \gamma k^2 - \frac{12U}{b^2} \left[ \frac{\mu_2 U^{(n-1)}}{b^{(n-1)}} - \mu_1 \right] \end{bmatrix} \begin{bmatrix} A_1 \\ A_2 \\ C \end{bmatrix} = \begin{bmatrix} 0 \\ 0 \\ 0 \end{bmatrix} \quad (3.102)$$



A non-trivial solution of the system (3.102) involves a zero determinant of the matrix  $A$ , leading to the dispersion relation,

$$\omega = i \left[ \left( \frac{b^2 \mu_0 - b^{(n+1)} U^{(1-n)} \mu_1}{b^2 \mu_0 + b^{(n+1)} U^{(1-n)} \mu_1} \right) U \alpha - T \alpha^3 \frac{b^{(n+1)}}{12} \left( \frac{U^{(1-n)}}{\mu_0 + b^{(n-1)} U^{(1-n)} \mu_1} \right) \right] \quad (3.103)$$

In the case of a low-viscosity fluid displacing a high-viscosity fluid such that  $\mu_0 \gg \mu_1$ , here it is considered  $\mu_1 = 0$ . Hence, equation (3.103) simplifies to

$$\begin{aligned} \omega &= i \left[ U \alpha - T \alpha^3 \frac{b^{(n+1)}}{12} \left( \frac{U^{(1-n)}}{\mu_0} \right) \right], \\ &= i U [\alpha - B \alpha^3 w^2], \end{aligned} \quad (3.104)$$

under the assumption that the viscosity of the driving fluid is negligible.  $B(\dot{\gamma}) = \frac{Tb^2}{12\mu(\dot{\gamma})Uw^2}$  is a control parameter, discussed later in this section. From equation (3.104), it can be concluded that the existence of the most unstable temporal mode (obtained by setting  $\frac{d\omega}{d\alpha} = 0$ , leading to a value  $\alpha_{\text{Temp}} = (w\sqrt{3B})^{-1}$ ). Based on the physical explanation by Chuoke (Chuoke, Van Meurs, and Poel, 1959), it is conjectured that the relative finger width of the advancing interface,  $\Lambda_{\text{Temp}}$ , is the wavelength of the instability found at the most unstable temporal mode, or

$$\Lambda_{\text{Temp}} = \frac{2\pi}{\alpha_{\text{Temp}}}. \quad (3.105)$$

TABLE 3.1: Viscosity data for the power-law model (equation (3.5)) for different concentrations of Xanthane and PEO, utilized in equations (3.72), (3.77) and (3.104) (Sources: (Bonn and Meunier, 1997; Lindner, Bonn, and Meunier, 2000)).

Xanthane		
Conc. (ppm)	$\mu_0$ (mPa s <sup>n</sup> )	n
50	2.06	0.930
100	5.23	0.818
500	40.62	0.607
1000	160.35	0.463
PEO		
Conc. (ppm)	$\mu_0$ (mPa s <sup>n</sup> )	n
5	7.9	1.018
50	29.2	1.032
500	70.7	1.052

Investigation of STI for polymer solutions allows us to consider the most common non-Newtonian effects: shear thinning behavior and the effect of normal stresses. Figure 3.3 (also refer table- 3.1 for the corresponding viscosity data) highlights the in vitro data for Xanthane gum, which is a shear thinning fluid, versus different polymer concentrations (fig 3.3a) as well as for different cell geometries (fig 3.3b) (Lindner,

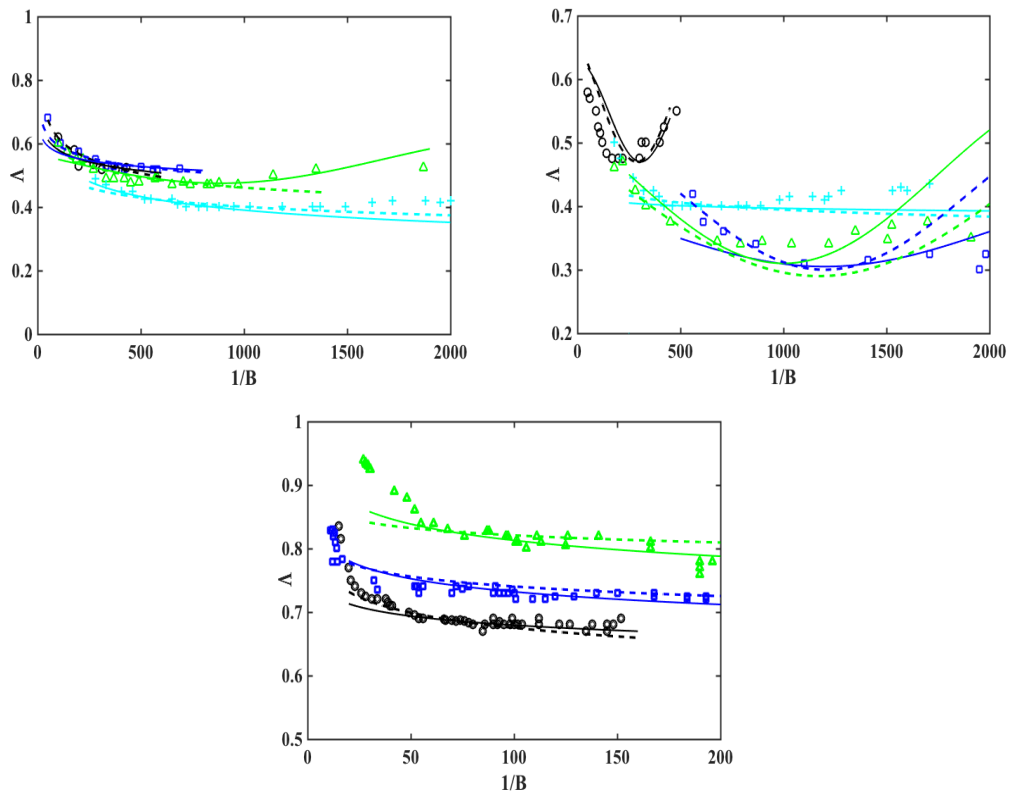


FIGURE 3.3: Finger width as a function of  $1/B$  for solutions of (a) Xanthane for concentrations of 50 ppm ( $\circ$ ), 100 ppm ( $\square$ ), 500 ppm ( $\triangle$ ), 1000 ppm ( $+$ ), and at fixed cell geometry,  $w = 2.0\text{cm}$  and  $b = 0.25\text{mm}$  (Source: (Lindner, Bonn, and Meunier, 2000)), (b) Xanthane at different cell geometries,  $w = 2.0\text{cm}$  and  $b = 0.66\text{mm}$  ( $\circ$ ),  $w = 2.0\text{cm}$  and  $b = 0.25\text{mm}$  ( $+$ ),  $w = 4.0\text{cm}$  and  $b = 0.5\text{mm}$  ( $\triangle$ ),  $w = 4.0\text{cm}$  and  $b = 0.25\text{mm}$  ( $\square$ ), and at fixed concentration of 1000 ppm (Source: (Lindner et al., 2002)), (c) PEO for concentrations of 5 ppm ( $\circ$ ), 50 ppm ( $\square$ ), 500 ppm ( $\triangle$ ), and at fixed cell geometry,  $w = 2.0\text{cm}$  and  $b = 0.5\text{mm}$  (Source: (Lindner et al., 2002)). (---) predictions from the linear stability analysis (equation (3.105)). (—) predictions from the theoretical estimate (equations (3.72), (3.77)).

Coussot, and Bonn, 2000). A reasonably good agreement is found between the experimental data, the one computed with the linearized model (equations (3.104), (3.105)) and the theoretical estimate (equation (3.72), (3.77)), for larger values of the parameter,  $1/B$ . For this class of fluids, the results of the finger width versus the control parameter are separated into two different regimes. For low polymer concentrations (e.g., for the case of 50 ppm and 100 ppm, fig 3.3a), the non-Newtonian (or shear thinning) effects are weak. These effects can be taken into account solely by incorporating the power-law viscosity in the dispersion relation (equation (3.104)) or the control parameter, thereby resolving the finger selection problem. For higher polymer concentrations (e.g., 1000 ppm, cyan curve in fig 3.3a, and all cases in fig 3.3b), the shear-thinning effects become prominent, and there is a discrepancy in the stacking of the numerical results onto the experimental dataset. This discrepancy (in the matching between the theory and the experiments) was explained by Rabaud (Rabaud, Couder, and Gerard, 1988a), who concluded that it is the radius of the fingertip, (equations (3.3), (3.6)) which is the selection (or the perturbation) parameter and which will (supposedly) resolve the finger selection mechanism for strong shear-thinning fluids.

Contrary to the observations for the shear thinning fluid, a widening of the finger for solutions of PEO, compared with the Newtonian case, is found. From fig 3.3c, it is observed that the finger decreases with increasing values of the (inverse) control parameter, followed by stabilization on a plateau value with  $\Lambda > 0.5$ . This widening becomes more pronounced as the polymer concentration increases. The finger selection mechanism for this class of shear thickening fluids is understood as follows: in a related experiment of the flow of finite bubbles in a capillary, Bonn (Bonn and Meunier, 1997) found that the observed thickness of the thin wetting film left between the moving bubble and the walls of the tube, was much larger when polymers were added in the solvent. The explanation for the increase in the film thickness was due to the presence of high normal stresses in the film exerting extra pressure on the bubble, which becomes more elongated. Bonn also suggested that for the viscoelastic fingers in the Hele-Shaw cell, a similar effect could lead to pressure buildup within the wetting film between the advancing finger and the glass plates of the cell, thereby causing a finger widening. Tabeling (Tabeling and Libchaber, 1986) incorporated the effect of the finite thickness of the wetting film by correcting the surface tension, as follows,

$$T^* = T \left[ \frac{\pi}{4} + 1.7 \left( \frac{\Lambda}{b/w} \right) \left( \frac{\mu U}{T} \right)^{2/3} \right], \quad (3.106)$$

ensuing in a renormalized control parameter,  $\frac{1}{B^*} = \frac{12\mu w^2}{b^2} \left( \frac{U}{T^*} \right)$ , which, again, leads to a rescaling of the linearized model onto the experimental dataset.

### 3.5 Concluding remark

This chapter provides an analytical treatment of predicting the Saffman-Taylor fingers for a class of non-Newtonian fluids. The first objective is to provide a systematic description of the way in which the singular perturbation introduced by the viscous and the capillary forces leads to a solvability mechanism for pattern selection. It is then

shown how the experimental observations for shear thinning fluids (Lindner, Coussot, and Bonn, 2000) and shear thickening fluids (Bonn and Meunier, 1997; Lindner et al., 2002) can be interpreted in terms suggested by this mechanism. The obtained results in this chapter extend the classical results for Newtonian fluids of Hong (Hong and Langer, 1986), Shraiman (Shraiman, 1986) and Combescot (Combescot et al., 1986), showing that the finger width has the form  $\Lambda - \frac{1}{2} \sim v_0^{2/3}$ , in the limit of small  $v_0$ . However, besides the cell geometry, finger velocity, and surface tension, this analysis highlights on how the power-law exponent of the viscosity, modifies the selected finger width to explain the finger thinning (finger thickening) for shear thinning (shear-thickening) fluids.

Although, the analysis presented here has generalized previous findings (Hong and Langer, 1986), via the introduction of a shear-dependent, power-law form of viscosity, certain shortcomings of the model must not be overlooked, including the absence of elastic stresses (especially important for shear thickening fluids), absence of a characteristic time scale and a characteristic viscosity and the presence of large errors in viscosity measurements near zero shear rates (Bird, Armstrong, and Hassager, 1987). A future endeavor is the perturbative expansion of the model via the radius of the fingertip to explain the selection mechanism for strong shear-thinning fluids.

## Chapter 4

# Conclusion

### 4.1 Introductory remark

The investigation of viscous fingering in a Hele-Shaw cell is a well-known issue that has evolved into an archetype of the development of interfacial patterns, yet it keeps bringing new surprises that challenge our knowledge of the non-local, nonlinear pattern dynamics of interfaces.

In the first section of this last chapter, the limitations and difficulties encountered when formulating the underlying assumptions for building the mathematical model are discussed, along with the key findings that has been arrived at about the finger width for a class of non-Newtonian fluids (Bansal, Ghosh, and Sircar, 2023). On the other hand, future directions in the context of viscous fingering have been discussed in the second section of this chapter.

### 4.2 Limitations of the current work

#### 4.2.1 In formulating the mathematical model

In this thesis, an analytical method is used to resolve the Saffman-Taylor finger selection mechanism for a class of non-Newtonian fluids. The spatiotemporal analysis of the viscoelastic flows is more recent and sparse. In order to derive the equations for the steady two-dimensional non-Newtonian flow produced by a finger inside a channel with surface tension effects resulting from lateral curvature, the literature on the temporal and spatiotemporal stability analysis of viscous and viscoelastic Hele-Shaw flows has been reviewed. This review allowed us to highlight specific and important hypotheses. The procedure of developing the hypothesis and validating the findings with previous experiments and numerical simulations is limited but challenging enough to be worth mentioning in this chapter. The following limitations are used as follows:

- The driving (Newtonian) fluid's viscosity and buoyancy forces are assumed to be negligible in accordance with the in vitro (Rabaud, Couder, and Gerard, 1988b; McLean, 1980) and in silico (Lindner, Bonn, and Meunier, 2000; Ostwald, 1925) experiments. In our analysis, a low-viscosity ( $\mu_1$ ) fluid pushes a high-viscosity ( $\mu_0$ ) fluid such that  $\mu_1 \ll \mu_0$ , the dispersion relation takes the form of equation (3.104) (Bansal, Ghosh, and Sircar, 2023).

- The assumption that the driving fluid expels the driven fluid completely is typically false in experimental setups (Sircar and Wang, 2010) because a thin film of the driven fluid is left adhering to the plates. In reality, the shape of the advancing interface is controlled by the presence of this finite, spatially varying, wetting film.
- In this study, the inertial term in the Navier-Stokes equation is neglected, and to do that, a low, steady, gap-averaged velocity of the fluid is considered.
- The main mathematical challenge posed by the 'viscoelastic fingering' instability is that pressure may no longer be a Laplacian field, complicating numerical prediction of finger width (Lindner et al., 2002). Lindner et al. (Lindner et al., 2002) have argued that the pressure,  $p$ , is essentially harmonic, as divergence-free condition applied to the modified Darcy's law can lead to,

$$\mu \nabla^2 p - \mu' \nabla(\mathbf{u} \cdot \mathbf{u}) \cdot \nabla p = 0.$$

- Although this work is largely focused on the shear thinning feature, the impacts of elastic stresses have been ignored as a result. This is a high-intensity problem in terms of computation, but in the Stokes-Darcy regime and in the absence of elastic effects, the flow was believed to be symmetric about the centerline. Costs gradually decrease as a consequence.
- There are several numerical difficulties as well since the problem is inherently nonlinear and nonlocal. Even for simpler models, such as the geometrical model where non-locality is completely neglected, disagreement existed between the theory and numerics on the prefactors of the cusp function. In light of this, it becomes desirable to carefully reexamine some of the mathematical approximations used in the original solvability theory proposals and perhaps improve them systematically in the context of the Hele-Shaw flow, where solving the entire nonlocal model is required. The prefactor of the cusp function is re-computed (in equations (3.78),(3.87),(3.90)) to include all nonlinear terms at the level of the WKB approximation, rather than just the leading term (Bansal, Ghosh, and Sircar, 2023). A 5% numerical difference is found between this extended method and the original theory for the Hele-Shaw flow problem.

#### 4.2.2 In determining a unique value of $\Lambda$

The fact that  $v_0$  appears in the equation as a single perturbation parameter is a critical aspect of the integro-differential equations (3.17) in general (Ramesh et al., 2020; Gupta, Kadalbajoo, and Dubey, 2019). The mathematical foundation of the issue is entirely altered because  $v_0$  multiplies the highest derivative. Equation (3.17) can be explicitly solved to provide the equation (3.19) when  $v_0 = 0$ . According to McLean (McLean, 1980), the equation (3.19) satisfies the family of solutions (3.1) put forth by Saffman. This solution fails to selectively determine a unique value of  $\Lambda$  since the equation (3.19) is automatically consistent with the boundary conditions (3.18) for any  $\Lambda$ . In general, it says that even for accurate solutions that operate smoothly without any finite-time singularities, the limit of vanishing surface tension generally does not converge to the precise zero-surface tension solutions after a time of order unity. This indicates that the solutions with and without surface tension do not

approach each other in the limit of vanishing surface tension after a time that is largely independent of surface tension. Mathematically, it was quite difficult to solve this astonishing finding. However, in the range of  $v_0 \rightarrow 0$ , I was able to offer a unique solution for  $\Lambda$  (Bansal, Ghosh, and Sircar, 2023).

## 4.3 Future problems

This section provides a quick overview of some recent advances and potential future research on the dynamics of fingering patterns. Now, this discussion goes into further depth when talking about the impact of changing the viscosity contrast parameter (Casademunt, 2004). Here, it demonstrates that the dynamics of fingered structures are quite sensitive to this parameter and that the competition between the typical Saffman-Taylor single-finger stationary solution and other attractors characterized by closed bubbles dominates the long-time asymptotics. Moreover, in this section, the future prospects in the field with regard to the existence of topological singularities in the form of interface pinch-off, wetting effects, and applications to other issues like interface roughening in the fluid invasion of porous media in this context while also taking into account recent results on rotating Hele-Shaw flows (McCloud and Maher, 1995), has been discussed.

### 4.3.1 The role of viscosity contrast

The broad picture of finger competition where fingers try to distinguish the Laplacian pressure field from each other, ending up with a single finger surviving and approaching the Saffman-Taylor solution. Including the singular effects of surface tension, is restricted to the one-sided Saffman-Taylor problem, that is, to viscosity contrast  $c = 1$ , where  $c = \frac{\mu_2 - \mu_1}{\mu_2 + \mu_1}$  is the viscosity contrast or Atwood ratio. The dynamics under consideration are basically controlled by these important dimensionless parameters: viscosity contrast ( $c$ ) and surface tension ( $v$ ). It has already been observed by Tryggvason and Aref (Tryggvason and Aref, 1983) and later on by Maher (Maher, 1985) that the viscosity contrast has a strong influence on the dynamics of Hele-Shaw flows and consequently in the morphology of the fingering patterns formed. In 1985, Tryggvason and Aref (Tryggvason and Aref, 1985) also studied the simple two-finger configurations to confirm the dramatic differences between high  $c$  and low  $c$  dynamics by direct numerical simulations. In conclusion, Curtis (Curtis and Maher, 1989) and Vinals (Vinals and Jasnow, 1992) showed that for low  $c$  the finger competition process was strongly inhibited, and the coarsening process observed for high  $c$  that leads to the formation of a single finger does not seem to take place.

In order to clarify the issue on more rigorous grounds, J. Casademunt and D. Jasnow (Casademunt and Jasnow, 1991; Casademunt and Jasnow, 1994) have developed a topological approach to study finger competition that allowed new insights on the dynamics of low  $c$ . They conjectured that the size of the basin of attraction of the Saffman-Taylor depended on the value of  $c$ . That is, even though a Saffman-Taylor finger solution exists and is stable for any value of  $c$ , it might not be the universal attractor of the dynamics for any viscosity contrast,  $c$ . It begs the question of what

will happen to the system in the long run if it is not drawn to a single-finger arrangement. Thus, it seemed crucial to take another look at those unanswered questions and attempt to provide fresh insight.

Another essential justification for investigating this matter with precise numerics is its applicability to the fundamental query regarding the occurrence of topological singularities (Eggers, 1997). In both experiments and simulations, for low  $c$ , an enhanced tendency to interface pinch-off can be observed. While the author did not specifically address in his work the nontrivial question of whether the dynamics leads spontaneously to finite-time pinch-off, he pushed the idea that the tendency to pinch-off can be related to the fact that attractors with different topologies coexist and compete. In comparison to the high viscosity case, the problem of Hele-Shaw flows with arbitrary viscosity contrast has received some attention also from a mathematical point of view. To draw the community's attention to this fundamental issue, Howison (Howison, 2000) has presented a formal method for locating explicit solutions to the two-phase flow in a Hele-Shaw cell.

#### 4.3.1.1 Basin of attraction of Saffman-Taylor finger

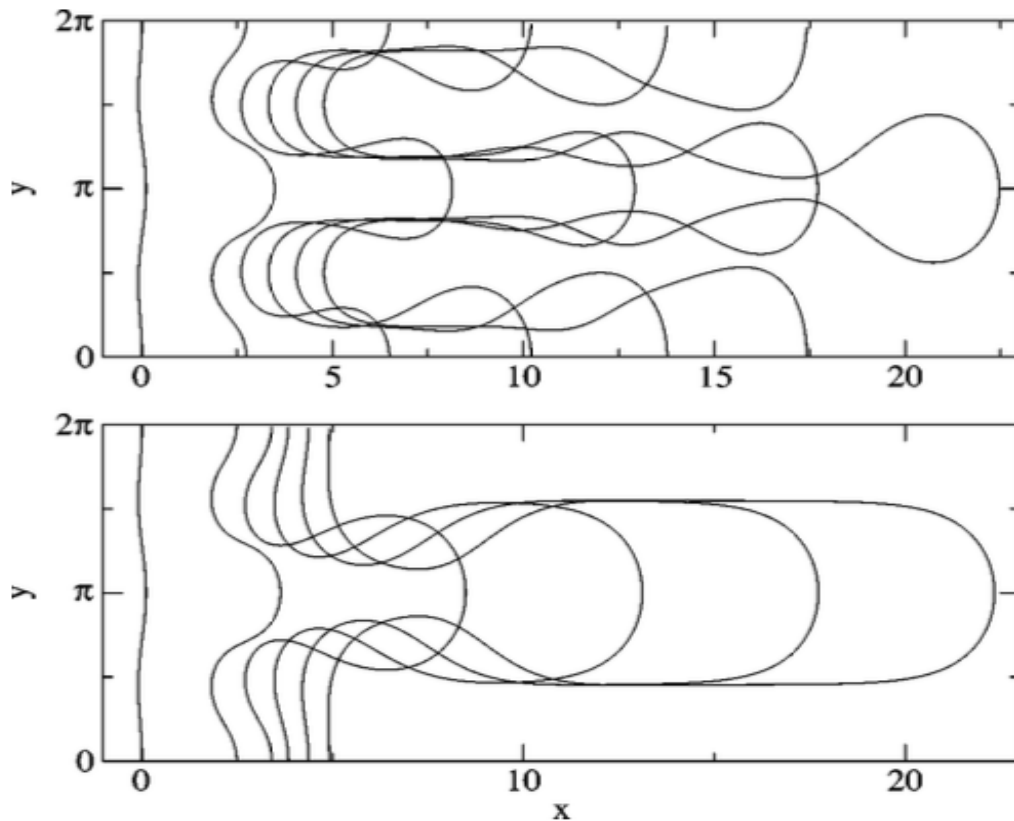


FIGURE 4.1: Two types of finger dynamics observed for  $c = 0$  (Upper plot) and  $c \neq 0$  (Lower plot) (Casademunt, 2004)

J. Casademunt and E. Paune (Pauné, Siegel, and Casademunt, 2002) aimed to add this subsection in order to present and characterize in a quantitative way the dependence of the basin of attraction of the ST finger on viscosity contrast  $c$  (See figure-4.1). It is clear from their literature (Pauné, Siegel, and Casademunt, 2002)



that the two-finger configurations will be adequate to study the finger competition. Although the authors did not address the small surface tension limit for general viscosity contrast, they recognized this as an interesting and completely open problem. They have shown that the basin of attraction of the Saffman–Taylor’s finger is only the full phase space for the strict limit of high viscosity contrast ( $c = 1$ ), while it decreases gradually with  $c$  to a small but not vanishing region for  $c = 0$ . The behavior for smaller  $c$ , for which no finger competition is evident, must be treated as more generic. The maximal sensitivity to  $c$  is precisely at  $c = 1$ .

#### 4.3.1.2 The competing attractors of Taylor-Saffman bubbles

For arbitrary viscosity contrast, finger competition is generically absent or weak, and the ST finger may not be reached. Instead, a more complex structure, such as a bubble-shaped tip connected to the rest of the interface by a long, narrow neck, that can be extremely thin next to the bubble region may arise, and attractors absent for high viscosity contrast may also appear (see figure-4.2). This bubble formation process has been observed (Casademunt, 2004) for a wide range of values of the viscosity contrast,  $c$ , except for values very close to 1. Formation of bubbles for low viscosity contrast has been previously reported by Tryggvason and Aref (Tryggvason and Aref, 1983) in more complex interfacial configurations. The (partial) attractors of the dynamics that compete with the ST finger have been identified as closed bubble solutions. The fact that these have a different topology than the initial condition provides an explanation of the observed tendency to interface pinch-off. A thorough study of the dynamics that lead to finite-time pinch-off is indeed one of the future directions to be explored. The fundamental idea is that regardless of whether or not there is a finite-time pinch-off, it seems clear that the isolated bubble solutions do behave in practice as attractors of the dynamics, at least partially.

J. Casademunt and D. Jasnow (Casademunt and Jasnow, 1991; Casademunt and Jasnow, 1994) in their computations showed that, for a given initial condition, as the viscosity contrast is decreased, the area of the bubble gets smaller. They have given a possible explanation for this behavior with more details in (Pauné, Siegel, and Casademunt, 2002). While many interesting questions remain open, most remarkably are those concerning finite-time pinch-off, the conclusions of this analysis are clear from (Casademunt and Jasnow, 1991; Pauné, Siegel, and Casademunt, 2002). On the one hand, the dynamics of low viscosity contrast appear to be more general than those of high viscosity contrast (which are more frequently discussed in the literature), in that the typical scenario of a finger competition only occurs for values of  $c$  that are extremely close to one. Thus, in the vicinity of  $c = 1$ , there is a very large sensitivity of the dynamics to  $c$ . On the other hand, they have strengthened the hypothesis that Saffman-Taylor’s basin of attraction is continuously decreasing with  $c$ . Furthermore, they have identified the isolated Taylor–Saffman bubbles as the missing attractors that compete with the Saffman–Taylor finger. The general tendency to pinch-off observed in experiments and simulation finds a natural explanation by having a different topology from that of the interface in the initial configuration (Casademunt, 2004).

Till now, the effect of viscosity contrast has only been studied for dimensionless surface tension of order one. It remains an open and challenging question to explore

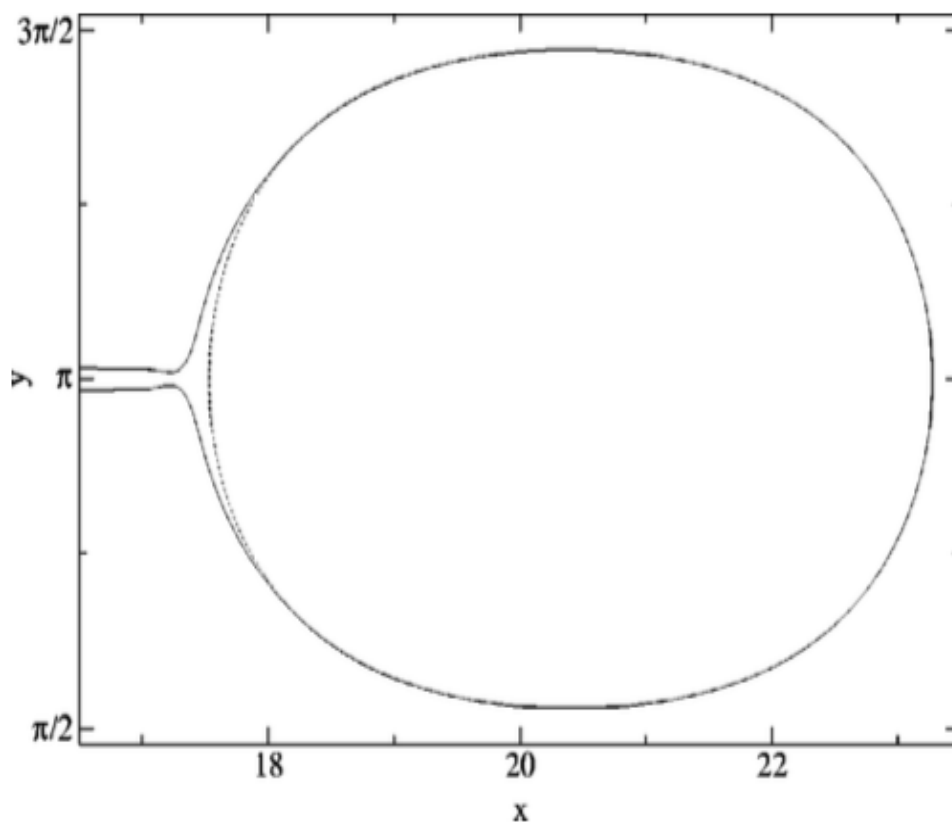


FIGURE 4.2: Bubble shaped region for a given surface tension and viscosity contrast (Casademunt, 2004)

how the perturbative picture of small surface tension is modified if viscosity contrast is different from  $c = 1$ . While classical (static) solvability theory is not fundamentally modified by varying  $c$ , the situation for the time-dependent behavior is expected to be much more involved, as suggested by the lack of explicit time-dependent solutions for  $B = 0$  and  $c \neq 1$ . As far as the (time-dependent) single-ST finger of relative width  $\Lambda = 1/2$  (Jacquard and Ségurier, 1962) is concerned, it is the only exact time-dependent solution for arbitrary  $c$  ( $B = 0$ ). Remarkably, other filling fractions  $\Lambda$  have time-dependent single-finger solutions only for (Pauné, Siegel, and Casademunt, 2002; Alvarez-Lacalle, Casademunt, and Ortín, 2001)  $c = 1$ . This finding reveals a fascinating relationship between the width selection issue and the dynamical function of viscosity contrast.

#### 4.3.1.3 Rotating Hele-Shaw flows

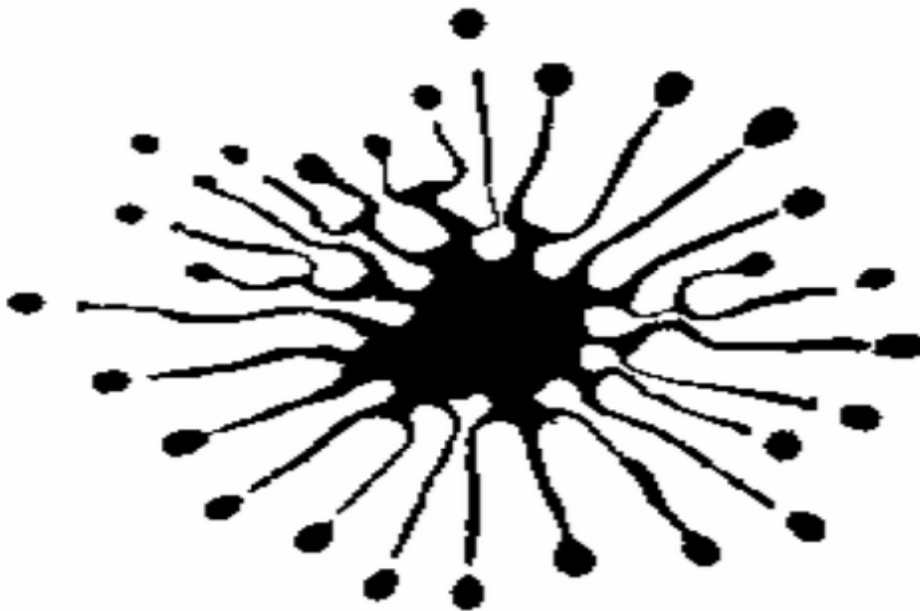


FIGURE 4.3: Typical experimental pattern of low viscosity contrast fingering under rotation (Casademunt, 2004)

The case of rotating Hele-Shaw flows has been studied only quite recently, both theoretically and experimentally, and has revealed a wealth of new phenomena and new interesting questions. Apart from the interplay between dynamics and interface morphology, the most salient feature in terms of future research has been the enhanced occurrence of topological singularities and their relation to viscosity contrast. While pinch-off singularities have been studied in Hele-Shaw problems in the past, it is, in particular, a usual setup to specifically design to produce pinch-off. In the case of rotating Hele-Shaw flows (see figure-4.3), it has been shown that the dynamics lead naturally to situations approaching pinch-off. However, a detailed study of the asymptotic approach to pinch-off within a lubrication approximation is still lacking. This point is currently being explored both analytically and numerically (Folch et al., 2004; Folch et al., 2009).

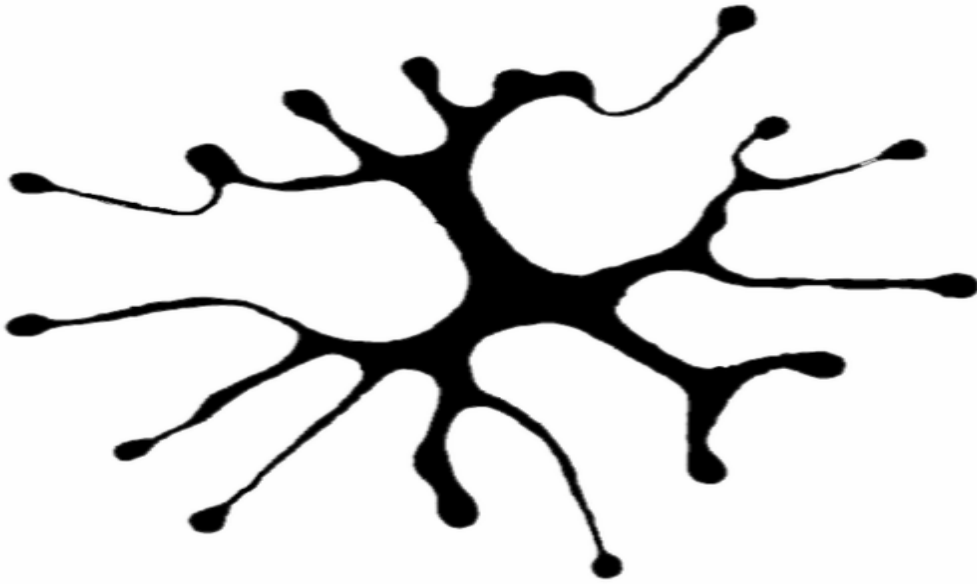


FIGURE 4.4: Typical experimental pattern for  $c = 1$ , with air as the outer fluid, if the cell is initially dry (Casademunt, 2004)

The study of rotating flows has also highlighted the need for a more thorough investigation of the effective boundary condition at the interface during the displacement of the wetting fluid by the non-wetting one (see figure-4.4), a circumstance that is typical for centrifugally driven flows but unusual in more conventional experiments. Having the cell prewetted makes a significant difference in the first scenario. A typical but frequently unsolved issue in fluid mechanics is the motion of a contact line, which is related to the description of the wetting fluid moving forward in a dry cell. An extremely intriguing early investigation demonstrates that the influence is not only perceptible computationally but also qualitatively in the overall shape of the generated patterns, even with a rather crude description of the contact line motion. The adoption of a microscopic length scale is necessary for the treatment of the contact line. (related to the thickness of the precursor wetting film). Thus, it is noteworthy that such a microscopic length scale has a significant impact on the macroscopic pattern morphology in a manner that is similar to the impact of the capillary length on pattern selection in the microscopic solvability scenario. This open question is also of great interest and also sets forth a promising future perspective.

Finally, one of the most interesting lines of future research in the context of Hele-Shaw flows consists of adding controlled modifications of the classical setup to define richer model systems and use them to pursue basic and general principles of more complicated systems, in the spirit of McCloud and Maher, 1995 (McCloud and Maher, 1995). The case of the random Hele-Shaw cell as a model of a porous medium is a paradigmatic and fruitful recent example (Pauné, Siegel, and Casademunt, 2002; Pauné and Casademunt, 2003). This specific instance has led to the preliminary derivation of an interface equation, which has allowed generalizations to be made regarding the issue of interface roughening in the fluid invasion of porous media. It has also provided a suitable theoretical framework within which renormalization group analysis and numerical simulation can operate with assurance.

The usefulness of the Hele-Shaw-type model-system analysis has thus been remarkable in a field where controversy and confusion have been too common. The explicit knowledge of all interface equation parameters enables one to design new experiments with the best possible parameter selection. This is more important than simply being able to reinterpret old experimental and simulational results after deriving the exact interface equation with all noise contributions. Experiments on Hele-Shaw cells with a random gap as a model system for porous media have already been carried out by J. Soriano and co-workers (see, for instance, (Soriano, Ortín, and Hernandez-Machado, 2002)). The possibility of a clear connection between theory and experiment and the good control that is possible in both aspects makes this line also a promising and exciting direction.

## 4.4 Concluding remark

The section summary concludes with the observation that viscous fingering and its modifications continue to be a challenging and consistently surprising model system despite years of research and study. It is useful for understanding fundamental physics, but it also provides a strong foundation for analyzing various issues with interfacial pattern generation through controlled experimentation and analytical insight.

Although the work on the analysis (Bansal, Ghosh, and Sircar, 2023) that is presented here has been built on earlier findings (Hong and Langer, 1986) by introducing a shear-dependent, power-law form of viscosity, there are some flaws in the model that shouldn't be ignored, including the lack of elastic stresses (which are crucial for fluids that thicken under shear), the absence of a characteristic time scale and viscosity, and the presence of significant measurement errors in the vicinity of zero shear rates (Bird, Armstrong, and Hassager, 1987). A future aim will be to explain the selection mechanism for strong shear-thinning fluids by perturbatively expanding the model via the radius of the fingertip. Also, notice that, with a large aspect ratio and in the inertial regime, the boundary effects are especially important for cell geometry. Hence, a deeper consideration of the impact of boundaries like: elastic boundaries and occlusions, the moving boundaries should be worthwhile in the future (Bansal, Chauhan, and Sircar, 2022).

## Bibliography

- Aharonov, E., M. Spiegelman, and P. Kelemen (1997). “Three-dimensional flow and reaction in porous media: Implications for the Earth’s mantle and sedimentary basins”. In: *Journal of Geophysical Research: Solid Earth* 102.B7, pp. 14821–14833.
- Ahmadikhamsi, Seyedarash, Fabrice Golfier, Constantin Oltean, Eric Lefèvre, and S. Amir Bahrani (2020). “Impact of surfactant addition on non-Newtonian fluid behavior during viscous fingering in Hele-Shaw cell”. In: *Physics of Fluids* 32.1, p. 012103.
- Akylas, T. R. (1982). “A nonlinear theory for the generation of water waves by wind”. In: *Studies in Applied Mathematics* 67, pp. 1–24.
- Akylas, T. R. and D. J. Benney (1980). “Direct resonance in nonlinear wave systems”. In: *Studies in Applied Mathematics* 63.209-226.
- Akylas, T. R. and D. J. Benney (1982). “The Evolution of Waves Near Direct-Resonance Conditions”. In: *Studies in Applied Mathematics* 67, pp. 107–123.
- Al-Housseiny, Talal T. and Howard A. Stone (2013). “Controlling viscous fingering in tapered Hele-Shaw cells”. In: *Physics of Fluids* 25.9, p. 092102.
- Alhushaybar, A. and J. Uddin (2019). “Convective and absolute instability of viscoelastic liquid jets in the presence of gravity”. In: *Physics of Fluids* 31, p. 044106.
- Alhushaybar, A. and J. Uddin (2020). “Absolute instability of free-falling viscoelastic liquid jets with surfactants”. In: *Physics of Fluids* 32, p. 013102.
- Alvarez-Lacalle, Enrique, J Casademunt, and Jordi Ortín (2001). “Systematic weakly nonlinear analysis of interfacial instabilities in Hele-Shaw flows”. In: *Physical Review E* 64.1, p. 016302.
- Amar, Martine Ben and Daniel Bonn (2005). “Fingering instabilities in adhesive failure”. In: *Physica D: Nonlinear Phenomena* 209.1-4, pp. 1–16.
- Araktingi, Udo Gaetan and FM Orr (1993). “Viscous fingering in heterogeneous porous media”. In: *SPE Advanced Technology Series* 1.01, pp. 71–80.
- Aranha, J.A., D.K.P. Yue, and C.C. Mei (1982). “Nonlinear waves near a cut off frequency in an acoustic duct- a numerical study”. In: *Journal of Fluid Mechanics* 121, pp. 465–485.
- Avendano, J, Nicolas Pannacci, Benjamin Herzhaft, Patrick Gateau, and Philippe Coussot (2013). “Enhanced displacement of a liquid pushed by a viscoelastic fluid”. In: *Journal of colloid and interface science* 410, pp. 172–180.
- Bansal, D, T Chauhan, and S Sircar (2022). “Spatiotemporal linear stability of viscoelastic Saffman–Taylor flows”. In: *Physics of Fluids* 34.10.
- Bansal, D., D. Ghosh, and S. Sircar (2021). “Spatiotemporal linear stability of viscoelastic free shear flows: non-affine response regime”. In: *Physics of Fluids* 33, p. 054106.

- Bansal, Diksha, Dipa Ghosh, and Sarthok Sircar (2023). “Selection Mechanism in Non-Newtonian Saffman–Taylor Fingers”. In: *SIAM Journal on Applied Mathematics* 83.2, pp. 329–353.
- Barbieri, Angelo, Daniel C. Hong, and J. S. Langer (1987). “Velocity selection in the symmetric model of dendritic crystal growth”. In: *Physical Review A* 35.4, pp. 1802–1808.
- Beeson-Jones, Tim H. and Andrew W. Woods (2015). “On the selection of viscosity to suppress the Saffman–Taylor instability in a radially spreading annulus”. In: *Journal of Fluid Mechanics* 782, pp. 127–143.
- Bekri, S, JF Thovert, and PM Adler (1995). “Dissolution of porous media”. In: *Chemical Engineering Science* 50, p. 17.
- Ben, Yuxing, Evgeny A Demekhin, and Hsueh-Chia Chang (2002). “A spectral theory for small-amplitude miscible fingering”. In: *Physics of Fluids* 14.3, pp. 999–1010.
- Ben-Jacob, Eshel, Ofer Schochet, Adam Tenenbaum, Inon Cohen, Andras Czirók, and Tamas Vicsek (1994). “Generic modelling of cooperative growth patterns in bacterial colonies”. In: *Nature* 368.6466, pp. 46–49.
- Benny, D. J. and L. H. Gustavsson (1981). “A new mechanism for linear and nonlinear hydrodynamic instability”. In: *Studies in Applied Mathematics* 64, pp. 185–209.
- Bensimon, D., L. P. Kadanoff, S. Liang, B. I. Shraiman, and C. Tang (1986). “Viscous flow in two dimensions”. In: *Reviews of Modern Physics* 58.977.
- Bernardi, Francesca, Shankararaman Chellam, NG Cogan, and MNJ Moore (2023). “Stokes flow solutions in infinite and semi-infinite porous channels”. In: *Studies in Applied Mathematics*.
- Bers, A. (1983). *Space-time evolution of plasma instabilities-absolute and convective*. Vol. 1. Handbook of Plasma Physics.
- Bihi, Ilyesse, Michael Baudoin, Jason E. Butler, Christine Faille, and Farzam Zouesh-tiagh (2016). “Inverse Saffman-Taylor Experiments with Particles Lead to Capillarity Driven Fingering Instabilities”. In: *Physical Review Letters* 117.3, p. 034501.
- Bird, R. B., R. C. Armstrong, and O. Hassager (1987). *Dynamics of polymeric liquids, Volume 1: Fluid Mechanics*. Wiley Intersciences.
- Bonn, D., H. Kellay, M. Bräunlich, M. Ben Amar, and J. Meunier (1995). “Viscous fingering in complex fluids”. In: *Physica A: Statistical Mechanics and its Applications* 220.1-2, pp. 60–73.
- Bonn, D. and J. Meunier (1997). “Viscoelastic Free-Boundary Problems: Non-Newtonian Viscosity vs Normal Stress Effects”. In: *Physical Review Letters* 79.14, pp. 2662–2665.
- Booth, R. J. S. (2010). “On the growth of the mixing zone in miscible viscous fingering”. In: *Journal of Fluid Mechanics* 655, pp. 527–539.
- Briggs, R. J. (1964). *Electron-stream interaction with plasmas*. MIT Press, Cambridge.
- Böckmann, Martin and Stefan C. Müller (2000). “Growth Rates of the Buoyancy-Driven Instability of an Autocatalytic Reaction Front in a Narrow Cell”. In: *Physical Review Letters* 85.12, pp. 2506–2509.
- Casademunt, J and David Jasnow (1991). “Defect dynamics in viscous fingering”. In: *Physical Review Letters* 67.26, p. 3677.

- Casademunt, J. and F.X. Magdaleno (2000). “Dynamics and selection of fingering patterns. Recent developments in the Saffman–Taylor problem”. In: *Physics Reports* 337.1-2, pp. 1–35.
- Casademunt, Jaume (2004). “Viscous fingering as a paradigm of interfacial pattern formation: Recent results and new challenges”. In: *Chaos: An Interdisciplinary Journal of Nonlinear Science* 14.3, pp. 809–824.
- Casademunt, Jaume and David Jasnow (1994). “Finger competition and viscosity contrast in viscous fingering. A topological approach”. In: *Physica D: Nonlinear Phenomena* 79.2-4, pp. 387–408.
- Chan, C. K. and N. Y. Liang (1997). “Observations of Surfactant Driven Instability in a Hele-Shaw Cell”. In: *Physical Review Letters* 79.22, pp. 4381–4384.
- Chandrasekhar, S (2013). *Hydrodynamic and Hydromagnetic Stability*.
- Chen, Jing-Den (1989). “Growth of radial viscous fingers in a Hele-Shaw cell”. In: *Journal of Fluid Mechanics* 201.-1, p. 223.
- Chevalier, C., A. Lindner, and E. Clément (2007). “Destabilization of a Saffman–Taylor Fingerlike Pattern in a Granular Suspension”. In: *Physical Review Letters* 99.17, p. 174501.
- Chevalier, Christophe, MARTINE BEN AMAR, Daniel Bonn, and Anke Lindner (2006). “Inertial effects on Saffman–Taylor viscous fingering”. In: *Journal of fluid mechanics* 552, pp. 83–97.
- Christie, MA, ADW Jones, and AH Muggeridge (1990). “Comparison between laboratory experiments and detailed simulations of unstable miscible displacement influenced by gravity”. In: *North Sea Oil and Gas Reservoirs—II*. Springer, pp. 245–250.
- Christie, MA, AH Muggeridge, and JJ Barley (1993). “3D simulation of viscous fingering and WAG schemes”. In: *SPE reservoir engineering* 8.01, pp. 19–26.
- Chuoque, RL, P Van Meurs, and C\_ van der Poel (1959). “The instability of slow, immiscible, viscous liquid-liquid displacements in permeable media”. In: *Transactions of the AIME* 216.01, pp. 188–194.
- Clemmow, P.C. and J.P. Dougherty (1969). *Electronics of particles and plasmas*. Reading, Mass: Addison-Wesley.
- Cogan, Nick G, John Spencer Gunn, and Daniel J Wozniak (2011). “Biofilms and infectious diseases: biology to mathematics and back again”. In: *FEMS microbiology letters* 322.1, pp. 1–7.
- Combescot, Roland, Thierry Dombre, Vincent Hakim, Yves Pomeau, and Alain Pumir (1986). “Shape Selection of Saffman-Taylor Fingers”. In: *Physical Review Letters* 56 (19), pp. 2036–2039.
- Corvera Poiré, Eugenia and Martine Ben Amar (1998). “Finger Behavior of a Shear Thinning Fluid in a Hele-Shaw Cell”. In: *Physical Review Letters* 81.10, pp. 2048–2051.
- Couder, Y. (2000). “Viscous fingering as an archetype of growth pattern”. In: ed. by Batchelor G. K., Moffatt H. K., and Worster M. G. Cambridge University Press, pp. 53–104.
- Coussot, Philippe (1999). “Saffman–Taylor instability in yield-stress fluids”. In: *Journal of Fluid Mechanics* 380, pp. 363–376.



- Cremer, L. (1953). “Theorie der Luftschall-Dämpfung im Rechteckkanal mit schluckender Wand und das sich dabei ergebende höchste Dämpfungsmag”. In: *Acustica* 8, pp. 249–263.
- Crighton, D.G. and M. Gaster (1976). “Stability of slowly-diverging jet flow”. In: *Journal of Fluid Mechanics* 77, pp. 397–413.
- Cueto-Felgueroso, Luis and Ruben Juanes (2014). “A phase-field model of two-phase Hele-Shaw flow”. In: *Journal of Fluid Mechanics* 758, pp. 522–552.
- Curtis, SA and JV Maher (1989). “Racetrack for competing viscous fingers”. In: *Physical Review Letters* 63.25, p. 2729.
- Daripa, Prabir and Xueru Ding (2012). “Universal stability properties for multilayer hele-shaw flows and application to instability control”. In: *SIAM Journal on Applied Mathematics* 72.5, pp. 1667–1685.
- De Wit, A. (2001). “Fingering of Chemical Fronts in Porous Media”. In: *Physical Review Letters* 87.5, p. 054502.
- De Wit, A. and G. M. Homsy (1999a). “Nonlinear interactions of chemical reactions and viscous fingering in porous media”. In: *Physics of Fluids* 11.5, pp. 949–951.
- De Wit, A. and G. M. Homsy (1999b). “Viscous fingering in reaction-diffusion systems”. In: *The Journal of Chemical Physics* 110.17, pp. 8663–8675.
- Demuth, Rainer and Eckart Meiburg (2003). “Chemical fronts in Hele-Shaw cells: Linear stability analysis based on the three-dimensional Stokes equations”. In: *Physics of Fluids* 15.3, pp. 597–602.
- Dias, Eduardo O. and José A. Miranda (2011). “Influence of inertia on viscous fingering patterns: Rectangular and radial flows”. In: *Physical Review E* 83.6, p. 066312.
- Eastham, PS, MNJ Moore, NG Cogan, Qingpu Wang, and Oliver Steinbock (2020). “Multiphase modelling of precipitation-induced membrane formation”. In: *Journal of Fluid Mechanics* 888, A20.
- Ecke, Robert E. and Scott Backhaus (2016). “Plume dynamics in Hele-Shaw porous media convection”. In: *Philosophical Transactions of the Royal Society A: Mathematical, Physical and Engineering Sciences* 374.2078, p. 20150420.
- Eggers, Jens (1997). “Nonlinear dynamics and breakup of free-surface flows”. In: *Reviews of modern physics* 69.3, p. 865.
- Fadoul, Oumar Abdoulaye and Philippe Coussot (2019). “Saffman–Taylor instability in yield stress fluids: Theory–experiment comparison”. In: *Fluids* 4.1, p. 53.
- Fast, Petri, L. Kondic, Michael J. Shelley, and Peter Palffy-Muhoray (2001). “Pattern formation in non-Newtonian Hele–Shaw flow”. In: *Physics of Fluids* 13.5, pp. 1191–1212.
- Fernandez, J., R. Krechetnikov, and G. M. Homsy (2005). “Experimental study of a surfactant-driven fingering phenomenon in a Hele-Shaw cell”. In: *Journal of Fluid Mechanics* 527, pp. 197–216.
- Fernandez, J, P Kurowski, P Petitjeans, and E Meiburg (2002). “Density-driven unstable flows of miscible fluids in a Hele-Shaw cell”. In: *Journal of Fluid Mechanics* 451, pp. 239–260.
- Folch, R, E Alvarez-Lacalle, J Ortín, and J Casademunt (2004). “Spontaneous pinch-off in rotating Hele-Shaw flows”. In: *arXiv preprint physics/0408092*.

- Folch, R, E Alvarez-Lacalle, J Ortín, and J Casademunt (2009). “Pattern formation and interface pinch-off in rotating Hele-Shaw flows: A phase-field approach”. In: *Physical Review E* 80.5, p. 056305.
- Franco-Gómez, Andrés, Alice B. Thompson, Andrew L. Hazel, and Anne Juel (2016). “Sensitivity of Saffman–Taylor fingers to channel-depth perturbations”. In: *Journal of Fluid Mechanics* 794, pp. 343–368.
- Fredd, Christopher N. and H. Scott Fogler (1998). “Influence of transport and reaction on wormhole formation in porous media”. In: *AIChE Journal* 44.9, pp. 1933–1949.
- Gaster, M., E. Kit, and I. Wygnanski (1985). “Large scale structures in a forced turbulent mixing layer”. In: *Journal of Fluid Mechanics* 150, pp. 23–29.
- Ghatak, A. (2006). “Confinement-induced instability of thin elastic film”. In: *Physical Review E* 73.4, p. 041601.
- Ghatak, Animangsu, Manoj K. Chaudhury, Vijay Shenoy, and Ashutosh Sharma (2000). “Meniscus Instability in a Thin Elastic Film”. In: *Physical Review Letters* 85.20, pp. 4329–4332.
- Goldstein, R. E., A. I. Pesci, and M. J. Shelley (1993). “Topology Transitions and Singularities in Viscous Flows”. In: *Physical Review Letters* 70, (20),3043–3047.
- Goyal, N. and E. Meiburg (2006). “Miscible displacements in Hele-Shaw cells: two-dimensional base states and their linear stability”. In: *Journal of Fluid Mechanics* 558, p. 329.
- Grillet, A. M., A. G. Lee, and E. S. G. Shaqfeh (1999). “Observations of ribbing instabilities in elastic fluid flows with gravity stabilization”. In: *Journal of Fluid Mechanics* 399, pp. 49–83.
- Gupta, Vikas, Mohan K Kadalbajoo, and Ritesh K Dubey (2019). “A parameter-uniform higher order finite difference scheme for singularly perturbed time-dependent parabolic problem with two small parameters”. In: *International Journal of Computer Mathematics* 96.3, pp. 474–499.
- Gustavsson, L. H. (1981). “Resonant growth of three-dimensional disturbances in plane Poiseuille flow”. In: *Journal of Fluid Mechanics* 112.253-264.
- Gustavsson, L. H. and L. S. Hultgren (1980). “A resonance mechanism in plane Couette flow”. In: *Journal of Fluid Mechanics* 98, pp. 149–159.
- Haudin, F., L. A. Riolfo, B. Knaepen, G. M. Homsy, and A. De Wit (2014). “Experimental study of a buoyancy-driven instability of a miscible horizontal displacement in a Hele-Shaw cell”. In: *Physics of Fluids* 26.4, p. 044102.
- Hazel, James, Kaspars Krutkramelis, Paul Mooney, Miroslav Tomschik, Ken Gerow, John Oakey, and J. C. Gatlin (2013). “Changes in Cytoplasmic Volume Are Sufficient to Drive Spindle Scaling”. In: *Science* 342.6160, pp. 853–856.
- Hele-Shaw, H. S. (1898). “Flow of Water”. In: *Nature* 58.1509, pp. 520–520.
- Heussler, F. H. C., R. M. Oliveira, M. O. John, and E. Meiburg (2014). “Three-dimensional Navier–Stokes simulations of buoyant, vertical miscible Hele-Shaw displacements”. In: *Journal of Fluid Mechanics* 752, pp. 157–183.
- Hirata, T. (1998). “Fracturing due to fluid intrusion into viscoelastic materials”. In: *Physical Review E* 57.2, pp. 1772–1779.
- Ho, C.M. and P. Huerre (1984). “Perturbed free shear layers”. In: *Annual review of fluid mechanics* 16, pp. 365–424.

- Ho, NguyenHo, Karin Leiderman, and Sarah Olson (2019). “A three-dimensional model of flagellar swimming in a Brinkman fluid”. In: *Journal of Fluid Mechanics* 864, pp. 1088–1124.
- Homsy, George M (1987). “Viscous fingering in porous media”. In: *Annual review of fluid mechanics* 19.1, pp. 271–311.
- Hong, D. C. and J. S. Langer (1986). “Analytic Theory of the Selection Mechanism in the Saffman-Taylor Problem”. In: *Physical Review Letters* 56.19, pp. 2032–2035.
- Hooshanginejad, Alireza, Benjamin C. Druecke, and Sungyon Lee (2019). “Stability analysis of a particle band on the fluid–fluid interface”. In: *Journal of Fluid Mechanics* 869, R2.
- Hosseinalipoor, Seyed Mostafa, Arash Nemati, Behrooz Zare Vamerzani, and Hamid Saffari (2020). “Experimental study of finger behavior due to miscible viscous and gravity contrast in a porous model”. In: *Energy Sources, Part A: Recovery, Utilization, and Environmental Effects* 42.19, pp. 2434–2447.
- Howison, Sam D (2000). “A note on the two-phase Hele-Shaw problem”. In: *Journal of Fluid Mechanics* 409, pp. 243–249.
- Huerre, Axel, Olivier Theodoly, Alexander M. Leshansky, Marie-Pierre Valignat, Isabelle Cantat, and Marie-Caroline Jullien (2015). “Droplets in Microchannels: Dynamical Properties of the Lubrication Film”. In: *Physical Review Letters* 115.6, p. 064501.
- Huerre, P. and P. A. Monkewitz (1985). “Absolute and convective instabilities in free shear layers”. In: *Journal of Fluid Mechanics* 159, pp. 151–168.
- Huerre, P. and P. A. Monkewitz (1990). “Local and global instabilities in spatially developing flows”. In: *Annual review of fluid mechanics* 22, pp. 473–537.
- Hultgren, L. S. and L. H. Gustavsson (1981). “Algebraic growth of disturbances in a laminar boundary layer”. In: *Physics of Fluids* 24, pp. 1000–1004.
- Islam, MR and Z Saghir (1999). “Experimental and numerical modelling studies of viscous fingering”. In: *Annual Technical Meeting. OnePetro*.
- Iyer, K, B Jamtveit, J Mathiesen, A Malthesorensen, and J Feder (2008). “Reaction-assisted hierarchical fracturing during serpentinization”. In: *Earth and Planetary Science Letters* 267.3-4, pp. 503–516.
- Jacquard, P and P Séguier (1962). “Mouvement de deux fluides en contact dans un milieu poreux”. In: *J. de Mec* 1, pp. 367–394.
- Jha, Anuradha and Mohan Krishen Kadalbajoo (2021). “Hybrid method for two parameter singularly perturbed elliptic boundary value problems”. In: *Computational and Mathematical Methods* 3.6, e1210.
- John, M. O., R. M. Oliveira, F. H. C. Heussler, and E. Meiburg (2013). “Variable density and viscosity, miscible displacements in horizontal Hele-Shaw cells. Part 2. Nonlinear simulations”. In: *Journal of Fluid Mechanics* 721, pp. 295–323.
- Johnsen, Ø., R. Toussaint, K. J. Måløy, and E. G. Flekkøy (2006). “Pattern formation during air injection into granular materials confined in a circular Hele-Shaw cell”. In: *Physical Review E* 74.1, p. 011301.
- Kambhammettu, Sri Krishna Sudhamsu, Abhijit P Deshpande, and Lakshmana Rao Chebolu (2021). “A Compressible Porous Media Model to Estimate Fluid Leak Through a Metal–Elastomer Interface”. In: *Transport in Porous Media* 136, pp. 191–215.

- Karmakar, Supriya and Priyanka Shukla (2023). “Instability of a plane Poiseuille flow bounded between inhomogeneous anisotropic porous layers”. In: *Thermal Science and Engineering Progress* 40, p. 101758.
- Karmakar, Supriya, R Usha, Geetanjali Chattopadhyay, Severine Millet, JV Ramana Reddy, and Priyanka Shukla (2022). “Stability of a plane Poiseuille flow in a channel bounded by anisotropic porous walls”. In: *Physics of Fluids* 34.3, p. 034103.
- Kim, Min Chan and Chang Kyun Choi (2011). “Linear analysis on the stability of miscible dispersion of shear-thinning fluids in porous media”. In: *Journal of Non-Newtonian Fluid Mechanics* 166.21–22, pp. 1211–1220.
- Koch, W. (1986). “Direct resonance in Orr-Sommerfeld problems”. In: *Acta mechanica* 59, pp. 11–29.
- Kondic, L., P. Palffy-Muhoray, and M. J. Shelley (1980). “Non-Newtonian Hele-Shaw flow and the Saffman-Taylor instability”. In: *Physical Review Letters* 80, pp. 1433–1436.
- Kondic, Ljubinko, Peter Palffy-Muhoray, and Michael J. Shelley (1996). “Models of non-Newtonian Hele-Shaw flow”. In: *Physical Review E* 54.5, R4536–R4539.
- Koval, E.J. (1963). “A Method for Predicting the Performance of Unstable Miscible Displacement in Heterogeneous Media”. In: *Society of Petroleum Engineers Journal* 3.02, pp. 145–154.
- Kupfer, K., A. Bers, and A. K. Ram (1987). “The cusp map in the complex-frequency plane for absolute instability”. In: *Physics of Fluids* 30.10, pp. 3075–3082.
- Lagrée, Bertrand, Stéphane Zaleski, and Igor Bondino (2016). “Simulation of Viscous Fingering in Rectangular Porous Media with Lateral Injection and Two- and Three-Phase Flows”. In: *Transport in Porous Media* 113.3, pp. 491–510.
- Lajeunesse, E., J. Martin, N. Rakotomalala, and D. Salin (1997). “3D Instability of Miscible Displacements in a Hele-Shaw Cell”. In: *Physical Review Letters* 79.26, pp. 5254–5257.
- Landau, L.D. and E.M. Lifshitz (1959). *Fluid Mechanics*. London: Pergamon Press.
- Lemaire, E., P. Levitz, G. Daccord, and H. Van Damme (1991). “From viscous fingering to viscoelastic fracturing in colloidal fluids”. In: *Physical Review Letters* 67.15, pp. 2009–2012.
- Liang, X., D. B. Weber, T. F. Edgar, L. W. Lake, M. Sayarpour, and A. Al-Yousef (2007). “Optimization of Oil Production Based on A Capacitance Model of Production and Injection Rates”. In: *All Days*. Dallas, Texas, U.S.A.: SPE, SPE–107713–MS.
- Lifshitz, E. M. and L.P. Pitaevskii (1981). “Physical kinetics”. In: London: Pergamon. Chap. 6.
- Lindner, A., D. Bonn, and J. Meunier (2000). “Viscous fingering in a shear-thinning fluid”. In: *Physics of Fluids* 12.2, pp. 256–261.
- Lindner, Anke, Daniel Bonn, Eugenia Corvera Poiré, Martine Ben Amar, and Jacques Meunier (2002). “Viscous fingering in non-Newtonian fluids”. In: *Journal of Fluid Mechanics* 469, pp. 237–256.
- Lindner, Anke, Philippe Coussot, and Daniel Bonn (2000). “Viscous Fingering in a Yield Stress Fluid”. In: *Physical Review Letters* 85.2, pp. 314–317.
- Lindner, Anke and Christian Wagner (2009). “Viscoelastic surface instabilities”. In: *Comptes Rendus Physique* 10.8, pp. 712–727.

- Lingwood, R. J. (1997). “Absolute instability of the Ekman layer and related rotating flows”. In: *Journal of Fluid Mechanics* 331, pp. 405–428.
- Lozar, Alberto de and Björn Hof (2009). “An experimental study of the decay of turbulent puffs in pipe flow”. In: *Philosophical Transactions of the Royal Society A: Mathematical, Physical and Engineering Sciences* 367.1888, pp. 589–599.
- Lu, Daihui, Federico Municchi, and Ivan C. Christov (2020). “Computational Analysis of Interfacial Dynamics in Angled Hele-Shaw Cells: Instability Regimes”. In: *Transport in Porous Media* 131.3, pp. 907–934.
- Madhavan, Nithin, Abhijit P Deshpande, Ethayaraja Mani, and Madivala G Basavaraj (2023). “Electrostatic Heteroaggregation: Fundamentals and Applications in Interfacial Engineering”. In: *Langmuir* 39.6, pp. 2112–2134.
- Maher, JV (1985). “Development of viscous fingering patterns”. In: *Physical review letters* 54.14, p. 1498.
- Manickam, O. and G. M. Homsy (1995). “Fingering instabilities in vertical miscible displacement flows in porous media”. In: *Journal of Fluid Mechanics* 288, pp. 75–102.
- Mannan, Forest O and Karin Leiderman (2020). “Weak inertial effects on arbitrarily shaped objects in the presence of a wall”. In: *Physical Review Fluids* 5.4, p. 044102.
- McCloud, Kathleen V and James V Maher (1995). “Experimental perturbations to Saffman-Taylor flow”. In: *Physics Reports* 260.3, pp. 139–185.
- McLean, J. W. (1980). “Fingering problem in flow through porous media”. PhD thesis. Pasadena: CalTech.
- McLean, J. W. and P. G. Saffman (1981). “The effect of surface tension on the shape of fingers in a Hele Shaw cell”. In: *Journal of Fluid Mechanics* 102, pp. 455–469.
- Merkine, L.O. (1977). “Convective and absolute instability of baroclinic eddies”. In: *Geophysical & Astrophysical Fluid Dynamics* 9, pp. 29–57.
- Michael, K., A. Golab, V. Shulakova, J. Ennis-King, G. Allinson, S. Sharma, and T. Aiken (2010). “Geological storage of CO<sub>2</sub> in saline aquifers—A review of the experience from existing storage operations”. In: *International Journal of Greenhouse Gas Control* 4.4, pp. 659–667.
- Miranda, José A. and Michael Widom (1998). “Weakly Nonlinear Investigation of the Saffman–Taylor Problem in a Rectangular Hele–Shaw Cell”. In: *International Journal of Modern Physics B* 12.09, pp. 931–949.
- Mora, S. and M. Manna (2010). “Saffman-Taylor instability of viscoelastic fluids: From viscous fingering to elastic fractures”. In: *Physical Review E* 81.2, p. 026305.
- Morrow, Liam C., Timothy J. Moroney, and Scott W. McCue (2019). “Numerical investigation of controlling interfacial instabilities in non-standard Hele-Shaw configurations”. In: *Journal of Fluid Mechanics* 877, pp. 1063–1097.
- Nagatsu, Yuichiro, Chika Iguchi, Kenji Matsuda, Yoshihito Kato, and Yutaka Tada (2010). “Miscible viscous fingering involving viscosity changes of the displacing fluid by chemical reactions”. In: *Physics of Fluids* 22.2, p. 024101.
- Nagel, Mathias and François Gallaire (2013). “A new prediction of wavelength selection in radial viscous fingering involving normal and tangential stresses”. In: *Physics of Fluids* 25.12, p. 124107.
- Nase, Julia, Didi Derks, and Anke Lindner (2011). “Dynamic evolution of fingering patterns in a lifted Hele–Shaw cell”. In: *Physics of Fluids* 23.12, p. 123101.

- Nelson, Anna C, Michael A Kelley, Laura M Haynes, and Karin Leiderman (2021). “Mathematical models of fibrin polymerization: past, present, and future”. In: *Current Opinion in Biomedical Engineering* 20, p. 100350.
- Newell, A. Coe and J.A. Whitehead (1969). “Finite bandwidth, finite amplitude convection”. In: *Journal of Fluid Mechanics* 38, pp. 279–303.
- Nguyen, Hoang-Ngan, Sarah D Olson, and Karin Leiderman (2019). “Computation of a regularized Brinkmanlet near a plane wall”. In: *Journal of Engineering Mathematics* 114, pp. 19–41.
- Nittmann, Johann, Gérard Daccord, and H. Eugene Stanley (1985). “Fractal growth viscous fingers: quantitative characterization of a fluid instability phenomenon”. In: *Nature* 314.6007, pp. 141–144.
- Nooranidoost, Mohammad, NG Cogan, Paul Stoodley, Erin S Gloag, and M Yousuff Hussaini (2023). “Bayesian estimation of *Pseudomonas aeruginosa* viscoelastic properties based on creep responses of wild type, rugose, and mucoid variant biofilms”. In: *Biofilm*, p. 100133.
- Oertel, J. H. (1990). “Wakes behind blunt bodies”. In: *Annual Review of Fluid Mechanics* 22, pp. 539–564.
- Oliveira, Rafael M. and Eckart Meiburg (2011). “Miscible displacements in Hele-Shaw cells: three-dimensional Navier–Stokes simulations”. In: *Journal of Fluid Mechanics* 687, pp. 431–460.
- Oliveira, R. M., F. H. C. Heussler, M. O. John, and E. Meiburg (2014). “Three-dimensional Navier–Stokes simulations of buoyant, vertical miscible Hele-Shaw displacements”. In: *Journal of Fluid Mechanics* 752, pp. 157–183.
- Ortoleva, P., J. Chadam, E. Merino, and A. Sen (1987). “Geochemical self-organization II; the reactive-infiltration instability”. In: *American Journal of Science* 287.10, pp. 1008–1040.
- Ostwald, W. (1925). “Ueber die Geschwindigkeitsfunktion der Viskosität disperser Systeme.” In: *Kolloid-Zeitschrift* 36, pp. 99–117.
- Pailha, M., A. L. Hazel, P. A. Glendinning, and A. Juel (2012). “Oscillatory bubbles induced by geometrical constraint”. In: *Physics of Fluids* 24.2, p. 021702.
- Park, C. W. and G. M. Homsy (1985). “The instability of long fingers in Hele–Shaw flows”. In: *Physics of Fluids* 28.6, p. 1583.
- Park, S. S. and D. J. Durian (1994). “Viscous and elastic fingering instabilities in foam”. In: *Physical Review Letters* 72.21, pp. 3347–3350.
- Pascal, H (1988). “Stability of non-Newtonian fluid interfaces in a porous medium and its applications in an oil displacement mechanism”. In: *Journal of colloid and interface science* 123.1, pp. 14–23.
- Paterson, Lincoln (1981). “Radial fingering in a Hele Shaw cell”. In: *Journal of Fluid Mechanics* 113, pp. 513–529.
- Patne, R. and V. Shankar (2017). “Absolute and convective instabilities in combined Couette-Poiseuille flow past a neo-Hookean solid”. In: *Physics of Fluids* 29, p. 124104.
- Pauné, E, M Siegel, and J Casademunt (2002). “Effects of small surface tension in Hele-Shaw multifinger dynamics: An analytical and numerical study”. In: *Physical Review E* 66.4, p. 046205.

- Pauné, Eduard and Jaume Casademunt (2003). “Kinetic roughening in two-phase fluid flow through a random Hele-Shaw cell”. In: *Physical Review Letters* 90.14, p. 144504.
- Petrolo, D., L. Chiapponi, S. Longo, M. Celli, A. Barletta, and V. Di Federico (2020). “Onset of Darcy–Bénard convection under throughflow of a shear-thinning fluid”. In: *Journal of Fluid Mechanics* 889, R2.
- Pierce, A. D. (1981). *Acoustics: An introduction to its physical principles and applications*. New York: McGraw-Hill.
- Pihler-Puzović, D, Pierre Illien, Matthias Heil, and Anne Juel (2012). “Suppression of complex fingerlike patterns at the interface between air and a viscous fluid by elastic membranes”. In: *Physical review letters* 108.7, p. 074502.
- Pihler-Puzović, Draga, Gunnar G Peng, John R Lister, Matthias Heil, and Anne Juel (2018). “Viscous fingering in a radial elastic-walled Hele-Shaw cell”. In: *Journal of Fluid Mechanics* 849, pp. 163–191.
- Pinilla, Andrés, Miguel Asuaje, and Nicolás Ratkovich (2021). “Experimental and computational advances on the study of Viscous Fingering: An umbrella review”. In: *Heliyon* 7.7.
- Pipe, C. (2005). “Experiments investigating the effects of fluid elasticity on laminar vortex shedding from a cylinder”. PhD thesis. MS Thesis, EPFL.
- Pramanik, Satyajit, GL Kulukuru, and Manoranjan Mishra (2012). “Miscible viscous fingering: Application in chromatographic columns and aquifers”. In: *COMSOL conference, Bangalore*.
- Pritchard, David (2009). “The linear stability of double-diffusive miscible rectilinear displacements in a Hele-Shaw cell”. In: *European Journal of Mechanics-B/Fluids* 28.4, pp. 564–577.
- Rabaud, M., Y. Couder, and N. Gerard (1988a). “Dynamics and stability of anomalous Saffman-Taylor fingers”. In: *Physical Review A* 37.3, pp. 935–947.
- Rabaud, M., Y. Couder, and N. Gerard (1988b). “Dynamics and stability of anomalous Saffman-Taylor fingers”. In: *Physical Review A* 37, pp. 935–947.
- Ramesh, VP, MK Kadalbajoo, M Prithvi, and B Priyanga (2020). “Exponentially refined mesh for singularly perturbed interior layer problem”. In: *International Journal of Applied and Computational Mathematics* 6.3, p. 82.
- Ray, P. K. and T. A. Zaki (2014). “Absolute instability in viscoelastic mixing layers”. In: *Physics of Fluids* 26, p. 014103.
- Ray, P. K. and T. A. Zaki (2015). “Absolute instability of planar viscoelastic jets”. In: *Physics of Fluids* 27, p. 014110.
- Reed, Ronald L, Robert N Healy, and DO Shah (1977). “Some physicochemical aspects of microemulsion flooding: a review”. In: *Improved oil recovery by surfactant and polymer flooding*, pp. 383–437.
- Romanov, Douchko, Franci Gabrovšek, and Wolfgang Dreybrodt (2003). “Dam sites in soluble rocks: a model of increasing leakage by dissolutional widening of fractures beneath a dam”. In: *Engineering Geology* 70.1-2, pp. 17–35.
- Ruith, Michael and Eckart Meiburg (2000). “Miscible rectilinear displacements with gravity override. Part 1. Homogeneous porous medium”. In: *Journal of Fluid Mechanics* 420, pp. 225–257.
- Sabet, Nasser, Hassan Hassanzadeh, and Jalal Abedi (2017). “Control of viscous fingering by nanoparticles”. In: *Physical Review E* 96.6, p. 063114.

- Saffman, P. G. (1959). “Exact solutions for the growth of fingers from a flat interface between two fluids in a porous medium or Hele-Shaw cell”. In: *The Quarterly Journal of Mechanics and Applied Mathematics* 12.2, pp. 146–150.
- Saffman, P. G. and G. I. Taylor (1958). “The penetration of a fluid into a porous medium or Hele-Shaw cell containing a more viscous liquid”. In: *Proceedings of the Royal Society of London. Series A, Mathematical and Physical Sciences* 245.1242, pp. 312–329.
- Saintyves, B., O. Dauchot, and E. Bouchaud (2013). “Bulk Elastic Fingering Instability in Hele-Shaw Cells”. In: *Physical Review Letters* 111.4, p. 047801.
- Sandnes, B., E.G. Flekkøy, H.A. Knudsen, K.J. Måløy, and H. See (2011). “Patterns and flow in frictional fluid dynamics”. In: *Nature Communications* 2.1, p. 288.
- Sandnes, B., H. A. Knudsen, K. J. Måløy, and E. G. Flekkøy (2007). “Labyrinth Patterns in Confined Granular-Fluid Systems”. In: *Physical Review Letters* 99.3, p. 038001.
- Sato, Kenji, Yasuhiro Sakai, and Manabu Chiga (1996). “Flame propagation along 90° bend in an open duct”. In: *Symposium (International) on Combustion* 26.1, pp. 931–937.
- Schmid, P.J. and D.S. Henningson (2001). *Stability and transition in shear flows*. New York: Springer.
- Schröder, M., K. Kassner, I. Rehberg, J. Claret, and F. Sagués (2002). “Experimental investigation of the initial regime in fingering electrodeposition: dispersion relation and velocity measurements”. In: *Physical Review E* 65.4, p. 041607.
- Shelley, Michael J, Fei-Ran Tian, and Krzysztof Włodarski (1997). “Hele - Shaw flow and pattern formation in a time-dependent gap”. In: *Nonlinearity* 10.6, pp. 1471–1495.
- Shoji, T., E. W. Harris, A. Bernard, S. G. Schein, and A. R. Karagozian (2020). “On the origins of transverse jet shear layer instability transition”. In: *Journal of Fluid Mechanics* 890, A7–1.
- Shokri, H., M. H. Kayhani, and M. Norouzi (2017). “Nonlinear simulation and linear stability analysis of viscous fingering instability of viscoelastic liquids”. In: *Physics of Fluids* 29.3, p. 033101.
- Shraiman, Boris I. (1986). “Velocity Selection and the Saffman-Taylor Problem”. In: *Physical Review Letters* 56.19, pp. 2028–2031.
- Shukla, Priyanka and Anne De Wit (2020). “Influence of the Péclet number on reactive viscous fingering”. In: *Physical Review Fluids* 5.1, p. 014004.
- Shull, Kenneth R., Dongchan Ahn, Wan-Lin Chen, Cynthia M. Flanigan, and Alfred J. Crosby (1998). “Axisymmetric adhesion tests of soft materials”. In: *Macromolecular Chemistry and Physics* 199.4, pp. 489–511.
- Siegel, Michael, Russel E. Caflisch, and Sam Howison (2004). “Global existence, singular solutions, and ill-posedness for the Muskat problem”. In: *Communications on Pure and Applied Mathematics* 57.10, pp. 1374–1411.
- Singh, Akhileshwar, Yogesh Singh, and Krishna Murari Pandey (2020). “Viscous fingering instabilities in radial Hele-Shaw cell: A review”. In: *Materials Today: Proceedings* 26, pp. 760–762.
- Singh, Brajeesh K and Jalel Azaiez (2001). “Numerical simulation of viscous fingering of shear-thinning fluids”. In: *The Canadian Journal of Chemical Engineering* 79.6, pp. 961–967.



- Sircar, S. and Q. Wang (2010). “Transient rheological responses in sheared biaxial liquid crystals”. In: *Rheologica Acta* 49.7, pp. 699–717.
- Slim, Anja C., M. M. Bandi, Joel C. Miller, and L. Mahadevan (2013). “Dissolution-driven convection in a Hele–Shaw cell”. In: *Physics of Fluids* 25.2, p. 024101.
- Sorbie, KS, Farag Feghi, GE Pickup, PS Ringrose, and JL Jensen (1994). “Flow regimes in miscible displacements in heterogeneous correlated random fields”. In: *SPE Advanced Technology Series* 2.02, pp. 78–87.
- Sorbie, KS, HR Zhang, and NB Tsibuklis (1995). “Linear viscous fingering: new experimental results, direct simulation and the evaluation of averaged models”. In: *Chemical engineering science* 50.4, pp. 601–616.
- Soriano, Jordi, Jordi Ortín, and Aurora Hernandez-Machado (2002). “Experiments of interfacial roughening in Hele-Shaw flows with weak quenched disorder”. In: *Physical Review E* 66.3, p. 031603.
- Steeffel, C. I. and A. C. Lasaga (1994). “A coupled model for transport of multiple chemical species and kinetic precipitation/dissolution reactions with application to reactive flow in single phase hydrothermal systems”. In: *American Journal of Science* 294.5, pp. 529–592.
- Stewartson, K. and I.T. Stuart (1971). “A nonlinear instability theory for a wave system in plane Poiseuille flow”. In: *Journal of Fluid Mechanics* 48, pp. 529–45.
- Sturrock, P.A. (1958). “Kinematics of growing waves”. In: *Physical Review* 112, pp. 1488–1503.
- Sudaryanto, Bagus and Yannis C. Yortsos (Sept. 2001). “Optimization of Displacements in Porous Media Using Rate Control”. In: *All Days*. New Orleans, Louisiana: SPE, SPE–71509–MS.
- Suzuki, Ryuta X., Yuichiro Nagatsu, Manoranjan Mishra, and Takahiko Ban (2020a). “Phase separation effects on a partially miscible viscous fingering dynamics”. In: *Journal of Fluid Mechanics* 898, A11.
- Suzuki, Ryuta X., Fu Wei Quah, Takahiko Ban, Manoranjan Mishra, and Yuichiro Nagatsu (2020b). “Experimental study of miscible viscous fingering with different effective interfacial tension”. In: *AIP Advances* 10.11, p. 115219.
- Tabeling, P. and A. Libchaber (1986). “Film draining and the Saffman-Taylor problem”. In: *Physical Review A* 33.1, pp. 794–796.
- Tabeling, P., G. Zocchi, and A. Libchaber (1987). “An experimental study of the Saffman-Taylor instability”. In: *Journal of Fluid Mechanics* 177, pp. 67–82.
- Talon, L, N Goyal, and E Meiburg (2013). “Variable density and viscosity, miscible displacements in horizontal Hele-Shaw cells. Part 1. Linear stability analysis”. In: *Journal of Fluid Mechanics* 721, pp. 268–294.
- Tchelepi, HA, FM Orr Jr, N Rakotomalala, D Salin, and R Woumeni (1993). “Dispersion, permeability heterogeneity, and viscous fingering: Acoustic experimental observations and particle-tracking simulations”. In: *Physics of Fluids A: Fluid Dynamics* 5.7, pp. 1558–1574.
- Thacker, W.C. (1976). “Spatial growth of Gulf stream meanders”. In: *Geophysical & Astrophysical Fluid Dynamics* 7.27, pp. 1–95.
- Tryggvason, Gretar and Hassan Aref (1983). “Numerical experiments on Hele Shaw flow with a sharp interface”. In: *Journal of Fluid Mechanics* 136, pp. 1–30.
- Tryggvason, Grétar and Hassan Aref (1985). “Finger-interaction mechanisms in stratified Hele-Shaw flow”. In: *Journal of Fluid Mechanics* 154, pp. 287–301.

- Tsuzuki, Reiko, Ryohei Tanaka, Takahiko Ban, and Yuichiro Nagatsu (2019). “Deviation from capillary number scaling of nonlinear viscous fingering formed by the injection of Newtonian surfactant solution”. In: *Physics of Fluids* 31.4, p. 042108.
- Twiss, R. Q. (1952). “Propagation in electron-ion streams”. In: *Physical Review* 88, pp. 1392–1407.
- Upchurch, E. and E. Meiburg (2008). “Miscible porous media displacements driven by non-vertical injection wells”. In: *Journal of Fluid Mechanics* 607, pp. 289–312.
- Veeramani, Naveen, Raja Samikannu, Abhijit P Deshpande, Sheril Varghese, and Vinutha Moses (2023). “Effects of polymeric microcapsules on self-healing composites reinforced with carbon fibers: a comparative study”. In: *International Polymer Processing*.
- Veiga-López, Fernando, Daniel Martínez-Ruiz, Eduardo Fernández-Tarrazo, and Mario Sánchez-Sanz (2019). “Experimental analysis of oscillatory premixed flames in a Hele-Shaw cell propagating towards a closed end”. In: *Combustion and Flame* 201, pp. 1–11.
- Vihinen, I., A. M. Honohan, and S. P. Lin (1997). “Image of absolute instability in a liquid jet”. In: *Physics of Fluids* 9, p. 3117.
- Vinals, Jorge and David Jasnow (1992). “Coarsening following a morphological instability in the one-sided model”. In: *Physical Review A* 46.12, p. 7777.
- Waele, A. De (1923). “Viscometry and plastometry”. In: *Journal of Oil and Color Chemists’ Association* 6, pp. 33–88.
- Wooding, R. A. (1969). “Growth of fingers at an unstable diffusing interface in a porous medium or Hele-Shaw cell”. In: *Journal of Fluid Mechanics* 39.3, pp. 477–495.
- Xu, Le, Piotr Szymczak, Renaud Toussaint, Eirik G. Flekkøy, and Knut J. Måløy (2019). “Experimental Observation of Dissolution Finger Growth in Radial Geometry”. In: *Frontiers in Physics* 7, p. 96.
- Yeo, K.S., B.C. Khoo, and H.Z. Zhao (1996). “The absolute instability of boundary-layer flow over viscoelastic walls”. In: *Theoretical and computational fluid dynamics* 8, pp. 237–252.
- Zhao, H. and J. V. Maher (1993). “Associating-polymer effects in a Hele-Shaw experiment”. In: *Physical Review E* 47.6, pp. 4278–4283.
- Zocchi, Giovanni, Patrick Tabeling, and Martine Ben Amar (1992). “Saffman-Taylor plumes”. In: *Physical Review Letters* 69.4, pp. 601–604.

## List of Publications

1. Diksha Bansal, Dipa Ghosh, Sarthok Sircar, Selection mechanism in non-Newtonian Saffman-Taylor fingers, *SIAM Journal on Applied Mathematics* **83(2)**, 329-353(2023). <https://doi.org/10.1137/22M1485838>
2. Dipa Ghosh, Tanisha Chauhan, Sarthok Sircar, Implicit-Explicit Time Integration Method for Fractional Advection-Reaction-Diffusion Equations, *ANZIAM Journal*, Submitted.
3. Diksha Bansal, Dipa Ghosh, Sarthok Sircar, Spatiotemporal linear stability of viscoelastic free shear flows: non-affine regime, *Phys. Fluids*, **33**, 054106 (2021). <https://doi.org/10.1063/5.0049504>

# Curriculum Vitae

## Dipa Ghosh

H1 Hostel  
IIT Delhi, Okhla Industrial area phase-3,  
New Delhi, Delhi-110020

dipag@iiitd.ac.in  
kdipa6@gmail.com  
+918345968493

### Personal info

Date of birth : 03-01-1990  
Nationality : Indian  
Languages : Bengali, Hindi and English  
Research gate : [https://www.researchgate.net/profile/Dipa\\_Ghosh2](https://www.researchgate.net/profile/Dipa_Ghosh2)

### Research Interests

Fluid Dynamics, CFD, Flow Instability, Viscoelasticity, Non-Newtonian fluid flow, Hele-Shaw Cell, Direct Numerical Simulations, Fourier analysis, Finite element method, Scientific Computing, Numerical PDE

### Education

2019–2024 : **Ph.D. Mathematics, Dept. Of mathematics, IIITD, Delhi**  
2012–2014 : M.Sc. Mathematics, IIT Madras, Chennai, Tamilnadu  
2009–2012 : B.Sc. Mathematics, University Of North Bengal, West Bengal

### Technical strengths

Language : C, C++, Python  
Software Skills : MS Office, Latex, MATLAB, Mathematica, Maple, Tecplot

### Teaching assistant/Lecturer Experience

July 2019-July 2023 : TA(Real analysis-II and Multivariate calculus)  
January 2020-July 2022 : NPTEL TA (Online mode: Integral Transform and their Appl. and Calculus of Variation)  
July 2015-November 2016 : Assistant Professor (Undergraduate Maths), Inspiria Knowledge Campus

### Conferences and Poster Presentation

- ICRAMDF Conference on Applied Mathematics, Recent advancement in Mathematical Fluid dynamics, MNIT Jaipur, Rajasthan, India, December 02, 2022

- ICIAM Conference on Applied Mathematics, Minisymposia invited talk, Waseda University, Tokyo, Japan, August 20th - 25th, 2023
- ICCEMT 2023 Conference on Energy Summit, Paper presentation, UPES, Dehradun, India, September 20th - 22nd, 2023
- ICAMM conference on Applied Mathematics and Mechanics, Paper presentation (Oral), IIT Indore, India, October 18th – 20th, 2023
- Mathematics Open House talk on Applied Mathematics and Mechanics, Paper presentation (Oral), Department of Mathematics, IIIT Delhi, India, November 25th, 2023
- Selected at Joint Mathematics Meetings for Contributed talk, Paper presentation (Oral) as a member of AMS, San Francisco, California, January 3rd to 6th, 2024
- ICIAM Conference on Applied mathematics, Poster Presentation, Waseda University, Tokyo, Japan, August 20th - 25th, 2023
- RIISE 2023 Poster Presentation, Poster Presentation on Cartilage Tissue, IIIT Delhi, India, May 11th, 2023

## Workshops and Seminars

- Interfacial Instability with Industrial Applications, GIAN course, IIT Ropar, July 11, 2022
- Cognitive Modelling, Winter School, IIT Mandi, Oct 16, 2022
- Nonlinear Dynamics and Applications, Lecture series, SERB, IIT Indore, Feb 13, 2023
- Recent advancement in fluid flow and heat transfer, E-colloquium, IIT Roorkee, Oct 19, 2020
- Numerical solutions of Differential Equation, Short Course, NIT Jalandhar, Sept 16, 2022
- Refresher course on Analysis, Tezpur University, NAC and INSA, Feb 18, 2019
- Optimization and Fuzzy Mathematics, National Workshop, Vidyasagar University, Sept 19, 2014
- National Workshop on PDE - TCA, DST, IIT Madras, May 20, 2013
- MTTTS (Mathematics Training and Talent Search) Programme, NBHM, Shantiniketan, Kolkata, May 24, 2010

## **Awards and Grants**

- UGC-CSIR in Mathematical Science, JRF and SRF, AIR-141, August 2019
- GATE in Mathematics, JRF, AIR-663, January 2018
- Travel awards, IIT Delhi Institution Travel Grants, August 2023
- Best Oral Presentation award, ACS Publication, Energy Summit 2023, UPES, August 2023

## **Membership**

American Mathematical Society (AMS)